Domain Decomposition Methods for Elastic Materials with Compressible and Almost Incompressible Components

Sabrina Gippert
geboren in Neuss

Fakultät für Mathematik
Universität Duisburg-Essen

November 2012

Dissertation im Fach Mathematik
zum Erwerb des Dr. rer. nat.
an der Fakultät für Mathematik
der Universität Duisburg-Essen

UNIVERSITÄT
DUISBURG
ESSEN

Erstgutachter: Prof. Dr. Axel Klawonn,
Mathematisches Institut, Universität zu Köln
Zweitgutachter: Prof. Dr. Gerhard Starke
Institut für Angewandte Mathematik, Leibniz Universität Hannover
Tag der mündlichen Prüfung: 11.01.2013

Contents

Acknowlegements

First of all, I like to thank all the people who supported me during my doctoral thesis. I owe special thanks to my advisor Prof. Dr. Axel Klawonn; I am grateful for his support in the last years, his time for discussion and offering me the possibility to spend the time of my doctorate in his working group. I would also like to thank him and Prof. Dr. Gerhard Starke for reviewing this work. Additionally, I like to thank Dr. Oliver Rheinbach for his excellent implementation tips as well as for the encouragement he gave me. I am happy to thank my colleagues, especially Patrick for all the discussions and time we spend in front of the blackboard in our office in Essen and Martin for his support, in mathematical topics but also for his friendship.

I would not be at this point of my life without my parents who have always supported and encouraged me continuously, and my sister Katja who always has a sympathetic ear for me, her support and inspiration means so much to me. Last but not least I want to thank my friends, who always tried to find a compensation for scientific work. Thank you Marion, among other things, for your interest in my work, even if you say, you don't like math-
I don't believe that!

Introduction

The finite element method (FEM) is a well established approximation method in engineering, physics and applied mathematics. In 1956 the FEM was first applied in structural and fluid mechanics for an aircraft wing [58]. The term finite element method was established four years later [9]. Today the finite element method is a frequently used tool to approximate solutions of partial differential equations (PDEs). Such approximations are inevitable since exact solutions of partial differential equations are known only for simple PDEs and simple geometries. In order to apply the finite element method a variational formulation is derived from a strong form of a partial differential equation. Minimization in a finite dimensional space then gives the finite element solution.

The discretization by finite elements leads, either directly or after linearization, to a large linear system of equations which needs to be solved. The number of unknowns is determined by the accuracy of the solution required for the specific application. Today the number of unknowns can range from millions to billions of unknowns in structural mechanics simulations. To solve linear systems of such size the use of parallel computers is necessary.

Domain decomposition methods (DDMs) are algorithms well suited for high performance parallel computers. They are inherently parallel methods based on an overlapping or nonoverlapping geometric decomposition of the computational domain. The solution of the original problem is then computed in an iterative process, typically accelerated by a Krylov subspace method such as conjugate gradients. In this work domain decomposition methods are thus always understood as preconditioned iterative methods.

In the construction of domain decomposition methods attention has to be paid to the different aspects of scalability. A DDM is called numerically scalable if the number of iterations is independent of the problem size. In order to obtain numerical scalability, a small coarse problem has to be solved in each iteration step in addition to the number of systems associated with the local subdomains. Such a coarse problem provides a mechanism for global exchange of information in each iteration step. Numerical scalability is a requirement to obtain parallel scalability of DDMs. Here, we distinguish between two versions of parallel scalability, i.e.,

strong and weak scalability. For a problem with a fixed number of unknowns, an algorithm is called strongly scalable, if ideally, it solves the problem twice as fast if the number of processors is doubled. An algorithm is called weakly scalable if doubling the number of unknowns and doubling the number of processors at the same time will, ideally, keep the solution time constant.

The convergence of preconditioned conjugate gradient methods is determined by the condition number of the problem. For the convergence theory of domain decomposition methods the derivation of condition number bounds is therefore essential. In this work new condition number bounds for classes of problems in linear elasticity for a well-known and widely applied family of nonoverlapping DDMs, the dual primal Finite Element Tearing and Interconnecting (FETI-DP) Method, are derived. These bounds also apply to the balancing DDM by constraints (BDDC) method, introduced by Dohrmann [13].

We focus on the equations of linear elasticity in three dimensions, where the task is to calculate the displacement of a linear elastic domain under the action of forces; see, e.g., [8, 3, 4, 57], or more precisely, we consider linear elasticity problems with compressible and almost incompressible components. To obtain the displacement we use dual-primal FETI methods (FETI-DP). These methods belong to the family of Finite Element Tearing and Interconnecting (FETI) domain decomposition methods, which have been first introduced by Farhat and Roux in 1991; see [20]. The computational domain, on which the given partial differential equation has to be solved, is decomposed into nonoverlapping subdomains. The continuity of the solution across the interface is established weakly by the introduction of Lagrange multipliers, thus enforcing continuity not before convergence of the iterative method. In FETI-DP methods, some continuity constraints are defined to be primal, which means that they are assembled before the iteration and therefore continuity is enforced in each iteration step. The primal constraints should be selected such that the subproblems are invertible and such that good condition number bounds can be derived. For the remaining dual variables Lagrange multipliers are introduced as in standard FETI methods. The basic idea of FETI-DP is to eliminate the primal variables by forming a Schur complement and then iterate on the Lagrange multipliers, usually using a preconditioner. For the numerical results presented in this dissertation only the Dirichlet preconditioner is used.

For linear elasticity problems in the plane, FETI-DP methods were introduced by Farhat et al. in [18] and extended to the three dimensional case by Farhat, Lesoinne, and Pierson [19]. To obtain the same quality of bounds for the condition number estimate of FETI-DP in case

of linear elasticity essential changes in the selection of primal constraints have to be made. While selecting an appropriate set of edge averages as primal constraints is sufficient to handle material coefficients without large jumps, for arbitrary jumps primal first-order moments and, sometimes, constraints over vertices are required; see [37, 31].

The first analysis for scalar second- and fourth-order elliptic partial differential equations in two dimensions was provided by Mandel and Tezaur [46] and it was extended to the three dimensional case in [38, 39, 36] and to three dimensional linear elasticity in [37]. In [34], a theory for irregular subdomains in 2D was introduced. In [29], FETI-DP methods for spectral element discretizations for a polynomial degree of up to $p = 32$ were considered. In [32], the weak parallel scalability of a new version of a FETI-DP method, introduced in [54], for up to $65\,000$ processor cores was shown. The work in Chapter 3 of this thesis can be understood as an extension of the theory in [37] for certain classes of problems with jumps inside subdomains. Problems in elasticity with coefficient jumps not aligned with the interface have been considered before in [31].

Coarse spaces for iterative substructuring methods that are robust either with respect to exact incompressibility constraints or with respect to almost incompressibility on the complete computational domain have been known for some time. For early works on Neumann-Neumann methods for incompressible elasticity, see [23, 24, 48, 49]. For a recent Neumann-Neumann method for almost incompressible elasticity, see [1]. A balancing domain decomposition method (BDDC) for the Stokes equation was introduced by Li and Widlund [42]; for a FETI-DP method for the Stokes and the incompressible Navier-Stokes equation, see Li [41, 40]. For an extension of a recent overlapping Schwarz method, see Dohrmann et al. [14], to almost incompressible elasticity problems, see Dohrmann and Widlund [15]. This overlapping Schwarz method borrows its coarse space from iterative substructuring methods. For a BDDC method with a coarse space that is robust with respect to the almost incompressibility, see, e.g., [13, 50, 11]. In [35, 55], a FETI-DP method for almost incompressible elasticity in 2D was discussed.

An application of FETI-DP methods to almost incompressible problems in biomechanics can be also found in Klawonn and Rheinbach [32], Brinkhues, Klawonn, Rheinbach, and Schröder [6], and Böse et al. [2].

BDDC methods, see, e.g., [12, 10, 44, 43, 45, 29] for references, are closely related to FETI-DP methods in the sense that they share essentially all eigenvalues. It was first shown in Mandel, Dohrmann, and Tezaur [45], that FETI-DP and BDDC methods have the same

eigenvalues, which are not zero or one. As a consequence all results presented are also valid for BDDC methods.

This thesis is organized as follows. In Chapter 1, we introduce the problem of linear elasticity. The finite element method and the discretization of the elastic domain, and a brief summary of the domain decomposition method FETI-DP is given in Chapter 2. After this introduction of the conceptual basics, we consider a special category of compressible and almost incompressible linear elasticity problems when using a FETI-DP domain decomposition method. We introduce convergence bounds of FETI-DP methods for problems in 3D with almost incompressible inclusions or compressible inclusions with different Young's modulus embedded in a compressible matrix material using the coarse space for compressible linear elasticity. For such problems, where the material is compressible in the vicinity of the subdomain interface, we show a polylogarithmic condition number estimate for the preconditioned FETI-DP system, which only depends on the thickness of the compressible hull, but is otherwise independent of coefficient jumps between the hulls and the inclusions. We expand the convergence analysis, given by Klawonn and Widlund [37] for compressible linear elasticity, to the case where each subdomain contains an inclusion surrounded by a compressible hull of thickness η. Similar results for the diffusion problem and FETI-1 are already obtained by Pechstein and Scheichl [51, 52, 53]. The theoretical findings are numerically confirmed and presented at the end of Chapter 3. In Chapter 4, we focus on the problem of almost incompressible linear elasticity on the whole domain. Since in the previous chapter we used the coarse space for compressible elasticity, we need to expand the coarse space by using the zero net flux condition. In this approach, the face contributions need to be enforced by projector preconditioning, but for the edge contributions it is possible to enforce the zero net flux condition by projector preconditioning or using a transformation of basis; see [26, 33, 30]. We consider both concepts and we present numerical results for different experiments.

1 Linear Elasticity

The problem of linear elasticity consists in finding the displacement of an elastic domain under the action of forces. An elastic solid will return to its original state after removing the force; for example, a steel body will only show permanent deformation if very large forces are applied. In linear elasticity the strain tensor is only a linear approximation and therefore valid only for small displacements. Let $\Omega \subset \mathbb{R}^3$ be an elastic domain, see, e.g., Figure 1.1, on which a volume force is applied. The deformation, or more precisely the displacement in each meshpoint is calculated; see, e.g., Figure 1.2. In the figures the cube is fixed on the back side and we see that it is displaced, when a volume force in the direction of the front side is applied.

Figure 1.1:

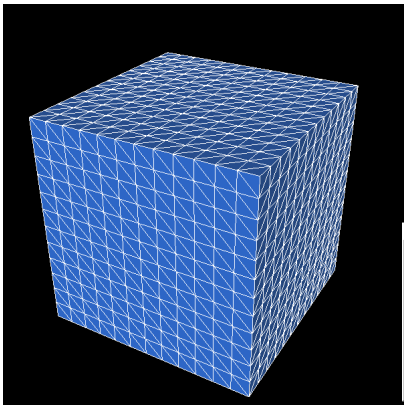

A cube of elastic material.

Figure 1.2:

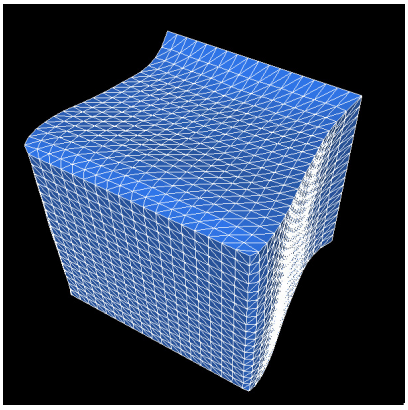

Deformation of a cube, after a volume force is applied.

1.1 Weak Formulation

We consider an isotropic elastic domain $\Omega \subset \mathbb{R}^3$. Let u be the displacement and f a given volume force. In the theory of linear elasticity u satisfies the partial differential equation given

by

$$\begin{aligned} -\mathrm{div}(\sigma(u)) &= f \qquad \text{in } \Omega \\ \sigma(u)\cdot n &= g \qquad \text{on } \partial\Omega_N \\ u &= 0 \qquad \text{on } \partial\Omega_D, \end{aligned} \tag{1.1}$$

where the stress tensor is defined as $\sigma(u) := G\ \varepsilon(u) + G\beta\ \mathrm{tr}(\varepsilon(u))\ I$, using the material parameters G and β. The linearized strain tensor $\varepsilon = (\varepsilon_{ij})_{ij}$ is defined as $\varepsilon_{ij}(u) = \frac{1}{2}\left(\frac{\partial u_i}{\partial x_j} + \frac{\partial u_j}{\partial x_i}\right)$. We also use the notation

$$\varepsilon(u) : \varepsilon(v) := \sum_{i,j=1}^{3} \varepsilon_{ij}(u)\varepsilon_{ij}(v) \text{ and } (\varepsilon(u), \varepsilon(v))_{L_2(\Omega)} := \int_\Omega \varepsilon(u) : \varepsilon(v)\ dx.$$

Note that we impose homogenous Dirichlet boundary conditions on $\partial\Omega_D$.
Assuming that equation (1.1) holds for $u \in H^2(\Omega)$, then for all $v \in H^1_0(\Omega, \partial\Omega_D)$, we obtain the weak formulation from integration by parts, see, e.g., [4, Chapter 11.2] or [3],

$$\begin{aligned} \int_\Omega f\cdot v\ dx &= -\int_\Omega \mathrm{div}(\sigma(u))\ v\ dx \\ &= \int_\Omega \sigma(u) : \nabla v\ dx - \int_{\partial\Omega} (\sigma(u)\cdot n)\ v\ ds \\ &= \int_\Omega \sigma(u) : \varepsilon(v)\ dx - \int_{\partial\Omega_N} g\cdot v\ ds \\ \Leftrightarrow \int_\Omega \sigma(u) : \varepsilon(v)\ dx &= \int_\Omega f\cdot v\ dx + \int_{\partial\Omega_N} g\cdot v\ ds. \end{aligned}$$

We consider

$$\begin{aligned} \int_\Omega \sigma(u) : \varepsilon(v)\ dx &= \int_\Omega (G\ \varepsilon(u) + G\beta\ \mathrm{tr}(\varepsilon(u))\ I) : \varepsilon(v)\ dx \\ &= \int_\Omega G\beta\ \mathrm{tr}(\varepsilon(u))\ I : \varepsilon(v)\ dx + \int_\Omega G\ \varepsilon(u) : \varepsilon(v)\ dx \\ &= \int_\Omega G\beta\ \mathrm{div}(u)\ \mathrm{div}(v)\ dx + \int_\Omega G\ \varepsilon(u) : \varepsilon(v)\ dx. \end{aligned}$$

Then, the problem of linear elasticity is defined as follows:

Find the displacement $u \in H^1_0(\Omega, \partial\Omega_D)$, such that

$$\int_\Omega G\varepsilon(u) : \varepsilon(v)\ dx + \int_\Omega G\beta\ \mathrm{div}(u)\ \mathrm{div}(v)\ dx = < F, v > \quad \forall v \in H^1_0(\Omega, \partial\Omega_D)$$

with the material parameters $G,\ \beta$, and the right hand side

$$< F, v > \ = \ \int_\Omega f^T v\ dx + \int_{\partial\Omega_N} g^T v\ ds.$$

Now, we can write the bilinear form for linear elasticity as

$$a(u,v) = (G\varepsilon(u), \varepsilon(v))_{L_2(\Omega)} + (G\beta \ \mathrm{div}(u), \mathrm{div}(v))_{L_2(\Omega)} .$$

For a domain Ω with diameter H, we use the scaled Sobolev space norm

$$\|u\|^2_{H^1(\Omega)} = |u|^2_{H^1(\Omega)} + \frac{1}{H^2} \|u\|^2_{L_2(\Omega)}$$

with $\|u\|^2_{L_2(\Omega)} := \sum_{i=1}^3 \int_\Omega |u_i|^2 \ dx$ and $|u|^2_{H^1(\Omega)} := \sum_{i=1}^3 \|\nabla u_i\|^2_{L_2(\Omega)}$.

The continuity of the bilinear form $a(\cdot,\cdot)$ with respect to $\|\cdot\|_{H^1(\Omega)}$ depends on the material parameters. For all $u, v \in H^1(\Omega)$, we have

$$|a(u,v)| \leq (1+3\beta)\, G\, |u|_{H^1(\Omega)}\, |v|_{H^1(\Omega)} \leq (1+3\beta)\, G\, \|u\|_{H^1(\Omega)}\, \|v\|_{H^1(\Omega)} ;$$

see, e.g., [37]. The ellipticity of $a(u,v)$ for $u, v \in H^1_0(\Omega, \partial\Omega_D)$ follows from Korn's first inequality, i.e., for all $u \in H^1_0(\Omega)$ we have

$$\|u\|_{H^1(\Omega)} \leq C\, (\varepsilon(u), \varepsilon(u))_{L_2(\Omega)} ;$$

see for example [8, 37].

Then, as a result of the lemma of Lax-Milgram, see, e.g., [4, Theorem (2.7.7)], there exists a unique solution of the variational formulation

$$a(u,v) =< F, v > .$$

1.2 Material Parameters

In our theory, we consider an isotropic elastic material, i.e., the material behaves identically in all directions. An example of isotropic material is steel while wood is anisotropic. We consider the material parameters G and β, which can be expressed using Young's modulus E and Poisson's ratio ν by

$$G \ = \ \frac{E}{1+\nu} \text{ and } \beta = \frac{\nu}{1-2\nu}.$$

The Young modulus $E > 0$ is a measure for the stiffness of an elastic material, since it relates strain to stress. As the value of E gets larger, the considered material becomes stiffer. In our numerical experiments, we use, e.g., $E = 21e5$ for steel and $E = 0.037e5$ for rubber.

The deformation by compression in one direction of an elastic domain results in an expansion in cross direction. This effect is called the Poisson effect; see Figure 1.3. Poisson's ratio $\nu \in [0, \frac{1}{2})$ is a measure of this effect. As the value of the Poisson ratio is smaller, the expansion is smaller. In our numerical experiments, we use $\nu = 0.28$ for steel and $\nu = 0.485$ for rubber; see [8].

Compressibility is a measure of the relative volume change of a solid as a response to a

Figure 1.3: Poisson's effect

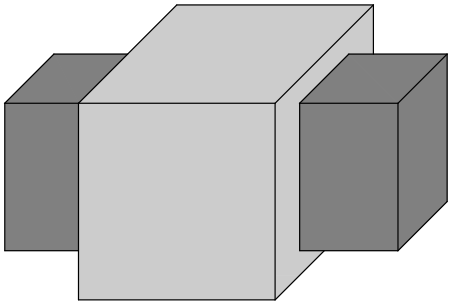

Compressing the smaller cuboid, we obtain an expansion in cross direction.

change in the pressure. Elastic material is called almost incompressible if ν tends to $\frac{1}{2}$, i.e., the volume does not change significantly under pressure. The limit of $\nu = \frac{1}{2}$ is called perfect incompressibility and only topic of theoretical considerations.

1.3 Mixed Formulation

For almost incompressible linear elasticity, i.e., $\nu \to \frac{1}{2}$, the value of β tends to infinity, and the discretization by standard finite elements leads to locking effects and slow convergence. For more information about the locking effect, see, e.g., [4, 3]. As a remedy the variational formulation of the pure displacement problem is replaced by a mixed formulation. Therefore, we introduce the pressure $p := G\beta \operatorname{div}(u) \in L_2(\Omega)$ as an auxiliary variable and consider the problem:

Find $(u, p) \in H_0^1(\Omega, \partial\Omega_D) \times L_2(\Omega)$, such that

$$\begin{aligned} \int_\Omega G\varepsilon(u) : \varepsilon(v)\ dx + \int_\Omega \operatorname{div}(v)\ p\ dx &= < F, v > \quad \forall v \in H_0^1(\Omega, \partial\Omega_D) \\ \int_\Omega \operatorname{div}(u)\ q\ dx - \int_\Omega \frac{1}{G\beta}\ p\ q\ dx &= 0 \quad \forall q \in L_2(\Omega). \end{aligned}$$

It is known, that in the case of almost incompressible linear elasticity the solution of this mixed

formulation exists and is unique, as a result of the $V-$ellipticity of the bilinear form and the inf-sup condition; see, e.g., [3, 57, 5]. The ellipticity of $\int_\Omega G\varepsilon(u) : \varepsilon(v)\ dx$ is ensured by the first Korn inequality, and an inf-sup condition for $\int_\Omega \mathrm{div}(v)\ p\ dx$ follows from the analysis of the Stokes problem; see [57]. The involving estimates are independent of $G\beta > 0$, thus, for low-order, conforming finite elements, the solution of the finite element method converges uniformly in $G\beta$; see [3].

In our numerical experiments, we will later choose for the almost incompressible part $\mathcal{Q}_2 - \mathcal{P}_0$ mixed finite elements. The finite space for the displacement is $V^h := (\mathcal{Q}_2(h))^n$, where $\mathcal{Q}_2$ is the space of triquadratic functions. The pressure space consists of discontinuous piecewise constant functions, i.e., $U^h := \{q \in L_2 :\ q\,|_T \in \mathcal{P}_0(T)\ \forall T \in \tau_h\}$. Both spaces are defined on the same hexahedral mesh. This finite element method satisfies an inf-sup condition in the sense that:

$$\sup_{v \in V^h} \frac{b_i(v,q)}{a_i(v,v)^{1/2}} \geq \gamma\ c_i(q,q)^{1/2}\ \forall q \in U^h \cap L_{2,0},\ \gamma > 0,$$

where $a_i(\cdot,\cdot),\ b_i(\cdot,\cdot)$, and $c_i(\cdot,\cdot)$ are the corresponding bilinear forms of the mixed formulation; see also the comments in Chapter 2 and [16].

2 Finite Elements and Domain Decomposition

In this chapter, we will introduce the assumptions needed for the convergence analysis of the FETI-DP algorithm, first for linear elasticity problems with different material components in Chapter 3 and then for the analysis of the zero net flux condition needed, for almost incompressible linear elasticity problems, considered in Chapter 4.

2.1 Finite Elements

The finite element method (FEM) is a numerical method to solve partial differential equations (PDEs) approximately. We consider the problem: Find $u \in V$, such that

$$a(u, v) = \langle f, v \rangle \ \forall v \in V,$$

where $a(\cdot, \cdot) : V \times V \to \mathbb{R}$ is the corresponding bilinear form of the weak formulation of a scalar partial differential equation and $f : V \to \mathbb{R}$ a linear functional. The infinite dimensional space V is approximated by the discrete finite dimensional space V^h and we solve the discrete problem: Find $u_h \in V^h$, such that

$$a(u_h, v_h) = \langle f, v_h \rangle \ \forall v_h \in V^h.$$

The discrete solution u_h can be written as

$$u_h = \sum_{i=1}^{n} u_i \varphi_i,$$

using the shape functions $\varphi_i,\ i = 1, \ldots, n$, of V^h. This presentation leads to the linear system

$$Au = b,$$

with the stiffness matrix $A = (a(\varphi_i, \varphi_j))_{i,j=1,\ldots,n}$ and the load vector $b = (f, \varphi_i)_{i=1,\ldots,n}$. The matrix A is positive definite since the bilinear form $a(\cdot, \cdot)$ is symmetric and $V-$elliptic.

The accuracy of this approximation can be improved by increasing the number of degrees of freedom. Accordingly, the computational effort increases.

In Chapter 3, we analyze linear elasticity problems with compressible and almost incompressible material components. For the compressible part, we use the standard displacement formulation, cf. Chapter 1, i.e., we discretize the displacement by piecewise quadratic tetrahedral finite elements. For almost incompressible linear elasticity, i.e., $\nu \to \frac{1}{2}$, the value of β tends to infinity, and the discretization of the displacement formulation by standard finite elements leads to locking effects and slow convergence; for an analysis of locking effects see, e.g., [4, 3]. Therefore, we use the mixed formulation for the almost incompressible part; cf. Chapter 1. For the discretization of this mixed problem we can principally use any inf-sup stable mixed finite element method. For simplicity we use $\mathcal{Q}_2 - \mathcal{P}_0$ mixed finite elements, i.e., we discretize the displacement with piecewise triquadratic hexahedral finite elements and the pressure with piecewise constant elements. To obtain again a symmetric positive definite problem, the pressure is statically condensated element-by-element. The discretization by $\mathcal{Q}_2 - \mathcal{P}_0$ elements is known to be inf-sup stable. It follows, for example, from the inf-sup stability of the $\mathcal{Q}_2 - \mathcal{P}_1^{\text{nc}}$ discretization with nonconforming piecewise linear pressure variables since the pressure space in the $\mathcal{Q}_2 - \mathcal{P}_0$ approach is smaller; see [47]. We are aware of the fact that this is not an optimal element with respect to finite element convergence, but we have used it due to its simple implementation. In general other elements, such as $\mathcal{Q}_2 - \mathcal{P}_1^{\text{nc}}$, i.e., piecewise triquadratic displacement and nonconforming piecewise linear pressure approximations, can be used. Let us note, that at the interface between the compressible part and the almost incompressible part a nonconformity of the finite element space can arise, because there the piecewise quadratic finite element functions and the piecewise triquadratic finite element functions intersect; cf. Section 2.2. For our analysis of the condition number estimate of our FETI-DP algorithm in Section 3.4, we do not need the inf-sup stability of the almost incompressible part but the stability is of course necessary for the convergence of the finite element solution in the almost incompressible part.

In Chapter 4, we consider a new coarse space for almost incompressible linear elasticity problems, i.e., the zero net flux condition. The elastic domain is discretized with piecewise triquadratic hexahedral finite elements on the whole domain. These finite elements are both, inf-sup stable and conform.

2.2 Nonconformity of the Combination of $\mathcal{P}_2$ and $\mathcal{Q}_2$ Finite Elements

Finite elements are conforming if their corresponding finite element functions are contained in the appropriate Sobolev spaces, in which the variational formulation holds. Note, that the condition number estimate of the algorithm is independent of the conformity, but conformity is needed for the quality of the finite element solution. It is well-known that the triangulation of $\mathcal{P}_2$ finite elements is conforming; also using only $\mathcal{Q}_2$ finite elements produces a conforming triangulation; see, e.g., [3]. We use both finite elements in our implementation, tetrahedra for the compressible and hexahedra for the almost incompressible part. In our geometrical configuration we have an inclusion which is discretized with piecewise triquadratic finite elements. Those are surrounded by layers of piecewise quadratic finite elements. The tetrahedra and hexahedra coincide on the nodes on that interface and the interface is the union of planar faces, cf. Section 2.3. To understand the nonconformity of this combination it is sufficient to consider the continuity of the finite element functions on that interface. Suppose, we consider a cube as one element, which is connected with a tetrahedron; see Figure 2.5(a). We may write $u(x,y,z) \in \mathcal{Q}_2$ as a linear combination of triquadratic shape functions $\varphi_i(x,y,z),\ i = 1,\ldots,27$, corresponding to the nodes in a hexahedral finite element, i.e.,

$$u(x,y,z) = \sum_{i=1}^{27} u_i \varphi_i(x,y,z).$$

For a global function we can choose, e.g., $u(x,y,z) = \varphi_6(x,y,z)$, such that $u_6 = 1$ and $u_i = 0$ for all $i \neq 6$. So, we have

$$\begin{aligned} u(x,y,z) &= \varphi_6(x,y,z) \\ &= \frac{1}{8}\left(x+x^2\right)\left(y+y^2\right)\left(2-2z^2\right). \end{aligned}$$

Since we restrict φ_6 to $y = 1$, we obtain

$$\begin{aligned} \varphi_6(x,1,z)\,|_{y=1} &= \frac{1}{4}\left(x+x^2\right)\left(2-2z^2\right) \\ &= \frac{1}{2}\left(x - xz^2 + x^2 - x^2z^2\right), \end{aligned}$$

as a possible $u(x,y,z) \in \mathcal{Q}_2$ on the face between a hexahedron and tetrahedron; see Figure 2.3(a) for the plot of the $\mathcal{Q}_2-$ shape function on the quadratic face, or Figure 2.3(b) for

a restriction on a triangle. For the corresponding $\mathcal{P}_2-$shape function, we obtain

$$\hat{\varphi}_6(x,1,z) = x - z + xz - z^2;$$

see Figure 2.2(a) for the plot of the $\mathcal{P}_2-$ shape function on the quadratic face, or Figure 2.2(b) for a restriction on a triangle. This means, we have a difference already between the shape function on one face, i.e.,

$$\varphi_6(x,1,z) - \hat{\varphi}_6(x,1,z) = -\frac{1}{2}x - \frac{1}{2}xz^2 + \frac{1}{2}x^2 - \frac{1}{2}x^2z^2 + z - xz + z^2.$$

Therefore, we cannot have continuity for all finite element functions on a face between hexahedral and tetrahedral finite elements; see Figure 2.4(c) for the difference on a triangle face or Figures 2.4(a), 2.4(b) for a quadratic face. Since the shape functions do not coincide, we do not have conformity of the combination of $\mathcal{P}_2$ and $\mathcal{Q}_2$ elements.

Figure 2.1: $\mathcal{P}_2-$shape function

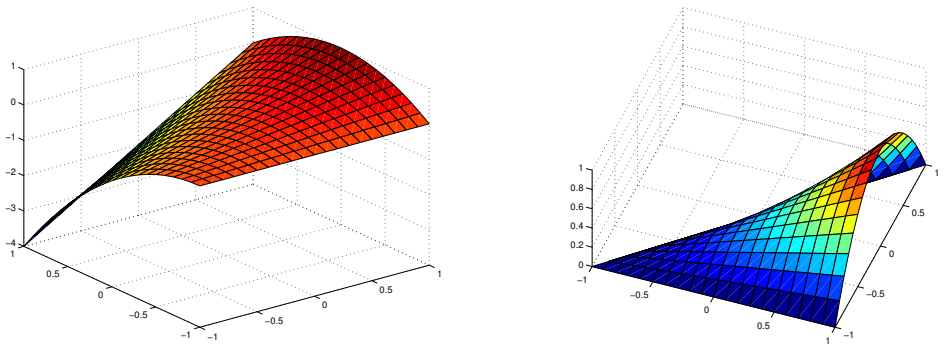

(a) $\mathcal{P}_2$- shape function on a quadratic face.

(b) $\mathcal{P}_2$- shape function restricted to a triangle face.

Figure 2.2: $\mathcal{Q}_2-$shape function

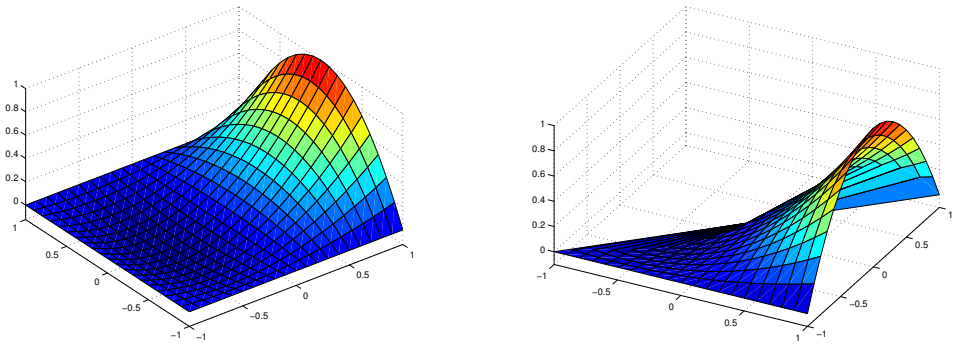

(a) $\mathcal{Q}_2$- shape function on a quadratic face.

(b) $\mathcal{Q}_2$- shape function restricted to a triangle face.

Figure 2.3: Difference

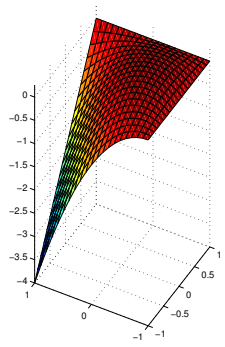

(a) Difference of both shape functions on a quadratic face.

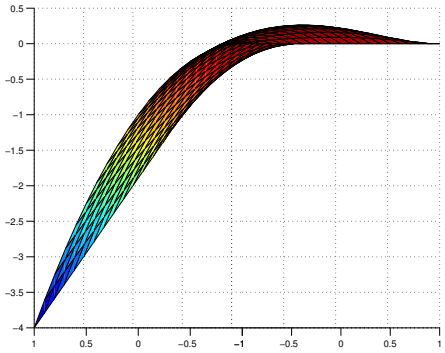

(b) Difference of both shape functions on a quadratic face (rotated).

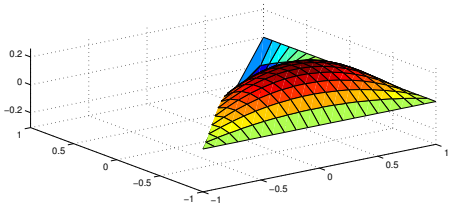

(c) Difference of both shape functions restricted to a triangle face.

Figure 2.4: Geometrical configuration

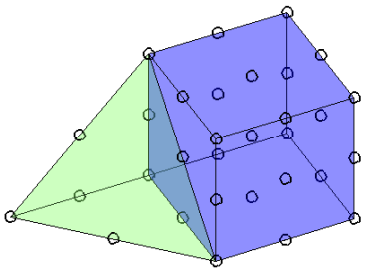

(a) Hexahedron connected with a tetrahedron. The elements coincide on the nodes on that interface.

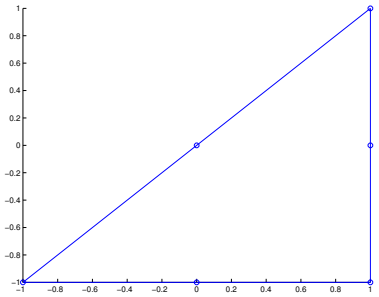

(b) Triangle face of the interface, with 6 nodes.

2.3 Scott-Zhang Interpolation

As we have mentioned before, we consider linear elasticity problems with different material components in Chapter 3. We will have an interior inclusion consisting of an almost incompressible material surrounded by a compressible hull. Our analysis will be established on a part of that hull which is bounded by straight edges and planar faces. So, on irregular meshes it might be necessary to cut through elements. We then define a slab of width η and define a regular mesh on this slab; see Figure 2.5. We have to assume that our irregular mesh resolves η in the sense that the incompressible inclusion is separated from the interface by at least one element; see Figure 2.5. For our analysis on irregular meshes we will use a Scott-Zhang interpolation; see [56, 4].

Figure 2.5:

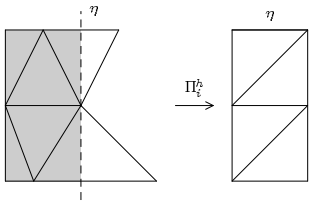

A slab in 2D: A slab (or a hull) is allowed to cut through finite elements. In such situations, an auxiliary mesh with a similar mesh size h is introduced such that the completion of the slab (or the hull) can be again represented as the union of finite elements.

We choose the operator, such that $\Pi_i^h : W^{(i)} \to \widetilde{V}^h$, i.e., a map from the original finite element trace space, into the finite element space on the regular mesh. The mesh size remains of the order of h. We assume the property $\Pi_i^h u \mid_{\partial\Omega_i} = u$ and the stability of the operator $\|\Pi_i^h u\|^2_{H^1(\Omega_i)} \leq C\|u\|^2_{H^1(\Omega_i)}$. Note that, since we cut through elements to separate the compressible and the almost incompressible part, this is only done in the theory, but never in the implementation. For simplicity, we assume in the proof that each slab can be represented as the union of finite elements. The generalization to the case where the interior boundary of a slab cuts through certain finite elements can be treated by using a Scott-Zhang interpolation operator, cf. the comment at the end of the proof of Lemma 3.17.

2.4 FETI-DP Domain Decomposition Method

The FETI-DP (**d**ual-**p**rimal **F**inite **E**lement **T**earing and **I**nterconnecting) Methods are nonoverlapping domain decomposition methods which are used to solve large linear systems arising, e.g., from finite element discretization. The problem is decomposed into smaller subproblems, which are solved, at the best, in parallel. The solutions of the subproblems are merged to a global solution. To obtain numerical scalability we need to solve a smaller, global coarse problem, which is traditionally solved exactly.

But first we give a brief introduction into FETI-DP, which is essentially taken from[54, 29]; for a complete description, see, e.g., [18, 19, 30, 31, 34]. Starting with the method, the computational domain $\Omega \subset \mathbb{R}^3$ is decomposed into N nonoverlapping subdomains $\Omega_i,\ i = 1, \dots N$, with diameter H_i. We obtain variables in the interior of the subdomains and those on the

Figure 2.6:

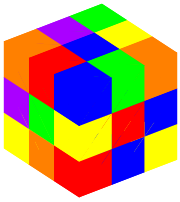

Decomposition into 27 subdomains.

Figure 2.7:

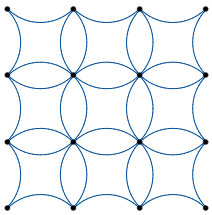

Cross section, assembled primal vertices.

interface $\Gamma := \bigcup_{i \neq j} (\partial\Omega_i \cap \partial\Omega_j) \setminus \partial\Omega_D$, to which we refer to $u_I^{(i)}$ and $u_\Gamma^{(i)}$, respectively. Concerning the interface Γ it is geometrically clear that Γ is the union of subdomain faces, edges, and vertices. Let us denote the sets of nodes on $\partial\Omega$ and Γ by $\partial\Omega_h,\ \Gamma_h$, and in Ω_i, by $\Omega_{i,h}$. For any interface node $x \in \Gamma_h$, we define

$$\mathcal{N}_x := \{j \in \{1, \dots, N\} :\ x \in \partial\Omega_{j,h}\}\,.$$

Thus, $\mathcal{N}_x$ is the set of subdomain indices which have x in their closure. A node x belongs to a face if x belongs to two subdomains, i.e., $|\mathcal{N}_x| = 2$, a node x belongs to an edge if $|\mathcal{N}_x| \geq 3$, and x is a vertex node if it is an endpoint of an edge. For more general meshes, i.e., outputs of graph partitioners, we refer to the detailed definition of faces, edges, and vertices in [37, Section 3].

Now the interface variables $u_\Gamma^{(i)}$ are partitioned into subdomain vertices, edges and faces. In FETI-DP methods, the variables on the subdomain boundaries are divided into two classes, the

primal and the dual variables. As primal variables $u_\Pi^{(i)}$, we call variables which are assembled before the iteration and in which continuity is enforced in each iteration step. For dual variables $u_\Delta^{(i)}$, continuity is established weakly by the introduction of Lagrange multipliers λ, thus enforcing continuity not before convergence.
However, we classify the variables into primal variables, associated with subdomain vertices and edge averages, and into nonprimal variables, associated with the interior variables and the subdomain edges and faces. For a description of the concept of primal constraints, we refer to Section 3.2 or [37].
For each subdomain we assemble the local stiffness matrix $K^{(i)}$ and the corresponding load vector $f^{(i)}$. Both are sorted according to the different sets of unknowns, this means the primal and the nonprimal variables

$$K^{(i)} = \begin{bmatrix} K_{BB}^{(i)} & K_{\Pi B}^{(i)T} \\ K_{\Pi B}^{(i)} & K_{\Pi\Pi}^{(i)} \end{bmatrix}, \quad f^{(i)} = \begin{bmatrix} f_B^{(i)} \\ f_\Pi^{(i)} \end{bmatrix}.$$

The nonprimal part is again partitioned into dual unknowns for which we later introduce Lagrange multipliers and interior variables. Thus we obtain

$$K_{BB}^{(i)} = \begin{bmatrix} K_{II}^{(i)} & K_{I\Delta}^{(i)T} \\ K_{I\Delta}^{(i)} & K_{\Delta\Delta}^{(i)} \end{bmatrix}, \quad f^{(i)} = \begin{bmatrix} f_I^{(i)} \\ f_\Delta^{(i)} \end{bmatrix}.$$

We define the corresponding block matrices

$$\begin{array}{lll} K_{II} = \mathrm{diag}(K_{II}^{(i)}) & K_{\Delta I} = \mathrm{diag}(K_{\Delta I}^{(i)}) & K_{\Delta\Delta} = \mathrm{diag}(K_{\Delta\Delta}^{(i)}) \\ K_{\Pi I} = \mathrm{diag}(K_{\Pi I}^{(i)}) & K_{\Pi\Delta} = \mathrm{diag}(K_{\Pi\Delta}^{(i)}) & K_{\Pi\Pi} = \mathrm{diag}(K_{\Pi\Pi}^{(i)}). \end{array}$$

By assembly of the local subdomain matrices in the primal variables, such that

$$\tilde{u}_\Pi = R_\Pi^T u_\Pi = \sum_{i=0}^{N} R_\Pi^{(i)T} u_\Pi^{(i)}$$

we obtain a partially assembled global stiffness matrix.

$$\begin{aligned} \widetilde{K} &= \begin{bmatrix} K_{BB} & \widetilde{K}_{\Pi B}^T \\ \widetilde{K}_{\Pi B} & \widetilde{K}_{\Pi\Pi} \end{bmatrix} = \begin{bmatrix} I_B & 0 \\ 0 & R_\Pi^T \end{bmatrix} \begin{bmatrix} K_{BB} & K_{\Pi B}^T \\ K_{\Pi B} & K_{\Pi\Pi} \end{bmatrix} \begin{bmatrix} I_B & 0 \\ 0 & R_\Pi \end{bmatrix} \\ \tilde{f} &= \begin{bmatrix} f_B \\ \tilde{f}_\Pi \end{bmatrix} = \begin{bmatrix} I_B & 0 \\ 0 & R_\Pi^T \end{bmatrix} \begin{bmatrix} f_B \\ f_\Pi \end{bmatrix}. \end{aligned}$$

The matrix $\widetilde{K}$ is coupled in the primal variables but has still a block structure in the nonprimal block K_{BB}.

Note, that the matrix $\widetilde{K}$ is symmetric positive definite, since we choose a sufficient number of primal variables to constrain the solution.

To enforce continuity on the remaining interface variables, we introduce a jump operator B_B with entries $\{-1, 0, 1\}$ and Lagrange multipliers λ. The constraint $B_B u_B = 0$ results in the FETI-DP saddle point problem

$$\begin{bmatrix} K_{BB} & \widetilde{K}_{\Pi B}^T & B_B^T \\ \widetilde{K}_{\Pi B} & \widetilde{K}_{\Pi\Pi} & 0 \\ B_B & 0 & 0 \end{bmatrix} \begin{bmatrix} u_B \\ \tilde{u}_\Pi \\ \lambda \end{bmatrix} = \begin{bmatrix} f_B \\ \tilde{f}_\Pi \\ 0 \end{bmatrix}.$$

We obtain the FETI-DP system $F\lambda = d$, where

$$\begin{aligned} F &= \begin{bmatrix} B_B & 0 \end{bmatrix} \begin{bmatrix} K_{BB} & \widetilde{K}_{\Pi B}^T \\ \widetilde{K}_{\Pi B} & \widetilde{K}_{\Pi\Pi} \end{bmatrix}^{-1} \begin{bmatrix} B_B^T \\ 0 \end{bmatrix} \\ d &= \begin{bmatrix} B_B & 0 \end{bmatrix} \begin{bmatrix} K_{BB} & \widetilde{K}_{\Pi B}^T \\ \widetilde{K}_{\Pi B} & \widetilde{K}_{\Pi\Pi} \end{bmatrix}^{-1} \begin{bmatrix} f_B \\ \tilde{f}_\Pi \end{bmatrix}, \end{aligned}$$

by calculating the Schur complement with respect first to the nonprimal and then again with respect to the assembled primal variables. The FETI-DP system is then solved iteratively with a preconditioned conjugate gradient algorithm using the Dirichlet preconditioner

$$M^{-1} = B_{B,D} \begin{bmatrix} 0 & I_\Delta \end{bmatrix}^T \left(K_{\Delta\Delta} - K_{\Delta I} K_{II}^{-1} K_{\Delta I}^T \right) \begin{bmatrix} 0 & I_\Delta \end{bmatrix} B_{B,D}^T.$$

For a full description of the Dirichlet preconditioner, see, e.g., [29, Section 3.2] or [30, 34, 37, 32].

2.5 Projector Preconditioning/Deflation

In substructuring methods as FETI-DP it is possible to expand the coarse space by additional constraints using projections; see, e.g., [33, 26]. For a given rectangular matrix U, which contains the constraints as columns, the condition $U^T B_B u_B = 0$ is enforced in each iteration of the preconditioned conjugate gradient method. We define the $F-$orthogonal projection

$$P = U \left(U^T F U \right)^{-1} U^T F$$

onto $\mathrm{range(U)}$ if F is symmetric positive definite or

$$P = U\left(U^T F U\right)^+ U^T F,$$

where $\left(U^T F U\right)^+$ denotes the pseudoinvers matrix of $U^T F U$, if F is symmetric positive semidefinite. We will then solve the projected system

$$(I-P)^T F\lambda = (I-P)^T d.$$

Since $\mathrm{range(P)}$ and $\ker(P)$ are $F-$orthogonal the projection P is called an $F-$conjugate projection. If $\lambda \in \mathrm{range(U)}$ we have

$$(I-P)^T F\lambda = F\lambda - P^T F\lambda = FU\hat{\lambda} - P^T FU\hat{\lambda} = 0 \Rightarrow U^T(I-P)^T F\lambda = 0$$

where $U\hat{\lambda} = \lambda$. Since U has full column rank, we have $\lambda \in \ker((I-P)^T F)$. For $\lambda \in \ker((I-P)^T F)$ we obtain $\lambda = F^+ FU(U^T FU)^+ U^T F\lambda + (I - F^+F)\hat{\lambda}$, with arbitrary solutions $\hat{\lambda}$. Using $\hat{\lambda} := U(U^T FU)^+ U^T F\lambda + (I-F^+F)\hat{\lambda}$ we get $\lambda = \hat{\lambda} \in \mathrm{range(U)}$. It follows, that

$$\ker((I-P)^T F) = \mathrm{range(U)}.$$

The matrix $(I-P)^T F$ is singular but the linear system is consistent and can therefore be solved using the conjugate gradient method. The preconditioned system is

$$M^{-1}(I-P)^T F\lambda = M^{-1}(I-P)^T d, \tag{2.1}$$

where M^{-1} denotes the Dirichlet preconditioner. Let λ^* be the solution of the original system $F\lambda = d$. We define

$$\overline{\lambda} := PF^+ d$$

for any pseudoinverse F^+ and additionally we denote by λ the solution of (2.1). The solution of the original problem can then be written as

$$\lambda^* = \overline{\lambda} + (I-P)\lambda \in \ker(I-P) \oplus \mathrm{range(I-P)}.$$

For construction of the Krylov space only the projections of the preconditioned residuals onto $\mathrm{range(I-P)}$ are relevant, since

$$M^{-1}(I-P)^T F = M^{-1}F(I-P) = M^{-1}F(I-P)^2 = M^{-1}(I-P)^T F(I-P).$$

We will include the projection $(I-P)^T$ into the preconditioner and project the correction onto $\mathrm{range(I-P)}$ in each iteration. We obtain the symmetric preconditioner

$$M_{PP}^{-1} = (I-P)M^{-1}(I-P)^T$$

and solve the original problem applying this preconditioner. This preconditioned system is singular but consistent. The solution λ of this system is in the subspace $\mathrm{range(I-P)}$. The solution λ^* of the original problem is then computed by

$$\lambda^* \quad = \overline{\lambda} + \lambda \in \ker(I-P) \oplus \mathrm{range(I-P)}.$$

If we include the computation of $\overline{\lambda}$ into the iteration we get the balancing preconditioner

$$M_{BP}^{-1} = (I-P)M^{-1}(I-P)^T + U(U^TFU)^{-1}U^T.$$

From [33] it is known, that the finite element solutions corresponding to the iterates generated by the FETI-DP method using projector preconditioning satisfy the condition $U^TB_Bu_B = 0$.

3 Compressible and Almost Incompressible Components

In this chapter we consider linear elasticity problems with varying coefficients inside subdomains. For each subdomain we will define an inclusion surrounded by a hull with a thickness of at least one element. For the inclusion we can choose either compressible or almost incompressible material and a different Young modulus, embedded in a compressible matrix material, because we use a coarse space for the FETI-DP algorithm designed for compressible linear elasticity. We expand the convergence analysis, given by Klawonn and Widlund [37] for compressible linear elasticity, to the case where each subdomain contains an inclusion surrounded by a compressible hull of thickness η. Similar results for the diffusion problem and FETI-1 are already obtained by Pechstein and Scheichl [51, 52, 53].
For such problems, where the material is compressible in the neighborhood of the subdomain interface, we show a polylogarithmic condition number estimate for the preconditioned FETI-DP system. The condition number bound only depends on the thickness of the compressible hull but is otherwise independent of coefficient jumps between the hull and the inclusion. These results are already published in [22] and the presentation here follows that in [22].

3.1 Technical Assumptions

First, we gather the assumptions that are made on the geometry of the finite element discretization and the domain decomposition and make some technical definitions.

We can write the bilinear form for linear elasticity as

$$a(u,v) = (G(x)\varepsilon(u),\varepsilon(v))_{L_2(\Omega)} + (G(x)\beta(x)\mathrm{div}(u),\mathrm{div}(v))_{L_2(\Omega)}\,.$$

For a domain Ω with diameter H, we use the scaled Sobolev space norm

$$\|u\|^2_{H^1(\Omega)} = |u|^2_{H^1(\Omega)} + \frac{1}{H^2}\,\|u\|^2_{L_2(\Omega)}$$

with $\|u\|^2_{L_2(\Omega)} := \sum_{i=1}^3 \int_\Omega |u_i|^2 \, dx$ and $|u|^2_{H^1(\Omega)} := \sum_{i=1}^3 \|\nabla u_i\|^2_{L_2(\Omega)}$.

We assume that a triangulation τ_h of Ω is given with shape regular finite elements, having a typical diameter h. In our numerical tests we use tetrahedra for the discretization of the compressible and hexahedra for the almost incompressible part, which coincide on the element nodes; cf. Chapter 2. We denote by $W^h := W^h(\Omega) \subset \left(H^1_0(\Omega, \partial\Omega_D)\right)^3$ our finite element space.

The domain Ω is decomposed into N nonoverlapping subdomains $\Omega_i, \ i = 1, \ldots, N$, with diameter H_i. For simplicity, we assume for our analysis, that the subdomains are well-shaped parallelepipeds. The theory could be extended to more general hexahedral subdomains with planar faces using the theory of mapped hexahedral elements in [47]. Since this would increase the technicality of our proofs even further, we restrict ourselves to parallelepipeds. The resulting interface is given by $\Gamma := \bigcup_{i \neq j} (\partial\Omega_i \cap \partial\Omega_j) \setminus \partial\Omega_D$. We assume matching finite element nodes on the neighboring subdomains across the interface Γ. We also introduce the local finite element trace spaces $W^{(i)} = W^h(\partial\Omega_i \cap \Gamma), \ i = 1, \ldots, N$; see also Remark 3.5.

For our analysis, we need the corresponding partition-of-unity functions.

Definition 3.1. *Let $\theta_{\mathcal{F}^{ij}}$, $\theta_{\mathcal{E}^{ik}}$, and $\theta_{\mathcal{V}^{il}}$ be the partition-of-unity functions associated with the decomposition of the interface Γ into subdomain faces, edges, and vertices. These functions are piecewise linear finite element functions on the decomposition $\tau_{h/2}$. Here, we denote by $\tau_{h/2}$ the decomposition which is obtained by decomposing each tetrahedron into seven new tetrahedra by using the midpoints of the edges of the quadratic elements as new vertices; see Figure 3.1. Let $\theta_{\mathcal{F}^{ij}}$, $\theta_{\mathcal{E}^{ik}}$, and $\theta_{\mathcal{V}^{il}}$ be discrete harmonic finite element functions which are piecewise linear on $\tau_{h/2}$ and vanish at all nodes of Γ except of those of $\mathcal{F}^{ij}, \mathcal{E}^{ik}$, and $\mathcal{V}^{il}$, respectively, where the value is 1; see [28, Section 7].*

In our analysis we allow that each of the N subdomains contains an almost incompressible part, here also called an inclusion, surrounded by a compressible hull. The inclusion may have a different Young modulus than the hull. It may also be compressible. We will now specify the definitions of a hull and a slab of a hull. We define the hull and the slab to be open sets.

Definition 3.2. *The hull of a subdomain Ω_i with width η is defined as*

$$\Omega_{i,\eta} := \{x \in \Omega_i : \operatorname{dist}(x, \partial\Omega_i) < \eta\}; \qquad \textit{see Figure 3.2.}$$

Definition 3.3. *Let $\mathcal{F}^{ij} \subset \partial\Omega_i$ be a face. Then a slab $\widetilde{\Omega}_{i,\eta}$ of the hull $\Omega_{i,\eta} \subset \Omega_i$ with $\mathcal{F}^{ij} \subset \partial\widetilde{\Omega}_{i,\eta}$ is defined as*

$$\widetilde{\Omega}_{i,\eta} := \left\{x \in \Omega_{i,\eta} : \ \operatorname{dist}(x, \mathcal{F}^{ij}) < \eta\right\}; \qquad \textit{see Figure 3.3.}$$

Figure 3.1:

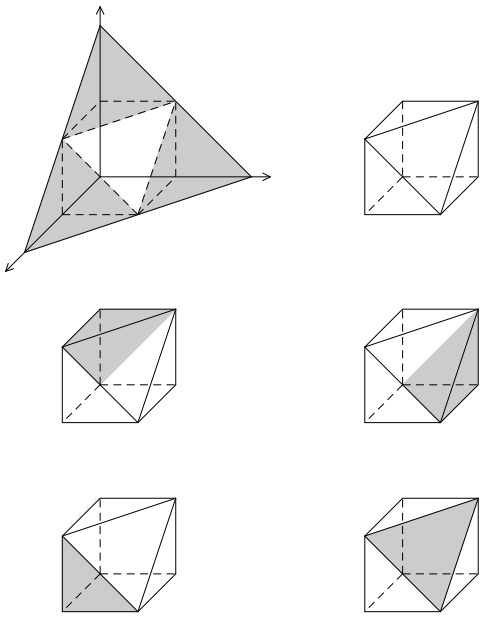

Decomposition of a tetrahedron into seven tetrahedra.

Since we made the assumption that our subdomains are parallelepipeds, the faces of a hull and of a slab are planar. In the following we assume that the completion of a hull and a slab are the union of finite elements. The inclusion can still be quite irregular in this situation; see Figure 3.4. Still, if the completion of a slab is not the union of finite elements, i.e., the boundary of a slab cuts through finite elements, then we remesh the slab with a mesh size similar to h, such that the auxiliary mesh satisfies the assumption. Note that this auxiliary mesh is only needed to extend our analysis to this case and is never used in the implementation of the algorithm. In the proof of Lemma 3.17, we then use a Scott-Zhang interpolation, cf. [56, 4], from the original finite element space to the finite element space on the auxiliary mesh; see Figure 2.5 and the end of the proof of Lemma 3.17. We assume that our original mesh resolves η in the sense that the inclusion is separated from the interface by at least one element; also see Figure 2.5.

Figure 3.2: Hull

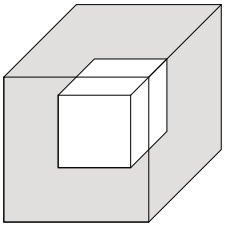

$\Omega_{i,\eta}$, hull of Ω_i; see Definition 3.2.

Figure 3.3: Slab

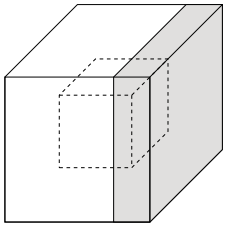

$\widetilde{\Omega}_{i,\eta}$, slab of $\Omega_{i,\eta}$; see Definition 3.3.

Figure 3.4:

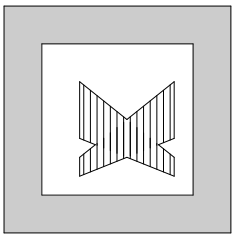

The inclusion may be irregular even for a hull with planar faces if it can be encased in the hull of width η.

Now, we define the discrete elastic extension and the corresponding discrete harmonic extension to the hull and to the slab.

Definition 3.4. *For $w \in W^{(i)}$ let $\mathcal{H}_\varepsilon w$ be the discrete elastic extension of w from $\partial\Omega_i$ to the subdomain Ω_i, i.e., $\mathcal{H}_\varepsilon w \in U_i := \left\{ v \in \left(H^1(\Omega_i)\right)^3 \cap W^h(\Omega_i) : \ v\,|_{\partial\Omega_i} = w \right\}$ defined by*

$$|a_i(\mathcal{H}_\varepsilon w, \mathcal{H}_\varepsilon w)| = \inf_{v \in U_i} |a_i(v,v)|$$

and let $\mathcal{H}_\eta w$ be the discrete harmonic extension of $w \in W^{(i)}$ from $\partial\Omega_i$ to the hull $\Omega_{i,\eta}$ with zero boundary conditions on the interior boundary of the hull, i.e., $\mathcal{H}_\eta w \in U_{i,\eta} := \{v \in \left(H^1(\Omega_{i,\eta})\right)^3 \cap W^h(\Omega_{i,\eta}) : \ v\,|_{\partial\Omega_i} = w, \ v\,|_{\partial\Omega_{i,\eta}\setminus\partial\Omega_i} = 0\}$ defined by

$$|\mathcal{H}_\eta w|_{H^1(\Omega_{i,\eta})} = \inf_{v \in U_{i,\eta}} |v|_{H^1(\Omega_{i,\eta})}.$$

Additionally, we have for $w \in W^{(i)}$ with $w(x) = 0$ for all $x \in \overline{\partial\Omega_i \setminus (\partial\widetilde{\Omega}_{i,\eta} \cap \partial\Omega_i)}$ the discrete harmonic extension $\widetilde{\mathcal{H}}_\eta w$ of w to the slab $\widetilde{\Omega}_{i,\eta}$, such that

$$\widetilde{\mathcal{H}}_\eta w = \begin{cases} w(x), & x \in \partial\Omega_i \\ 0, & x \in \overline{\Omega_i \setminus \widetilde{\Omega}_{i,\eta}} \\ \text{discrete harmonic in } \widetilde{\Omega}_{i,\eta}. \end{cases}$$

Remark 3.5. *In order to avoid an excessive use of extension operators, in the following, we will always tacitly assume that a function $u \in W^{(i)}$ is discrete elastically extended to the interior of the subdomain.*

3.2 Coarse Space

In FETI-DP algorithms primal constraints are used to make certain local problems invertible and to introduce a coarse problem. For simplicity, we consider FETI-DP methods with primal vertex constraints and edge averages over all edges as primal constraints. As a result all faces are fully primal in the sense of [37] and of Definition 3.6. For each subdomain Ω_i, we assemble the local linear system

$$K^{(i)} u^{(i)} = f^{(i)}.$$

Then, the FETI-DP saddle point problem is of the form

$$\begin{bmatrix} \widetilde{K} & B^T \\ B & 0 \end{bmatrix} \begin{bmatrix} \tilde{u} \\ \lambda \end{bmatrix} = \begin{bmatrix} \tilde{f} \\ 0 \end{bmatrix},$$

where the matrix $\widetilde{K}$ and right hand side $\tilde{f}$ are obtained from the local matrices $K^{(i)}$ and local load vectors $f^{(i)}$ by partial assembly in the primal variables; see, e.g., [31] or Section 2.4. The

continuity of the solution $\tilde{u}$ across the interface Γ is enforced by the constraint $Bu = 0$, where $B = [B^{(1)}, \ldots, B^{(N)}]$ with entries from $\{-1, 0, 1\}$. The restriction of B to the interface Γ is denoted by B_Γ. In standard FETI-DP algorithms, the variables $\tilde{u}$ are eliminated and the resulting Schur complement system $F\lambda = d$, with $F = B\widetilde{K}^{-1}B^T$ and $d = B\widetilde{K}^{-1}\tilde{f}$, is solved iteratively with a preconditioned conjugate gradient method. As a preconditioner we consider here exclusively the Dirichlet preconditioner M^{-1}, cf. [29, Section 3.2] or [30, 34, 37, 32]. For a complete description of FETI-DP algorithms, see, e.g., [18, 19, 29, 30, 31, 34]. Here we consider, in particular, the algorithm given in [37] and [31, 30]. See the latter references for an algorithmic description of parallel FETI-DP methods using primal edge constraints and a transformation of basis.

For the convenience of the reader we now recall the concept of edge average primal constraints, as given in [37, Section 5] .

The null space $\ker(\varepsilon)$ is the space of rigid body modes. For a generic domain $\hat{\Omega}$ with diameter H, a basis for $\ker(\varepsilon)$ is given by the three translations

$$r_1 = \begin{pmatrix} 1 \\ 0 \\ 0 \end{pmatrix}, \; r_2 = \begin{pmatrix} 0 \\ 1 \\ 0 \end{pmatrix}, \; r_3 = \begin{pmatrix} 0 \\ 0 \\ 1 \end{pmatrix}, \text{ and the three rotations}$$

$$r_4 = \frac{1}{H}\begin{pmatrix} x_2 - \hat{x}_2 \\ -x_1 + \hat{x}_1 \\ 0 \end{pmatrix}, \; r_5 = \frac{1}{H}\begin{pmatrix} -x_3 + \hat{x}_3 \\ 0 \\ x_1 - \hat{x}_1 \end{pmatrix}, \; r_6 = \frac{1}{H}\begin{pmatrix} 0 \\ x_3 - \hat{x}_3 \\ -x_2 + \hat{x}_2 \end{pmatrix}$$

where $\hat{x} \in \hat{\Omega}$.

In our proof of the condition number estimate we need to control the rigid body modes on each face. We use the concept of fully primal faces. A face is called fully primal, if there are at least six linearly independent constraints, given by appropriately selected averages over edges, which belong to the boundary of that face and which control the rigid body modes on that face. For a detailed description, see [37, Section 5]. The edge averages of the components of the displacements define linear functionals g_n, given by

$$g_n(w^{(i)}) = \frac{\int_{\mathcal{E}^{ik}} w_l^{(i)} \, dx}{\int_{\mathcal{E}^{ik}} 1 \, dx}, \quad n = 1, \ldots, 6, \; l = 1, 2, 3$$

for $w^{(i)} = \left(w_1^{(i)}, w_2^{(i)}, w_3^{(i)}\right) \in W^{(i)}$ and edges $\mathcal{E}^{ik} \subset \partial\mathcal{F}^{ij}$. The edges $\mathcal{E}^{ik}$ and the displacement components have to be chosen, such that the rigid body modes are controlled on $\mathcal{F}^{ij}$, i.e., if r is an arbitrary rigid body mode and $\sum_{i=1}^{6} g_n(r)^2 = 0$, then $r = 0$.

The functionals $g_n,\ n = 1,\dots,6$, provide a basis of the dual space $(\ker(\varepsilon))'$. There exists a dual basis of $(\ker(\varepsilon))'$, spanned by the functionals $f_1,\dots,f_6$, defined by $f_m(r_l) = \delta_{ml},\ m,l = 1,\dots,6$. Thus, there exist $\beta_{lk} \in \mathbb{R},\ l,k = 1,\dots,6$, such that for $w \in W^{(i)}$

$$f_m(w) = \sum_{n=1}^{6} \beta_{mn} g_n(w), \quad m = 1,\dots,6.$$

For further details, see, e.g., [37, Section 5].

Using a Cauchy-Schwarz inequality, we obtain

$$\left|g_m(w^{(i)})\right|^2 \leq C H_i^{-1} \left\|w^{(i)}\right\|^2_{L_2(\mathcal{E}^{ik})}.$$

With Lemma 3.11 we can show that

$$\left|g_m(w^{(i)})\right|^2 \leq C H_i^{-1} \left(1 + \log\left(\frac{H_i}{h_i}\right)\right) \left\|w^{(i)}\right\|^2_{H^1(\Omega_i)},$$

and, accordingly,

$$\left|g_m(w^{(i)})\right|^2 \leq C \eta^{-1} \left(1 + \log\left(\frac{\eta}{h_i}\right)\right) \left\|w^{(i)}\right\|^2_{H^1(\widetilde{\Omega}_{i,\eta})},$$

where $\widetilde{\Omega}_{i,\eta}$ is a slab which contains $\mathcal{E}^{ik}$ in its boundary. This motivates the definition of a fully primal face; see [37, Definition 5.3]. In contrast to [37], where trace spaces are used, we use standard Sobolev spaces.

Definition 3.6 (fully primal face). *A face $\mathcal{F}^{ij}$ is fully primal if, in the space of primal constraints over $\mathcal{F}^{ij}$, there exists a set $f_m^{\mathcal{F}^{ij}},\ m = 1,\dots,6$, of linear functionals on $W^{(i)}$ with the following properties:*

(i) $\left|f_m^{\mathcal{F}^{ij}}(w^{(i)})\right|^2 \leq C H_i^{-1} \left(1 + \log\left(\frac{H_i}{h_i}\right)\right) \left\{\left|w^{(i)}\right|^2_{H^1(\Omega_i)} + \frac{1}{H_i^2}\left\|w^{(i)}\right\|^2_{L_2(\Omega_i)}\right\}$

(ii) $\left|f_m^{\mathcal{F}^{ij}}(w^{(i)})\right|^2 \leq C \eta^{-1} \left(1 + \log\left(\frac{\eta}{h_i}\right)\right) \left\{\left|w^{(i)}\right|^2_{H^1(\widetilde{\Omega}_{i,\eta})} + \frac{1}{H_i^2}\left\|w^{(i)}\right\|^2_{L_2(\widetilde{\Omega}_{i,\eta})}\right\}$

(iii) $f_m^{\mathcal{F}^{ij}}(r_l) = \delta_{ml} \quad \forall m,l = 1,\dots,6,\ r_l \in \ker(\varepsilon).$

Finally, we need an additional Korn inequality; see, e.g., [37, Lemma 6.2], where a corresponding version for trace spaces is given. The Korn constant of a domain depends on its aspect ratio; for an ellipse with semi-axes H and η it is explicitly known, i.e., $K_e = 2(1+(\frac{H}{\eta})^2)$; see [25]. In particular, we need Korn's inequality on a slab.

Lemma 3.7. *Let $\Omega \subset \mathbb{R}^3$ be a Lipschitz domain of diameter H, and let $r \in \ker(\varepsilon)$ be the minimizing rigid body mode. Then, there exists a positive constant $C > 0$, independent of h and H, such that for all $u \in H^1(\Omega)$, we have*

$$\|u - r\|^2_{H^1(\Omega)} \leq C \, \|\varepsilon(u)\|^2_{L_2(\Omega)} \, .$$

For an estimate on the slab $\widetilde{\Omega}_{i,\eta}$, we have

$$\|u - r\|^2_{H^1(\widetilde{\Omega}_{i,\eta})} \leq C \left(\frac{H_i}{\eta}\right)^2 \|\varepsilon(u)\|^2_{L_2(\widetilde{\Omega}_{i,\eta})} \, .$$

Proof. For a proof of the first part, see [37, Lemma 6.2]. Here, we prove the second inequality. The idea is to transform the slab to the smaller cube of length η, estimate by the first inequality, and transform it back to the slab. Let us denote the cube of length η by Ω_η and let T be the transformation from the slab $\widetilde{\Omega}_{i,\eta} := [0, H]^2 \times [0, \eta]$ to this cube $\Omega_\eta := [0, \eta]^3$, such that

$$T(x, y, z) = \begin{pmatrix} \frac{\eta}{H} & 0 & 0 \\ 0 & \frac{\eta}{H} & 0 \\ 0 & 0 & 1 \end{pmatrix} \begin{pmatrix} x \\ y \\ z \end{pmatrix} .$$

Then we obtain

$$\begin{aligned}
\|u - r\|^2_{H^1(\widetilde{\Omega}_{i,\eta})} &= |u - r|^2_{H^1(\widetilde{\Omega}_{i,\eta})} + \frac{1}{H^2} \|u - r\|^2_{L_2(\widetilde{\Omega}_{i,\eta})} \\
&= \int_{\widetilde{\Omega}_{i,\eta}} |\nabla(u - r)|^2 \; dx + \frac{1}{H^2} \|u - r\|^2_{L_2(\widetilde{\Omega}_{i,\eta})} \\
&= \int_{\Omega_\eta} \nabla(\hat{u} - \hat{r})^T DT^T DT \; \nabla(\hat{u} - \hat{r}) |\det DT^{-1}| \; d\hat{x} + \frac{1}{H^2} \|u - r\|^2_{L_2(\widetilde{\Omega}_{i,\eta})} \\
&\leq \left(\frac{H}{\eta}\right)^2 \int_{\Omega_\eta} |\nabla(\hat{u} - \hat{r})|^2 \; d\hat{x} + \left(\frac{H}{\eta}\right)^2 \frac{1}{H^2} \|\hat{u} - \hat{r}\|^2_{L_2(\Omega_\eta)} \\
&= \left(\frac{H}{\eta}\right)^2 |\hat{u} - \hat{r}|^2_{H^1(\Omega_\eta)} + \frac{1}{\eta^2} \|\hat{u} - \hat{r}\|^2_{L_2(\Omega_\eta)} \\
&\leq C \left(\frac{H}{\eta}\right)^2 \|\varepsilon(\hat{u})\|^2_{L_2(\Omega_\eta)} \, .
\end{aligned}$$

Transforming back to the slab, we get with

$$\begin{aligned} & C\left(\frac{H}{\eta}\right)^2 \|\varepsilon(\hat{u})\|^2_{L_2(\Omega_\eta)} \\ = \; & C\left(\frac{H}{\eta}\right)^2 \int_{\widetilde{\Omega}_{i,\eta}} \left(\nabla u + \nabla u^T\right)^T DT^{-T} DT^{-1} \left(\nabla u + \nabla u^T\right) |\det DT| \, dx \\ \leq \; & C\left(\frac{H}{\eta}\right)^2 \|\varepsilon(u)\|^2_{L_2(\widetilde{\Omega}_{i,\eta})} \end{aligned}$$

a Korn inequality on a slab.

□

3.3 Technical Tools

In this section, we introduce some technical tools which we need for the analysis of the condition number bound in Section 3.4
The following lemma is directly related to [15, Lemma 5.4].

Lemma 3.8. *Let $\mathcal{F}^{ij}$ be a common face of Ω_i and Ω_j. There exists a piecewise linear finite element function $\bar{\vartheta}_{\mathcal{F}^{ij}}$ on $\widetilde{\Omega}_{i,\eta}$, which is equal to one at the nodal points of $\mathcal{F}^{ij}$, vanishes on $\Gamma_h \setminus \mathcal{F}^{ij}$, and satisfies*

$$\left|\bar{\vartheta}_{\mathcal{F}^{ij}}\right|^2_{H^1(\widetilde{\Omega}_{i,\eta})} \leq C\left(1 + \log\left(\frac{H_i}{h_i}\right)\right)\frac{H_i^2}{\eta}.$$

Proof. We follow the proof for cubes in Casarin [7, Lemma 3.3.6]; also see [57, Lemma 4.25]. In [15, Proof of Lemma 5.4] the proof is given for cubes and then, by discussing the effects of compressing the cube, the result for cuboids is obtained. Here, we introduce a proof directly modified for a cuboid and obtain a result which is slightly different to the one in [15, Lemma 5.4], in the sense that we have also a dependency on the number of elements in each slab.

Let us consider a cuboid $\widetilde{\Omega}_\eta$ which has the dimension $H \times H \times \eta$. The finite element function $\bar{\vartheta}_{\mathcal{F}^{ij}}$ is equal to 1 on the face $\mathcal{F}^{ij}$ and vanishes on the rest of the boundary nodes of $\partial\widetilde{\Omega}_\eta \setminus \mathcal{F}^{ij}$. We divide $\widetilde{\Omega}_\eta$ into 24 tetrahedra by connecting the center of the cuboid C to all its vertices and all centers of its faces $\mathcal{F}^{ik}$ and by dividing these faces by their diagonals; see Figure 3.5. The function $\bar{\vartheta}_{\mathcal{F}^{ij}}$ associated with the face $\mathcal{F}^{ij}$ is defined to take the value $\frac{1}{6}$

Figure 3.5:

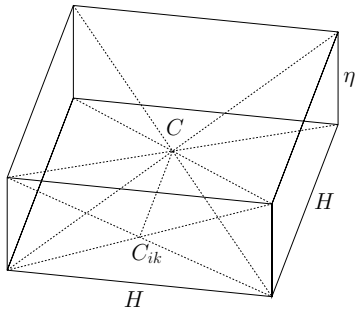

Decomposition of the cuboid into 24 tetrahedra.

at the center of the cuboid C. All six functions $\bar{\vartheta}_{\mathcal{F}^{ik}},\ k = 1, \ldots, 6$, corresponding to the six faces of the cuboid form a partition of unity at all nodes belonging to the closure of $\widetilde{\Omega}_\eta$ except those on the wire basket, formed by the union of the edges and vertices of the cuboid, where $\bar{\vartheta}_{\mathcal{F}^{ij}} = 0$. The values at the centers of the faces C_{ik} are $\bar{\vartheta}_{\mathcal{F}^{ij}}(C_{ik}) = \delta_{jk},\ k = 1, \ldots, 6$. On the segments $\overline{CC_{ik}}$ the function $\bar{\vartheta}_{\mathcal{F}^{ij}}$ is linear, this means on the straight line $\overline{CC_{ij}}$ the function $\bar{\vartheta}_{\mathcal{F}^{ij}}$ rises from $\frac{1}{6}$ to 1, on the other segments $\overline{CC_{ik}}$ the function $\bar{\vartheta}_{\mathcal{F}^{ij}}$ decreases from $\frac{1}{6}$ to 0. The values inside each tetrahedron, formed by a segment $\overline{CC_{ik}}$ and one edge of $\mathcal{F}^{ij}$, are defined to be constant on the intersection of any plane through that edge with the segment $\overline{CC_{ik}}$.

The value on the plane is given by the value of the intersection point, which we call E; see Figure 3.6.

Figure 3.6:

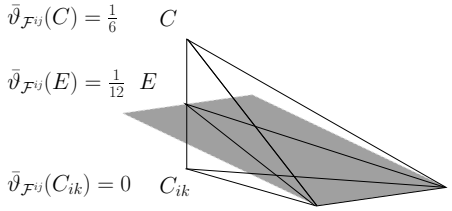

Plane (in gray) through one edge of $\mathcal{F}^{ij}$ and the point E. The point E is the intersection of the plane with the segment $\overline{CC_{ik}}$. The value of $\bar{\vartheta}_{\mathcal{F}^{ij}}$ is constant on this plane and defined by $\bar{\vartheta}_{\mathcal{F}^{ij}}(E)$. Since, in this picture, the point E is the center of the segment $\overline{CC_{ik}}$, we have $\bar{\vartheta}_{\mathcal{F}^{ij}}(E) = \frac{1}{12}$.

Such functions may not be finite element functions on our mesh. Therefore, we have to interpolate the functions $\bar{\vartheta}_{\mathcal{F}^{ij}}$ to obtain corresponding finite element functions. Note, that

the interpolated functions still form a partition of unity.

We first only discuss finite elements that do not touch an edge of the cuboid. Our face $\mathcal{F}^{ij}$ is the base of the cuboid in Figures 3.7, 3.8, and 3.9. There are two possibilities for the distance of the center of the cuboid C to the center of the different faces; either the distance is of the order of H, see Figure 3.7 and 3.8, or the distance is of the order of η, see Figure 3.9.

Figure 3.7:

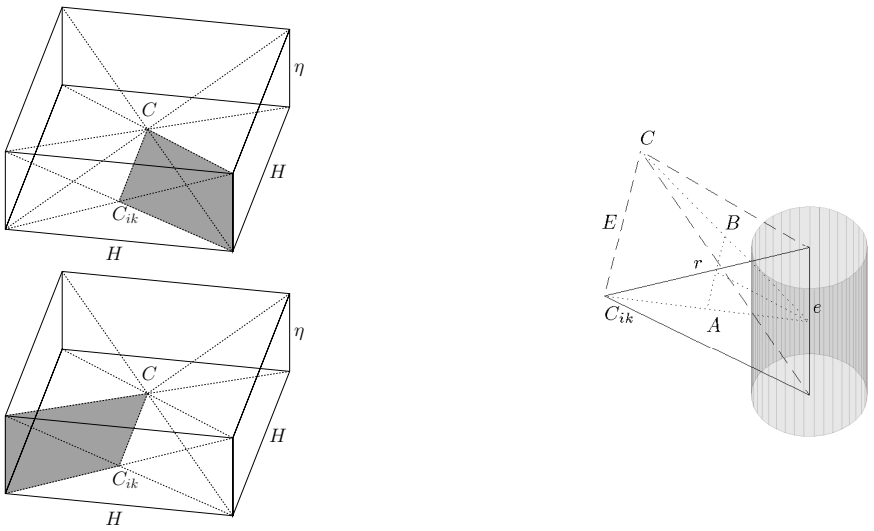

$\bar{\vartheta}_{\mathcal{F}^{ij}} \neq 1$ on all faces of the tetrahedron.

We first consider the situations as in Figures 3.7 and 3.8, where the distance between C and C_{ik} is of the order of H. On the segment $\overline{CC_{ik}}$ the function $\bar{\vartheta}_{\mathcal{F}^{ij}}$ decreases from $\frac{1}{6}$ to 0 and therefore here the Euclidean norm of the gradient can be bounded by

$$\|\nabla \bar{\vartheta}_{\mathcal{F}^{ij}}\|_{l_2} \leq \frac{\hat{C}}{H}.$$

Let e be a point on the edge of the cuboid, see Figures 3.7 and 3.8, and consider a plane through the points e, C, and C_{ik}. When moving closer to the point e the segment $\overline{CC_{ik}}$ becomes the segment $\overline{AB}$; see Figures 3.7-3.8. Since $\bar{\vartheta}_{\mathcal{F}^{ij}}(C) = \bar{\vartheta}_{\mathcal{F}^{ij}}(A)$ and $\bar{\vartheta}_{\mathcal{F}^{ij}}(C_{ik}) = \bar{\vartheta}_{\mathcal{F}^{ij}}(B)$ the gradient grows by a factor of $\frac{\overline{CC_{ik}}}{\overline{AB}}$, i.e.,

$$\|\nabla \bar{\vartheta}_{\mathcal{F}^{ij}}\|_{l_2} \quad \leq \quad \frac{\hat{C}}{H} \cdot \frac{\overline{CC_{ik}}}{\overline{AB}} = \frac{\hat{C}}{H} \cdot \frac{\overline{eE}}{r} \leq \frac{\hat{C}}{H} \cdot \frac{H}{r} \leq \frac{\hat{C}}{r},$$

where r is the distance of e to the midpoint of the segment $\overline{AB}$. Here, $\hat{C}$ is a generic constant independent of $H,\ h,\ \eta$ and r. The tetrahedra fulfilling this bound are not critical for our analysis since the bound does not depend on η.

Figure 3.8:

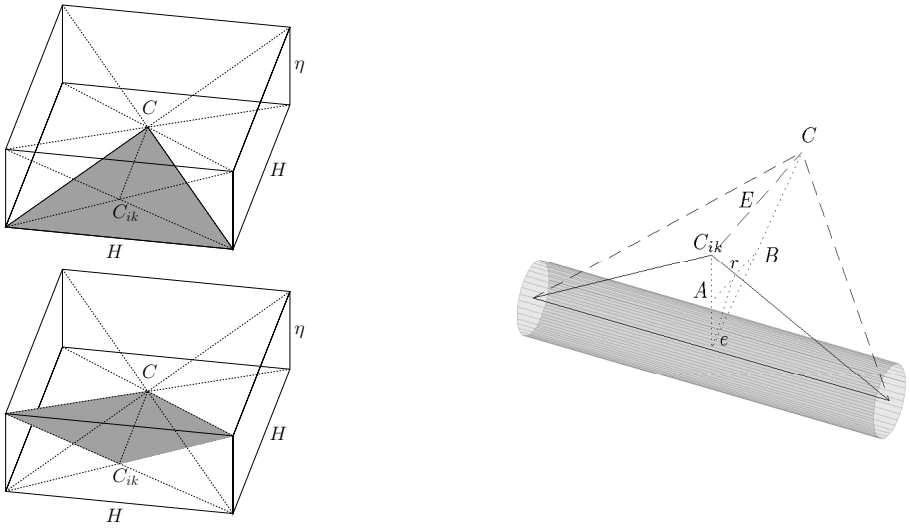

$\bar{\vartheta}_{\mathcal{F}^{ij}} \neq 1$ on all faces of the tetrahedron.

Figure 3.9:

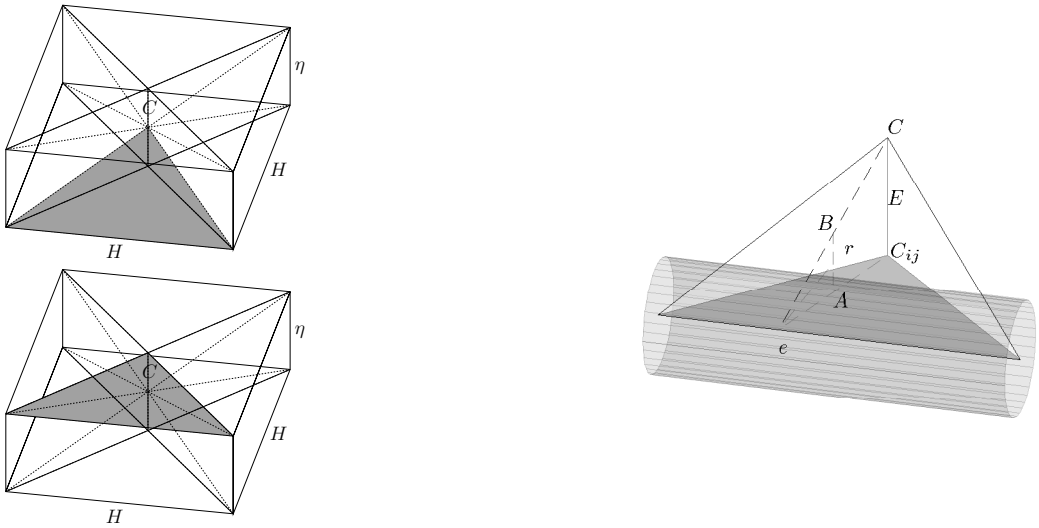

$\bar{\vartheta}_{\mathcal{F}^{ij}} = 1$ on the gray face, i.e., $\bar{\vartheta}_{\mathcal{F}^{ij}}(C_{ij}) = 1$ and $\bar{\vartheta}_{\mathcal{F}^{ij}}(C) = \frac{1}{6}$.

Next, we consider a tetrahedron, see Figure 3.9 (upper and left), which coincides on one face with $\mathcal{F}^{ij}$, i.e., $\bar{\vartheta}_{\mathcal{F}^{ij}} = 1$ on this face. Thus, the length of the segment $\overline{CC_{ij}}$ is of the order of η and on the segment $\overline{CC_{ij}}$ the value of the function $\bar{\vartheta}_{\mathcal{F}^{ij}}$ increases from $\frac{1}{6}$ to 1. This means, $\|\nabla\bar{\vartheta}_{\mathcal{F}^{ij}}\|_{l_2} \leq \frac{\hat{C}}{\eta}$ and again the gradient grows in proportion to $\frac{\overline{CC_{ik}}}{\overline{AB}}$ when moving closer to the edge of the cuboid. Thus, the norm of the gradient can be estimated by

$$\|\nabla\bar{\vartheta}_{\mathcal{F}^{ij}}\|_{l_2} \quad \leq \quad \frac{\hat{C}}{\eta}\cdot\frac{\overline{CC_{ik}}}{\overline{AB}} = \frac{\hat{C}}{\eta}\cdot\frac{\overline{eE}}{r} \leq \frac{\hat{C}}{\eta}\cdot\frac{H}{r},$$

in which $\hat{C}$ is a generic, positive constant independent of $H,\ h,\ \eta$, and r.

Next, we consider local cylindrical coordinates around the edges of the cuboid. The critical tetrahedra are the ones where the bound depends on H/η; see Figure 3.9. It is therefore sufficient to consider integrals in local cylindrical coordinates around edges of length H. We need to integrate over an angle of $\arctan(\eta/H) \leq \eta/H$; see Figure 3.10. We split the integral

Figure 3.10:

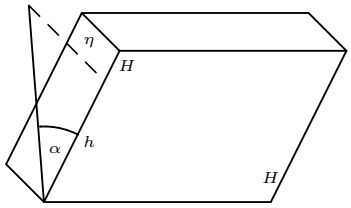

Integral around an edge in cylindrical coordinates.

into two parts. First one we integrate only over elements which do not touch edges of the cuboid. In the second term we consider a thin layer of elements of thickness h touching the edge. Note, that in the latter, the norm of the gradient of $\bar{\vartheta}_{\mathcal{F}^{ij}}$ is bounded by $\frac{\hat{C}}{h}\cdot\frac{H}{\eta}$ since $\bar{\vartheta}_{\mathcal{F}^{ij}}$ decreases to zero towards the outer boundary of the layer. Let U be a neighborhood of the edge. Then, we obtain

$$\begin{aligned}
&|\bar{\vartheta}_{\mathcal{F}^{ij}}|^2_{H^1(U)}\\
\leq\ & \hat{C}\left\{\int_0^H\int_h^H\int_0^{\frac{C\eta}{H}}\left(\frac{H}{\eta r}\right)^2 r\ d\alpha\ dr\ dz + \int_0^H\int_0^h\int_0^{\frac{C\eta}{H}}\left(\frac{H}{\eta h}\right)^2 r\ d\alpha\ dr\ dz\right\}\\
\leq\ & \hat{C}\frac{H^2}{\eta}\left(1+\log\left(\frac{H}{h}\right)\right).
\end{aligned}$$

The same bound applies to the tetrahedron in Figure 3.9 (lower and left), where $\bar{\vartheta}_{\mathcal{F}^{ij}}$ decreases from $\frac{1}{6}$ to 0 on a segment of length η.

By considering the cases in Figure 3.7 and 3.8, we have covered 16 of the total of the 24 tetrahedra. From the cases in Figure 3.9, we obtain our bounds for the remaining cases by symmetry, where in four cases $\bar{\vartheta}_{\mathcal{F}^{ij}}$ decreases from 1 to $\frac{1}{6}$ and in the other cases $\bar{\vartheta}_{\mathcal{F}^{ij}}$ increases from $\frac{1}{6}$ to 1.

□

We also need a discrete Sobolev inequality for a rectangle in two dimensions.

Lemma 3.9. *Let $\widehat{\Omega}_{i,\eta} \subset \mathbb{R}^2$ be a rectangle with side lengths H and η. Then, for finite element functions $u \in H^1(\widehat{\Omega}_{i,\eta})$,*

$$\|u\|^2_{L^\infty(\widehat{\Omega}_{i,\eta})} \leq C\frac{H}{\eta}\left(1+\log\left(\frac{\eta}{h}\right)\right)\left(|u|^2_{H^1(\widehat{\Omega}_{i,\eta})}+\frac{1}{H^2}\|u\|^2_{L^2(\widehat{\Omega}_{i,\eta})}\right),$$

where $C>0$ is a constant independent of H and h.

Proof. Let $\widetilde{\Omega}$ be a square with side length η. Then we define $\tilde{u}$ on $\widetilde{\Omega}$ as

$$\tilde{u}(\tilde{x},\tilde{y}) := (u\circ T)(\tilde{x},\tilde{y}) = u(x,y)$$

where the transformation T maps the square $\widetilde{\Omega}$ to the rectangle $\widehat{\Omega}_{i,\eta}$, i.e., $T:\widetilde{\Omega}\to\widehat{\Omega}_{i,\eta}$, and

$$\begin{pmatrix}\tilde{x}\\ \tilde{y}\end{pmatrix} \mapsto \begin{pmatrix}\frac{H}{\eta} & 0\\ 0 & 1\end{pmatrix}\begin{pmatrix}\tilde{x}\\ \tilde{y}\end{pmatrix} = \begin{pmatrix}x\\ y\end{pmatrix}.$$

We have

$$\|u\|^2_{L^\infty(\widehat{\Omega}_{i,\eta})} = \|\tilde{u}\|^2_{L^\infty(\widetilde{\Omega})}.$$

On the square $\widetilde{\Omega}$ we may apply the standard Sobolev inequality, see, e.g., [4, Lemma (4.9.1)].

$$\begin{aligned}\|\tilde{u}\|^2_{L^\infty(\widetilde{\Omega})} &\leq C\left(1+\log\left(\frac{\eta}{h}\right)\right)\|\tilde{u}\|^2_{H^1(\widetilde{\Omega})}\\ &= C\left(1+\log\left(\frac{\eta}{h}\right)\right)\left\{|\tilde{u}|^2_{H^1(\widetilde{\Omega})}+\frac{1}{\eta^2}\|\tilde{u}\|^2_{L_2(\widetilde{\Omega})}\right\}.\end{aligned}$$

By transforming back to the rectangle, we have for the first part

$$\begin{aligned}|\tilde{u}|^2_{H^1(\widetilde{\Omega})} &= \int_{\widetilde{\Omega}}|\nabla\tilde{u}|^2\,d\tilde{x}\\ &= \int_{\widehat{\Omega}_{i,\eta}}(\nabla u)^T\begin{pmatrix}\left(\frac{H}{\eta}\right)^2 & 0\\ 0 & 1\end{pmatrix}(\nabla u)\left(\frac{\eta}{H}\right)\,dx\\ &\leq \frac{H}{\eta}|u|^2_{H^1(\widehat{\Omega}_{i,\eta})},\end{aligned}$$

and for the L_2 term

$$\|\tilde{u}\|^2_{L_2(\widetilde{\Omega})} = \int_{\widetilde{\Omega}} |\tilde{u}|^2 \, d\tilde{x} = \int_{\widehat{\Omega}_{i,\eta}} \frac{\eta}{H}(u)^2 \, dx = \frac{\eta}{H}\|u\|^2_{L_2(\widehat{\Omega}_{i,\eta})}.$$

With

$$\begin{aligned} |\tilde{u}|^2_{H^1(\widetilde{\Omega})} + \frac{1}{\eta^2}\|\tilde{u}\|^2_{L_2(\widetilde{\Omega})} &\leq \frac{H}{\eta}|u|^2_{H^1(\widehat{\Omega}_{i,\eta})} + \frac{1}{\eta H}\|u\|^2_{L_2(\widehat{\Omega}_{i,\eta})} \\ &= \frac{H}{\eta}\left\{|u|^2_{H^1(\widehat{\Omega}_{i,\eta})} + \frac{1}{H^2}\|u\|^2_{L_2(\widehat{\Omega}_{i,\eta})}\right\} \end{aligned}$$

we obtain the Sobolev inequality on a cuboid

$$\|u\|^2_{L^\infty(\widehat{\Omega}_{i,\eta})} \leq C\frac{H}{\eta}\left(1 + \log\left(\frac{\eta}{h}\right)\right)\|u\|^2_{H^1(\widehat{\Omega}_{i,\eta})}.$$

□

The next lemma is a version of Casarin [7, Lemma 3.3.7], modified for cuboids; see also Dryja, Smith, and Widlund [17, Lemma 4.5] or [57]. A version related to the first part of our lemma can be found in [15, Lemma 5.4].

Lemma 3.10. *Let $\mathcal{F}^{ij}$ be a face common to Ω_i and Ω_j. Furthermore let $\widetilde{\Omega}_{i,\eta}$ be a slab as defined in Definition 3.3. Let $\bar{\vartheta}_{\mathcal{F}^{ij}}$ be given as constructed in Lemma 3.8. Then, for $u \in W^{(i)}$,*

$$1.\ |I^h(\bar{\vartheta}_{\mathcal{F}^{ij}}u)|^2_{H^1(\widetilde{\Omega}_{i,\eta})} \leq C\frac{H}{\eta}\left(1 + \log\left(\frac{H}{h}\right)\right)^2\|u\|^2_{H^1(\Omega_i)} \tag{3.1}$$

$$2.\ |I^h(\bar{\vartheta}_{\mathcal{F}^{ij}}u)|^2_{H^1(\widetilde{\Omega}_{i,\eta})} \leq C\left(\frac{H}{\eta}\right)^2\left(1 + \log\left(\frac{H}{h}\right)\right)\left(1 + \log\left(\frac{\eta}{h}\right)\right)\|u\|^2_{H^1(\widetilde{\Omega}_{i,\eta})}. \tag{3.2}$$

Proof. Here, we give a scalar version of the proof. In the proof of Lemma 3.8, we have established bounds for the gradient of $\bar{\vartheta}_{\mathcal{F}^{ij}}$. On each element let $\tilde{\bar{\vartheta}}_{\mathcal{F}^{ij}} \in [0,1]$ be the value of $\bar{\vartheta}_{\mathcal{F}^{ij}}$ at an arbitrary point of that element. For convenience we can choose some kind of average of $\bar{\vartheta}_{\mathcal{F}^{ij}}$ on each element. Then, by the mean value theorem, we obtain $\left|\bar{\vartheta}_{\mathcal{F}^{ij}} - \tilde{\bar{\vartheta}}_{\mathcal{F}^{ij}}\right| \leq h\, C\frac{H}{\eta r}$ or $\left|\bar{\vartheta}_{\mathcal{F}^{ij}} - \tilde{\bar{\vartheta}}_{\mathcal{F}^{ij}}\right| \leq h\, \frac{C}{r}$ for elements which do not touch edges, which belong to the boundary of the face $\mathcal{F}^{ij}$ and, accordingly, $\left|\bar{\vartheta}_{\mathcal{F}^{ij}} - \tilde{\bar{\vartheta}}_{\mathcal{F}^{ij}}\right| \leq h\, C\frac{H}{\eta h}$ or $\left|\bar{\vartheta}_{\mathcal{F}^{ij}} - \tilde{\bar{\vartheta}}_{\mathcal{F}^{ij}}\right| \leq h\, \frac{C}{h}$ for the thin layer of elements of thickness h touching the edge. First, we will only distinguish between elements which touch the edge or do not touch the edge, so we denote the estimates by

$\left|\bar{\vartheta}_{\mathcal{F}^{ij}} - \tilde{\bar{\vartheta}}_{\mathcal{F}^{ij}}\right| \leq h \cdot b_E$ and $\left|\bar{\vartheta}_{\mathcal{F}^{ij}} - \tilde{\bar{\vartheta}}_{\mathcal{F}^{ij}}\right| \leq h \cdot b_I$, respectively. Additionally, we denote by ω_η the union of all elements K which have a vertex on the edge $\mathcal{E}^{ik}$, which corresponds to the face $\mathcal{F}^{ij}$. Thus, we have

$$
\begin{aligned}
|I^h(\bar{\vartheta}_{\mathcal{F}^{ij}} u)|^2_{H^1(\widetilde{\Omega}_{i,\eta})} &= \sum_{K \subset \widetilde{\Omega}_{i,\eta}} \left| I^h\left((\bar{\vartheta}_{\mathcal{F}^{ij}} - \tilde{\bar{\vartheta}}_{\mathcal{F}^{ij}} + \tilde{\bar{\vartheta}}_{\mathcal{F}^{ij}}) u \right) \right|^2_{H^1(K)} \\
\leq\ & 2 \sum_{K \subset \widetilde{\Omega}_{i,\eta}} \left| \tilde{\bar{\vartheta}}_{\mathcal{F}^{ij}} u \right|^2_{H^1(K)} + 2 \sum_{K \subset \widetilde{\Omega}_{i,\eta}} \left| I^h\left((\bar{\vartheta}_{\mathcal{F}^{ij}} - \tilde{\bar{\vartheta}}_{\mathcal{F}^{ij}}) u \right) \right|^2_{H^1(K)} \\
\leq\ & 2\, |u|^2_{H^1(\widetilde{\Omega}_{i,\eta})} + 2 \sum_{K \subset \widetilde{\Omega}_{i,\eta} \setminus \omega_\eta} \left| I^h\left((\bar{\vartheta}_{\mathcal{F}^{ij}} - \tilde{\bar{\vartheta}}_{\mathcal{F}^{ij}}) u \right) \right|^2_{H^1(K)} \\
& + 2 \sum_{K \subset \omega_\eta} \left| I^h\left((\bar{\vartheta}_{\mathcal{F}^{ij}} - \tilde{\bar{\vartheta}}_{\mathcal{F}^{ij}}) u \right) \right|^2_{H^1(K)} .
\end{aligned}
$$

Using an inverse estimate for finite element functions, i.e., $|v_h|_{H^t(\Omega_i)} \leq \hat{C} h^{m-t} |v_h|_{H^m(\Omega_i)}$, see, e.g.,[3, p. 78 and p. 80], the H^1-seminorm in the second and the third term can be replaced by the L_2-norm with an additional factor h^{-2}. Therefore, we have to estimate

$$
\begin{aligned}
& \sum_{K \subset \widetilde{\Omega}_{i,\eta} \setminus \omega_\eta} h^{-2} \left\| I^h\left((\bar{\vartheta}_{\mathcal{F}^{ij}} - \tilde{\bar{\vartheta}}_{\mathcal{F}^{ij}}) u \right) \right\|^2_{L_2(K)} + \sum_{K \subset \omega_\eta} h^{-2} \left\| I^h\left((\bar{\vartheta}_{\mathcal{F}^{ij}} - \tilde{\bar{\vartheta}}_{\mathcal{F}^{ij}}) u \right) \right\|^2_{L_2(K)} \\
\leq\ & \sum_{K \subset \widetilde{\Omega}_{i,\eta} \setminus \omega_\eta} (b_I)^2 \, \|u\|^2_{L_2(K)} + \sum_{K \subset \omega_\eta} (b_E)^2 \, \|u\|^2_{L_2(K)} .
\end{aligned}
$$

So far we have used sums over elements, now we return to the integral in cylindrical coordinates. For the critical tetrahedra, where the bounds depend on H/η, z is of the order of H since the edge $\mathcal{E}^{ik}$ belongs to the face $\mathcal{F}^{ij}$; r is also of the order of H and the angle over which we integrate is of the order of $\frac{\eta}{H}$.

On the critical segment, we have

$$
\begin{aligned}
& \sum_{K \subset \widetilde{\Omega}_{i,\eta} \setminus \omega_\eta} \left(\frac{H}{\eta r} \right)^2 \|u\|^2_{L_2(K)} + \sum_{K \subset \omega_\eta} \left(\frac{H}{\eta h} \right)^2 \|u\|^2_{L_2(K)} \\
\leq\ & C \Big\{ \int_0^H \int_h^H \int_0^{\frac{\hat{C}\eta}{H}} \frac{H^2}{\eta^2 r^2} u^2 \; r \; d\alpha \; dr \; dz + \int_0^H \int_0^h \int_0^{\frac{\hat{C}\eta}{H}} \frac{H^2}{\eta^2 h^2} u^2 \; r \; d\alpha \; dr \; dz \Big\} \\
\leq\ & C \Big\{ \int_h^H \int_0^{\frac{\hat{C}\eta}{H}} \frac{H^2}{\eta^2 r} \Big(\int_0^H u^2 \; dz \Big) \; d\alpha \; dr + \int_0^h \int_0^{\frac{\hat{C}\eta}{H}} \frac{H^2}{\eta^2 h^2} r \Big(\int_0^H u^2 \; dz \Big) \; d\alpha \; dr \Big\}
\end{aligned}
$$

We have to estimate the line segment $\int_0^H u^2 \; dz$ which is dependent of z, α, and r. Building a smaller cuboid of size $\eta \times \eta \times H$ around this segment, we can estimate the line segment

by an edge of this cuboid, which is also of the order of H. We use the presentation of the estimate of $\|u\|^2_{L_2(\mathcal{E}^{ik})}$, given in [28, Lemma A.3]; see [27, Section 5, Proof of Lemma 2] for the proof. Combined with Lemma 3.9, we obtain

$$\|u\|^2_{L_2(\mathcal{E}^{ik})} \leq C\frac{H}{\eta}\left(1+\log\left(\frac{\eta}{h}\right)\right)\left(|u|^2_{H^1(\widetilde{\Omega}_{i,\eta})}+\frac{1}{H^2}\|u\|^2_{L_2(\widetilde{\Omega}_{i,\eta})}\right).$$

From this, we obtain the estimate (3.2)

$$\begin{aligned}&|I^h(\bar{\vartheta}_{\mathcal{F}^{ij}})|^2_{H^1(\widetilde{\Omega}_{i,\eta})}\\ \leq\ & C\left(\frac{H}{\eta}\right)^2\left(1+\log\left(\frac{\eta}{h}\right)\right)\left(1+\log\left(\frac{H}{h}\right)\right)\left(|u|^2_{H^1(\widetilde{\Omega}_{i,\eta})}+\frac{1}{H^2}\|u\|^2_{L_2(\widetilde{\Omega}_{i,\eta})}\right).\end{aligned}$$

If we can afford to estimate with respect to the whole subdomain Ω_i, we can use the standard edge estimate, see Toselli and Widlund [57, Lemma 4.16], and obtain

$$\|u\|^2_{L_2(\mathcal{E}^{ik})} \leq C\left(1+\log\left(\frac{H}{h}\right)\right)\left(|u|^2_{H^1(\Omega_i)}+\frac{1}{H^2}\|u\|^2_{L_2(\Omega_i)}\right).$$

From this, we obtain the inequality (3.1)

$$|I^h(\bar{\vartheta}_{\mathcal{F}^{ij}}u)|^2_{H^1(\widetilde{\Omega}_{i,\eta})} \leq C\frac{H}{\eta}\left(1+\log\left(\frac{H}{h}\right)\right)^2\left(|u|^2_{H^1(\Omega_i)}+\frac{1}{H^2}\|u\|^2_{L^2(\Omega_i)}\right).$$

□

In the next lemma, we just summarize the results for the estimates of the edges obtained in the proof of Lemma 3.10. It is therefore a combination of [57, Lemma 4.19] and [57, Lemma 4.16], and an edge estimate in terms of the energy on a corresponding slab.

Lemma 3.11. *Let $\mathcal{E}^{ik}$ be an edge of Ω_i, or rather an edge of $\widetilde{\Omega}_{i,\eta}$ of the order of H_i. Let $\theta_{\mathcal{E}^{ik}}$ be the finite element function which vanishes at all nodes of Γ except of those of $\mathcal{E}^{ik}$ where it takes the value 1, and which is discrete harmonically extended to Ω_i. Let $\bar{\vartheta}_{\mathcal{E}^{ik}}$ be the function that vanishes on all nodes of $\overline{\Omega}_i$ except on those of $\mathcal{E}^{ik}$ where it takes the value 1. By $I^h(\bar{\vartheta}_{\mathcal{E}^{ik}}u)$ we denote the extension by zeros of the values of u on $\mathcal{E}^{ik}$. Then, for $u \in W^{(i)}$,*

(i) $\left|\mathcal{H}(I^h(\theta_{\mathcal{E}^{ik}}u))\right|^2_{H^1(\Omega_i)} \leq \left|I^h(\bar{\vartheta}_{\mathcal{E}^{ik}}u)\right|^2_{H^1(\Omega_i)} \leq C\,\|u\|^2_{L_2(\mathcal{E}^{ik})}$,

since it is a local argument, the estimate is also valid for the slab, i.e.,

$$\left|\mathcal{H}(I^h(\theta_{\mathcal{E}^{ik}}u))\right|^2_{H^1(\widetilde{\Omega}_{i,\eta})} \leq \left|I^h(\bar{\vartheta}_{\mathcal{E}^{ik}}u)\right|^2_{H^1(\widetilde{\Omega}_{i,\eta})} \leq C\,\|u\|^2_{L_2(\mathcal{E}^{ik})},$$

(ii) $\|u\|^2_{L_2(\mathcal{E}^{ik})} \leq C\left(1+\log\left(\frac{H}{h}\right)\right)\left\{|u|^2_{H^1(\Omega_i)} + \frac{1}{H_i^2}\|u\|^2_{L_2(\Omega_i)}\right\},$

(iii) $\|u\|^2_{L_2(\mathcal{E}^{ik})} \leq C\frac{H}{\eta}\left(1+\log\left(\frac{\eta}{h}\right)\right)\left\{|u|^2_{H^1(\widetilde{\Omega}_{i,\eta})} + \frac{1}{H^2}\|u\|^2_{L_2(\widetilde{\Omega}_{i,\eta})}\right\}.$

Furthermore, we need an extension lemma to extend a function from one slab to a neighboring one.

Lemma 3.12. *Let $\widetilde{\Omega}_{i,\eta}$ and $\widetilde{\Omega}_{j,\eta}$ be two cuboids of the same width η, which share a face $\mathcal{F}^{ij} \subset \partial\widetilde{\Omega}_{i,\eta} \cap \partial\widetilde{\Omega}_{j,\eta}$, and let*

$$\begin{aligned} V_i &:= \{v \in W^h(\widetilde{\Omega}_{i,\eta}) : \ v(x) = 0 \ \forall x \in \partial\widetilde{\Omega}_{i,\eta} \setminus \mathcal{F}^{ij}\} \\ V_j &:= \{v \in W^h(\widetilde{\Omega}_{j,\eta}) : \ v(x) = 0 \ \forall x \in \partial\widetilde{\Omega}_{j,\eta} \setminus \mathcal{F}^{ij}\}. \end{aligned}$$

Then, there exists an extension operator $E_{ji} : \ V_j \to V_i$ with the following properties

1. $(E_{ji}u)\,|_{\widetilde{\Omega}_{j,\eta}} = u \quad \forall u \in V_j$
2. $|E_{ji}u|_{H^1(\widetilde{\Omega}_{i,\eta})} = |u|_{H^1(\widetilde{\Omega}_{j,\eta})} \quad \forall u \in V_j;$

see also Figure 3.11.

Figure 3.11: Extension

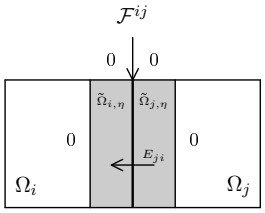

Cross section of two neighboring slabs. An extension from $\widetilde{\Omega}_{i,\eta}$ to $\widetilde{\Omega}_{j,\eta}$.

Proof. Without loss of generality we suppose that $\mathcal{F}^{ij}$ is a subset of the $x-y-$plane. Then it is sufficient to choose a reflection for the extension operator such that

$$E_{ji}u(x,y,z) = \begin{cases} u(x,y,-z) & x,y,z \in \widetilde{\Omega}_{i,\eta} \\ u(x,y,z) & x,y,z \in \widetilde{\Omega}_{j,\eta}. \end{cases}$$

We may write $E_{ji}u(x,y,z) = u(x,y,-z) = u \circ T$ with $T = \begin{pmatrix} x & 0 & 0 \\ 0 & y & 0 \\ 0 & 0 & -z \end{pmatrix}$ for $x, y, z \in \widetilde{\Omega}_{i,\eta}$ and we obtain

$$\begin{aligned} |E_{ji}u|^2_{H^1(\widetilde{\Omega}_{i,\eta})} &= \int_{\widetilde{\Omega}_{i,\eta}} |\nabla (E_{ji}u(x,y,z))|^2 \; dx \; dy \; dz \\ &= \int_{\widetilde{\Omega}_{i,\eta}} |\nabla (u \circ T)|^2 \; dx \; dy \; dz \\ &= \int_{\widetilde{\Omega}_{j,\eta}} (\nabla u)^T (DT)^T (DT) (\nabla u) \left|\det(DT^{-1})\right| \; d\hat{x} \; d\hat{y} \; d\hat{z} \\ &= \int_{\widetilde{\Omega}_{j,\eta}} |\nabla u|^2 \; d\hat{x} \; d\hat{y} \; d\hat{z} \\ &= |u|^2_{H^1(\widetilde{\Omega}_{j,\eta})} . \end{aligned}$$

□

3.4 Convergence Analysis

In this section, we will prove our central theorem on the condition number estimate for the FETI-DP algorithm. Let us first repeat the spaces usually used in the analysis of FETI-DP methods. We denote by $W := \prod_{i=1}^{N} W^{(i)}$ the product space associated with the spaces $W^{(i)}$, i.e., $W^{(i)} = W^h(\partial\Omega_i \cap \Gamma)$; see also Remark 3.5. Furthermore, we define

$$\widetilde{W} := \left\{ u : \; \exists u^{(i)} \in W^{(i)}, i = 1, \ldots, N, \text{ such that } u = \sum_{i=1}^{N} R^{(i)T} u^{(i)} \right\}$$

as the subspace of partially assembled finite element functions with an assembly in the primal variables of FETI-DP, where $R^{(i)T}$ is the local assembly operator. In our analysis we need the local Schur complement matrices $S_\varepsilon^{(i)}$ obtained from $K^{(i)}$ by the elimination of the interior variables in Ω_i and the partially assembled Schur complement matrix $\widetilde{S}_\varepsilon = \sum_{i=1}^{N} R^{(i)T} S_\varepsilon^{(i)} R^{(i)}$.

In order to provide a condition number estimate for the preconditioned FETI-DP matrix $M^{-1}F$, we expand the convergence analysis, given in [37] for compressible linear elasticity, to the case where each subdomain contains an almost incompressible or compressible inclusion surrounded by a compressible hull of thickness η.

As in [37, Section 8.1], we introduce the projection

$$P_D : \widetilde{W} \to \widetilde{W},\ P_D := B_{D,\Gamma}^T B_\Gamma.$$

Note that P_D and also P_D^T preserve jumps for $u \in \widetilde{W}$ in the sense that $B_\Gamma P_D u = B_\Gamma u$ and $B_{D,\Gamma} P_D^T u = B_{D,\Gamma} u$. In this notation we have $F = B_\Gamma \widetilde{S}_\varepsilon^{-1} B_\Gamma^T$ and the Dirichlet preconditioner $M^{-1} = B_{D,\Gamma} \widetilde{S}_\varepsilon B_{D,\Gamma}^T$. Let $w \in \widetilde{W}$, then, we have

$$\left(R^{(i)} P_D w\right)(x) = \sum_{j \in \mathcal{N}_x} \delta_j^\dagger \left((R^{(i)} w)(x) - (R^{(j)} w)(x)\right),\ x \in \partial\Omega_{i,h} \cap \Gamma_h,$$

where $\delta_j^\dagger(x) = \frac{G_{1,j}^\gamma}{\sum_{k \in \mathcal{N}_x} G_{1,k}^\gamma}$ and $\gamma \in [\frac{1}{2}, \infty)$. For the analysis, we make the following assumption.

Assumption 3.13. *For each subdomain, we have an inclusion which can be either almost incompressible or compressible, surrounded by a hull $\Omega_{i,\eta}$ of compressible material. The material coefficients $G(x)$ and $\beta(x)$ have a constant value in the interior inclusion and in the hull respectively, i.e.,*

$$G(x) = \begin{cases} G_{1,i} & x \in \overline{\Omega}_{i,\eta} \\ G_{2,i} & x \in \Omega_i \setminus \Omega_{i,\eta} \end{cases} \qquad \beta(x) = \begin{cases} \beta_{1,i} & x \in \overline{\Omega}_{i,\eta} \\ \beta_{2,i} & x \in \Omega_i \setminus \Omega_{i,\eta}. \end{cases}$$

Note, that this assumption could be easily generalized such that the Young modulus and the Poisson ratio are piecewise constant on each finite element and have positive, arbitrarily bounded values in the inclusion and only mildly varying values on the hull.

Remark 3.14. *Note that Assumption 3.13 allows that the Young modulus in the inclusion can be different from the one in the hull and that their quotient can be arbitrarily small or large. Hence, we can allow for arbitrarily large coefficient jumps of the Young modulus across the boundary of the inclusion in addition to an arbitrary Poisson ratio within the inclusion.*

The following assumption allows for the improved bound (3.4) in Lemma 3.17 and Theorem 3.18, respectively, which contains a linear factor H/η compared to the $(H/\eta)^4$ −factor in (3.3).

Assumption 3.15. *For each subdomain Ω_i, $i = 1, \ldots, N$, we assume that $G_{1,i} \leq k_i \cdot G_{2,i}$, where $k_i > 0$ is a constant independent of $h, H, \eta, G_{1,i}$, and $G_{2,i}$.*

For the edge term estimate in the proof of Lemma 3.17, we need a further assumption.

Assumption 3.16. *For any pair of subdomains (Ω_i, Ω_k) which have an edge in common, we assume that there exists an acceptable path $(\Omega_i, \Omega_{j_1}, \ldots, \Omega_{j_n}, \Omega_k)$ from Ω_i to Ω_k, via a uniformly bounded number of other subdomains $\Omega_{i_q},\ q = 1, \ldots n$, such that the coefficients G_{1,j_q} of the Ω_{i_q} satisfy the condition*

$$TOL \cdot G_{1,j_q} \geq \min(G_{1,i}, G_{1,k}),\ q = 1, \ldots, n,$$

where $TOL > 0$ is a chosen tolerance.

For a detailed description of the concept of acceptable paths, see [37, Section 5].

Next, we formulate the central technical lemma of this section.

Lemma 3.17. *Given Assumptions 3.13 and 3.16, for all $w \in \widetilde{W}$, we have*

$$|P_D w|^2_{\widetilde{S}_\varepsilon} \leq C \max(1, TOL) \left(1 + \log\left(\frac{H}{h}\right)\right) \left(1 + \log\left(\frac{\eta}{h}\right)\right) \left(\frac{H}{\eta}\right)^4 |w|^2_{\widetilde{S}_\varepsilon}, \tag{3.3}$$

where $C > 0$ is independent of h, H, η, and the values of G_i and $\beta_i,\ i = 1, \ldots, N$, and hence also of the values of E_i and $\nu_i, i = 1, \ldots, N$.
If additionally Assumption 3.15 is satisfied, we have

$$|P_D w|^2_{\widetilde{S}_\varepsilon} \leq C \max(1, TOL) \left(1 + \log\left(\frac{H}{h}\right)\right)^2 \left(\frac{H}{\eta}\right) |w|^2_{\widetilde{S}_\varepsilon}, \tag{3.4}$$

where $C > 0$ is independent of h, H, η, and the values of G_i and $\beta_i,\ i = 1, \ldots, N$, and hence also of the values of E_i and $\nu_i, i = 1, \ldots, N$.

We will prove this lemma after the next theorem.

Theorem 3.18. *Given Assumptions 3.13 and 3.16, the condition number of the preconditioned FETI-DP system satisfies*

$$\kappa(M^{-1}F) \leq C \max(1, TOL) \left(1 + \log\left(\frac{H}{h}\right)\right) \left(1 + \log\left(\frac{\eta}{h}\right)\right) \left(\frac{H}{\eta}\right)^4$$

where $C > 0$ is independent of h, H, η and the values of G_i and $\beta_i,\ i = 1, \ldots, N$, and hence also of the values of E_i and $\nu_i, i = 1, \ldots, N$.

If additionally Assumption 3.15 is satisfied, we have

$$\kappa(M^{-1}F) \leq C \max(1, TOL) \left(1 + \log\left(\frac{H}{h}\right)\right)^2 \left(\frac{H}{\eta}\right)$$

where $C > 0$ is independent of h, H, η and the values of G_i and $\beta_i,\ i = 1, \ldots, N$, and hence also of the values of E_i and $\nu_i, i = 1, \ldots, N$.

Proof. Using Lemma 3.17, the proof can be carried out exactly as in [37, Theorem 8.2]. For the sake of completeness, we give a sketch of the proof. We need to constrain the smallest eigenvalue $\lambda_{\min}(M^{-1}F)$ from below and the largest eigenvalue $\lambda_{\max}(M^{-1}F)$ from above. Therefore we consider the following equations in terms of the energy norm F. For all $\lambda \in \mathrm{range}(\mathrm{M}^{-1})$, we have

$$\langle \lambda, \lambda \rangle_F \leq \langle M^{-1}F\lambda, \lambda \rangle_F \leq C \max(1, TOL) \left(1 + \log\left(\frac{H}{h}\right)\right) \left(1 + \log\left(\frac{\eta}{h}\right)\right) \left(\frac{H}{\eta}\right)^4 \langle \lambda, \lambda \rangle_F$$

and accordingly

$$\langle \lambda, \lambda \rangle_F \leq \langle M^{-1}F\lambda, \lambda \rangle_F \leq C \max(1, TOL) \left(1 + \log\left(\frac{H}{h}\right)\right)^2 \left(\frac{H}{\eta}\right) \langle \lambda, \lambda \rangle_F.$$

First we consider the lower bound

$$\begin{aligned}
\langle \lambda, \lambda \rangle_F^2 &= \langle \lambda, B_{D,\Gamma} B_\Gamma^T \lambda \rangle_F^2 \\
&= \langle \lambda, B_{D,\Gamma} \widetilde{S}_\varepsilon^{1/2} \widetilde{S}_\varepsilon^{-1/2} B_\Gamma^T \lambda \rangle_F^2 \\
&= \langle F\lambda, B_{D,\Gamma} \widetilde{S}_\varepsilon^{1/2} \widetilde{S}_\varepsilon^{-1/2} B_\Gamma^T \lambda \rangle_F^2 \\
&\leq \langle \widetilde{S}_\varepsilon^{1/2} B_{D,\Gamma}^T F\lambda, \widetilde{S}_\varepsilon^{1/2} B_{D,\Gamma}^T F\lambda \rangle \langle \widetilde{S}_\varepsilon^{-1/2} B_\Gamma^T \lambda, \widetilde{S}_\varepsilon^{-1/2} B_\Gamma^T \lambda \rangle \\
&= \langle M^{-1}F\lambda, F\lambda \rangle \langle F\lambda, \lambda \rangle \\
&= \langle M^{-1}F\lambda, \lambda \rangle_F \langle \lambda, \lambda \rangle_F
\end{aligned}$$

For the upper bound we just prove the first estimate. The second estimate is obtained

analogously.

$$
\begin{aligned}
& \langle M^{-1}F\lambda,\lambda\rangle_F \\
= \;& \langle M^{-1}F\lambda,F\lambda\rangle \\
= \;& \langle B_{D,\Gamma}^T B_\Gamma \widetilde{S}_\varepsilon^{-1} B_\Gamma^T\lambda, B_{D,\Gamma}^T B_\Gamma \widetilde{S}_\varepsilon^{-1} B_\Gamma^T\lambda\rangle_{\widetilde{S}_\varepsilon} \\
= \;& \left|P_D(\widetilde{S}_\varepsilon^{-1}B_\Gamma^T\lambda)\right|^2_{\widetilde{S}_\varepsilon} \\
\leq \;& C\max(1,TOL)\left(1+\log\left(\frac{H}{h}\right)\right)\left(1+\log\left(\frac{\eta}{h}\right)\right)\left(\frac{H}{\eta}\right)^4\left|\widetilde{S}_\varepsilon^{-1}B_\Gamma^T\lambda\right|^2_{\widetilde{S}_\varepsilon} \\
= \;& C\max(1,TOL)\left(1+\log\left(\frac{H}{h}\right)\right)\left(1+\log\left(\frac{\eta}{h}\right)\right)\left(\frac{H}{\eta}\right)^4\langle\widetilde{S}_\varepsilon^{-1}B_\Gamma^T\lambda,\widetilde{S}_\varepsilon^{-1}B_\Gamma^T\lambda\rangle_{\widetilde{S}_\varepsilon} \\
= \;& C\max(1,TOL)\left(1+\log\left(\frac{H}{h}\right)\right)\left(1+\log\left(\frac{\eta}{h}\right)\right)\left(\frac{H}{\eta}\right)^4\langle F\lambda,\lambda\rangle \\
= \;& C\max(1,TOL)\left(1+\log\left(\frac{H}{h}\right)\right)\left(1+\log\left(\frac{\eta}{h}\right)\right)\left(\frac{H}{\eta}\right)^4\langle\lambda,\lambda\rangle_F
\end{aligned}
$$

□

Now, we will establish Lemma 3.17.

Proof of Lemma 3.17. For simplicity we first assume in this proof that each slab can be represented as the union of finite elements. The generalization to the case where the interior boundary of a slab cuts through certain finite elements can be treated by using a Scott-Zhang interpolation operator, cf. the comment at the end of this proof.

Let $w \in \widetilde{W}$, $Rw := \left(R^{(1)}w,\ldots,R^{(N)}w\right) \in W$ and note that $|P_D w|^2_{\widetilde{S}_\varepsilon} = |RP_D w|^2_{S_\varepsilon}$ as well as $|w|^2_{\widetilde{S}_\varepsilon} = |Rw|^2_{S_\varepsilon}$. Let $v^{(i)} = R^{(i)}P_D w$, then

$$
|RP_D w|^2_{S_\varepsilon} = \sum_{i=1}^N \left|v^{(i)}\right|^2_{S_\varepsilon^{(i)}}.
$$

We note that $Rw = \left(R^{(1)}w,\ldots,R^{(N)}w\right) = \left(w^{(1)},\ldots,w^{(N)}\right) \in W$. Thus, it is sufficient to prove

$$
\left|v^{(i)}\right|^2_{S_\varepsilon^{(i)}} \leq C\max(1,TOL)\left(1+\log\left(\frac{H}{h}\right)\right)\left(1+\log\left(\frac{\eta}{h}\right)\right)\left(\frac{H}{\eta}\right)^4\sum_{j\in\mathcal{N}_i}\left|w^{(j)}\right|^2_{S_\varepsilon^{(j)}}.
$$

We consider the local bilinear form for linear elasticity

$$
a_i(u,v) = (G(x)\varepsilon(u),\varepsilon(v))_{L_2(\Omega_i)} + (G(x)\beta(x)\mathrm{div}(u),\mathrm{div}(v))_{L_2(\Omega_i)}.
$$

Using the discrete elastic extension $\mathcal{H}_\varepsilon$ of $v^{(i)}$ to Ω_i and the discrete harmonic extension $\mathcal{H}_\eta$ of $v^{(i)}$ to the hull $\Omega_{i,\eta}$, see Definition 3.4, we have

$$\begin{aligned}
&|v^{(i)}|^2_{S^{(i)}_\varepsilon} = |a_i(\mathcal{H}_\varepsilon v^{(i)}, \mathcal{H}_\varepsilon v^{(i)})| \leq |a_i(\mathcal{H}_\eta v^{(i)}, \mathcal{H}_\eta v^{(i)})| \\
= \;& \left| \Big(G_{1,i}\, \varepsilon(\mathcal{H}_\eta v^{(i)}), \varepsilon(\mathcal{H}_\eta v^{(i)}) \Big)_{L_2(\Omega_{i,\eta})} + \Big(G_{1,i}\beta_{1,i}\, \mathrm{div}(\mathcal{H}_\eta v^{(i)}), \mathrm{div}(\mathcal{H}_\eta v^{(i)}) \Big)_{L_2(\Omega_{i,\eta})} \right| \\
\leq \;& (1+3\beta_{1,i})\, G_{1,i} \left| \mathcal{H}_\eta v^{(i)} \right|^2_{H^1(\Omega_{i,\eta})}.
\end{aligned}$$

For the proof we use the partition-of-unity functions $\theta_{\mathcal{F}^{ij}}$, $\theta_{\mathcal{E}^{ik}}$, and $\theta_{\mathcal{V}^{il}}$ associated with faces, edges, and vertices; see Definition 3.1. Since all vertices are primal, the vertex terms vanish and we obtain

$$v^{(i)} = \sum_{\mathcal{F}^{ij}} I^h(\theta_{\mathcal{F}^{ij}} v^{(i)}) + \sum_{\mathcal{E}^{ik}} I^h(\theta_{\mathcal{E}^{ik}} v^{(i)}).$$

Face terms

Let $\mathcal{F}^{ij}$ be a face, shared by the subdomains Ω_i and Ω_j. Then, the contribution to $v^{(i)}$ is $I^h(\theta_{\mathcal{F}^{ij}} \delta_j^\dagger(w^{(i)} - w^{(j)}))$, and

$$\left| I^h(\theta_{\mathcal{F}^{ij}} \delta_j^\dagger(w^{(i)} - w^{(j)})) \right|^2_{S^{(i)}_\varepsilon} \leq (1+3\beta_{1,i})\, G_{1,i} \left| \mathcal{H}_\eta \left(I^h(\theta_{\mathcal{F}^{ij}} \delta_j^\dagger(w^{(i)} - w^{(j)})) \right) \right|^2_{H^1(\Omega_{i,\eta})}.$$

Using $G_{1,i}[\delta_j^\dagger(x)]^2 \leq \min(G_{1,i}, G_{1,j})$, for details, see, e.g., [37, Lemma 8.4], we get

$$\begin{aligned}
&\left| I^h(\theta_{\mathcal{F}^{ij}} \delta_j^\dagger(w^{(i)} - w^{(j)})) \right|^2_{S^{(i)}_\varepsilon} \\
\leq \;& (1+3\beta_{1,i}) \min(G_{1,i}, G_{1,j}) \left| \mathcal{H}_\eta \left(I^h(\theta_{\mathcal{F}^{ij}} (w^{(i)} - w^{(j)})) \right) \right|^2_{H^1(\Omega_{i,\eta})}.
\end{aligned}$$

Let $\bar{\vartheta}_{\mathcal{F}^{ij}}$ be the finite element function, defined in Lemma 3.8, which is piecewise linear on $\tau_{h/2}$, coincides with $\theta_{\mathcal{F}^{ij}}$ on $\mathcal{F}^{ij}$, and vanishes on $\partial\widetilde{\Omega}_{i,\eta} \setminus \mathcal{F}^{ij}$ and on $\overline{\Omega_i \setminus \widetilde{\Omega}_{i,\eta}}$. Let $\widetilde{\mathcal{H}}_\eta$ be the discrete harmonic extension to the slab $\widetilde{\Omega}_{i,\eta}$, as in Definition 3.4. Then, we have

$$\begin{aligned}
& \min(G_{1,i}, G_{1,j}) \left| \mathcal{H}_\eta \left(I^h(\theta_{\mathcal{F}^{ij}} (w^{(i)} - w^{(j)})) \right) \right|^2_{H^1(\Omega_{i,\eta})} \\
= \;& \min(G_{1,i}, G_{1,j}) \left| \mathcal{H}_\eta \left(I^h(\bar{\vartheta}_{\mathcal{F}^{ij}} (w^{(i)} - w^{(j)})) \right) \right|^2_{H^1(\Omega_{i,\eta})} \\
\leq \;& \min(G_{1,i}, G_{1,j}) \left| \widetilde{\mathcal{H}}_\eta \left(I^h(\bar{\vartheta}_{\mathcal{F}^{ij}} (w^{(i)} - w^{(j)})) \right) \right|^2_{H^1(\Omega_{i,\eta})} \\
= \;& \min(G_{1,i}, G_{1,j}) \left| \widetilde{\mathcal{H}}_\eta \left(I^h(\bar{\vartheta}_{\mathcal{F}^{ij}} (w^{(i)} - w^{(j)})) \right) \right|^2_{H^1(\widetilde{\Omega}_{i,\eta})}.
\end{aligned}$$

All faces are fully primal; cf. Definition 3.6. Thus, there exist functionals $f_m^{\mathcal{F}^{ij}}$ with $f_m^{\mathcal{F}^{ij}}(w^{(i)}) = f_m^{\mathcal{F}^{ij}}(w^{(j)})$, $m = 1, \dots, 6$, $f_m^{\mathcal{F}^{ij}}(r_n) = \delta_{mn}$, $m, n = 1, \dots, 6$, such that

$$w^{(i)} - w^{(j)} = \Big(w^{(i)} - \sum_{m=1}^{6} f_m^{\mathcal{F}^{ij}}(w^{(i)}) r_m\Big) - \Big(w^{(j)} - \sum_{m=1}^{6} f_m^{\mathcal{F}^{ij}}(w^{(j)}) r_m\Big).$$

Using the representation of an arbitrary rigid body mode in terms of the basis $(r_m)_{m=1,\dots,6}$ of $\ker(\varepsilon)$, we obtain

$$r^{(i)} = \sum_{m=1}^{6} f_m^{\mathcal{F}^{ij}}(r^{(i)}) r_m.$$

The combination of these properties leads to

$$\begin{aligned} & \min(G_{1,i}, G_{1,j}) \left| \widetilde{\mathcal{H}}_\eta \left(I^h(\bar{\vartheta}_{\mathcal{F}^{ij}}(w^{(i)} - w^{(j)})) \right) \right|^2_{H^1(\widetilde{\Omega}_{i,\eta})} \qquad (3.5) \\ \leq \; & 2\, G_{1,i} \left| \widetilde{\mathcal{H}}_\eta \left(I^h(\bar{\vartheta}_{\mathcal{F}^{ij}}(w^{(i)} - r^{(i)} - \sum_{m=1}^{6} f_m^{\mathcal{F}^{ij}}(w^{(i)} - r^{(i)}) r_m)) \right) \right|^2_{H^1(\widetilde{\Omega}_{i,\eta})} \\ & + 2\, G_{1,j} \left| \widetilde{\mathcal{H}}_\eta \left(I^h(\bar{\vartheta}_{\mathcal{F}^{ij}}(w^{(j)} - r^{(j)} - \sum_{m=1}^{6} f_m^{\mathcal{F}^{ij}}(w^{(j)} - r^{(j)}) r_m)) \right) \right|^2_{H^1(\widetilde{\Omega}_{i,\eta})}. \end{aligned}$$

With Lemma 3.12, we obtain for the second term

$$\begin{aligned} & G_{1,j} \left| \widetilde{\mathcal{H}}_\eta \left(I^h(\bar{\vartheta}_{\mathcal{F}^{ij}}(w^{(j)} - r^{(j)} - \sum_{m=1}^{6} f_m^{\mathcal{F}^{ij}}(w^{(j)} - r^{(j)}) r_m)) \right) \right|^2_{H^1(\widetilde{\Omega}_{i,\eta})} \\ \leq \; & G_{1,j} \left| E_{ji} \widetilde{\mathcal{H}}_\eta \left(I^h(\bar{\vartheta}_{\mathcal{F}^{ij}}(w^{(j)} - r^{(j)} - \sum_{m=1}^{6} f_m^{\mathcal{F}^{ij}}(w^{(j)} - r^{(j)}) r_m)) \right) \right|^2_{H^1(\widetilde{\Omega}_{i,\eta})} \\ = \; & G_{1,j} \left| \widetilde{\mathcal{H}}_\eta \left(I^h(\bar{\vartheta}_{\mathcal{F}^{ij}}(w^{(j)} - r^{(j)} - \sum_{m=1}^{6} f_m^{\mathcal{F}^{ij}}(w^{(j)} - r^{(j)}) r_m)) \right) \right|^2_{H^1(\widetilde{\Omega}_{j,\eta})}. \end{aligned}$$

Here, we have tacitly assumed that $\widetilde{\mathcal{H}}_\eta$ extends to both slabs $\widetilde{\Omega}_{i,\eta}$ and $\widetilde{\Omega}_{j,\eta}$, respectively. Clearly, it is sufficient to estimate the first term

$$\begin{aligned} & G_{1,i} \left| \widetilde{\mathcal{H}}_\eta \left(I^h(\bar{\vartheta}_{\mathcal{F}^{ij}}(w^{(i)} - r^{(i)} - \sum_{m=1}^{6} f_m^{\mathcal{F}^{ij}}(w^{(i)} - r^{(i)}) r_m)) \right) \right|^2_{H^1(\widetilde{\Omega}_{i,\eta})} \\ \leq \; & G_{1,i} \left| I^h(\bar{\vartheta}_{\mathcal{F}^{ij}}(w^{(i)} - r^{(i)} - \sum_{m=1}^{6} f_m^{\mathcal{F}^{ij}}(w^{(i)} - r^{(i)}) r_m)) \right|^2_{H^1(\widetilde{\Omega}_{i,\eta})} \\ \leq \; & 7\, G_{1,i} \Big\{ \underbrace{\left| I^h(\bar{\vartheta}_{\mathcal{F}^{ij}}(w^{(i)} - r^{(i)})) \right|^2_{H^1(\widetilde{\Omega}_{i,\eta})}}_{\text{(I)}} + \sum_{m=1}^{6} \underbrace{\left| f_m^{\mathcal{F}^{ij}}(w^{(i)} - r^{(i)}) \right|^2}_{\text{(II)}} \underbrace{\left| I^h(\bar{\vartheta}_{\mathcal{F}^{ij}} r_m) \right|^2_{H^1(\widetilde{\Omega}_{i,\eta})}}_{\text{(III)}} \Big\}. \end{aligned}$$

Next, we will estimate the three terms (I), (II), and (III) separately. Let us first consider (I). This term can be estimated by Lemma 3.10.

$$\begin{aligned}&\left|I^h(\bar{\vartheta}_{\mathcal{F}^{ij}}(w^{(i)}-r^{(i)}))\right|^2_{H^1(\widetilde{\Omega}_{i,\eta})}\\ \leq\ & C\left(\frac{H_i}{\eta}\right)^2\left(1+\log\left(\frac{\eta}{h_i}\right)\right)\left(1+\log\left(\frac{H_i}{h_i}\right)\right)\left\|w^{(i)}-r^{(i)}\right\|^2_{H^1(\widetilde{\Omega}_{i,\eta})}.\end{aligned}$$

Next, we estimate (II). All faces are fully primal and with Definition 3.6, we obtain

$$\left|f_m^{\mathcal{F}^{ij}}(w^{(i)}-r^{(i)})\right|^2 \leq C\frac{1}{\eta}\left(1+\log\left(\frac{\eta}{h_i}\right)\right)\left\|w^{(i)}-r^{(i)}\right\|^2_{H^1(\widetilde{\Omega}_{i,\eta})}.$$

Finally, we consider (III). Since $\bar{\vartheta}_{\mathcal{F}^{ij}}r_m$ is at most piecewise quadratic on $\tau_{h/2}$, using the stability of the interpolation operator for piecewise quadratic functions on $\tau_{h/2}$ into the space of piecewise quadratic functions on τ_h, we can follow the arguments given in [57, Lemma 3.9] or the detailed arguments in [28, Lemma A.1], and we obtain

$$\left|I^h(\bar{\vartheta}_{\mathcal{F}^{ij}}r_m)\right|^2_{H^1(\widetilde{\Omega}_{i,\eta})} \leq C\Big\{\underbrace{\left\|\nabla\bar{\vartheta}_{\mathcal{F}^{ij}}\right\|^2_{L_2(\widetilde{\Omega}_{i,\eta})}}_{\text{(a)}}\underbrace{\|r_m\|^2_{L^\infty(\widetilde{\Omega}_{i,\eta})}}_{\text{(b)}}+\underbrace{\left\|\bar{\vartheta}_{\mathcal{F}^{ij}}\right\|^2_{L^\infty(\widetilde{\Omega}_{i,\eta})}}_{\text{(c)}}\underbrace{\|\nabla r_m\|^2_{L_2(\widetilde{\Omega}_{i,\eta})}}_{\text{(d)}}\Big\}.$$

First, we consider (a) and obtain by Lemma 3.8

$$\left\|\nabla\bar{\vartheta}_{\mathcal{F}^{ij}}\right\|^2_{L_2(\widetilde{\Omega}_{i,\eta})} \leq C\left(1+\log\left(\frac{H_i}{h_i}\right)\right)\frac{H_i^2}{\eta}.$$

Next, we consider (b). By estimating $|(r_m)_k|^2$ we get the upper bound independent of H_i

$$\begin{aligned}&|(r_m)_k|^2 = \begin{cases}1 & \text{for } m=1,2,3\\ \frac{1}{H_i^2}\left((x_i-\hat{x}_i)^2-(-x_j+\hat{x}_j)\right)^2 \leq \frac{1}{H_i^2}\cdot 2CH_i^2 & \text{for } m=4,5,6\end{cases}\\ &\Rightarrow \|(r_m)_k\|^2_{L^\infty(\widetilde{\Omega}_{i,\eta})} \leq C\ \forall k=1,2,3\\ &\Rightarrow \|r_m\|^2_{L^\infty(\widetilde{\Omega}_{i,\eta})} = \sum_{k=1}^{3}\|(r_m)_k\|^2_{L^\infty(\widetilde{\Omega}_{i,\eta})} \leq C.\end{aligned}$$

Considering (c), we have $\left\|\bar{\vartheta}_{\mathcal{F}^{ij}}\right\|^2_{L^\infty(\widetilde{\Omega}_{i,\eta})}=1$. Finally, we estimate (d) by

$$\|\nabla r_m\|^2_{L_2(\widetilde{\Omega}_{i,\eta})} = \sum_{k=1}^{3}\|\nabla\,(r_m)_k\|^2_{L_2(\widetilde{\Omega}_{i,\eta})} \leq 2\int_{\widetilde{\Omega}_{i,\eta}}\frac{1}{H_i^2}\,dx = C\eta.$$

Combining the estimates (a)-(d), we obtain as an estimate for (III)

$$\left|I^h(\bar{\vartheta}_{\mathcal{F}^{ij}}r_m)\right|^2_{H^1(\widetilde{\Omega}_{i,\eta})} \leq C\left(1+\log\left(\frac{H_i}{h_i}\right)\right)\frac{H_i^2}{\eta}.$$

Figure 3.12:

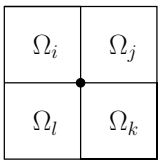

Cross section of four subdomains sharing an edge.

Combining (I)-(III), we have

$$\begin{aligned} & G_{1,i}\left\{\left|I^h(\bar{\vartheta}_{\mathcal{F}^{ij}}(w^{(i)}-r^{(r)}))\right|^2_{H^1(\widetilde{\Omega}_{i,\eta})}+\sum_{m=1}^{6}\left|f_m^{\mathcal{F}^{ij}}(w^{(i)}-r^{(i)})\right|^2\left|I^h(\bar{\vartheta}_{\mathcal{F}^{ij}}r_m)\right|^2_{H^1(\widetilde{\Omega}_{i,\eta})}\right\} \\ \leq\ & C\ G_{1,i}\left(\frac{H_i}{\eta}\right)^2\left(1+\log\left(\frac{\eta}{h_i}\right)\right)\left(1+\log\left(\frac{H_i}{h_i}\right)\right)\left\|w^{(i)}-r^{(i)}\right\|^2_{H^1(\widetilde{\Omega}_{i,\eta})}. \end{aligned}$$

With an appropriate Korn inequality, see Lemma 3.7, we obtain

$$\begin{aligned} & C\ G_{1,i}\left(\frac{H_i}{\eta}\right)^2\left(1+\log\left(\frac{\eta}{h_i}\right)\right)\left(1+\log\left(\frac{H_i}{h_i}\right)\right)\left\|w^{(i)}-r^{(i)}\right\|^2_{H^1(\widetilde{\Omega}_{i,\eta})} \\ \leq\ & C\ G_{1,i}\left(\frac{H_i}{\eta}\right)^4\left(1+\log\left(\frac{\eta}{h_i}\right)\right)\left(1+\log\left(\frac{H_i}{h_i}\right)\right)\left\|\varepsilon(w^{(i)})\right\|^2_{L_2(\widetilde{\Omega}_{i,\eta})} \\ \leq\ & C\ \left(\frac{H_i}{\eta}\right)^4\left(1+\log\left(\frac{\eta}{h_i}\right)\right)\left(1+\log\left(\frac{H_i}{h_i}\right)\right) \\ & \qquad\qquad \left\{G_{1,i}\left\|\varepsilon(w^{(i)})\right\|^2_{L_2(\Omega_{i,\eta})}+G_{2,i}\left\|\varepsilon(w^{(i)})\right\|^2_{L_2(\Omega_i\setminus\Omega_{i,\eta})}\right\}. \end{aligned}$$

Under the additional Assumption 3.15 we can obtain an improved estimate following basically the same arguments. The only difference is that we can be a bit more lenient and can always estimate the energy on the whole subdomain Ω_i instead of estimating on the slab $\widetilde{\Omega}_{i,\eta}$. Then, using Lemma 3.10, Definition 3.6, and Lemma 3.7, we obtain

$$\begin{aligned} & G_{1,i}\left\{\left|I^h(\bar{\vartheta}_{\mathcal{F}^{ij}}(w^{(i)}-r^{(r)}))\right|^2_{H^1(\widetilde{\Omega}_{i,\eta})}+\sum_{m=1}^{6}\left|f_m^{\mathcal{F}^{ij}}(w^{(i)}-r^{(i)})\right|^2\left|I^h(\bar{\vartheta}_{\mathcal{F}^{ij}}r_m)\right|^2_{H^1(\widetilde{\Omega}_{i,\eta})}\right\} \\ \leq\ & C\ \left(\frac{H_i}{\eta}\right)\left(1+\log\left(\frac{H_i}{h_i}\right)\right)^2\left\{G_{1,i}\left\|\varepsilon(w^{(i)})\right\|^2_{L_2(\Omega_{i,\eta})}+G_{2,i}\left\|\varepsilon(w^{(i)})\right\|^2_{L_2(\Omega_i\setminus\Omega_{i,\eta})}\right\}. \end{aligned}$$

Edge terms

Let $\mathcal{E}^{ik}$ be the edge shared by the four subdomains $\Omega_i,\ \Omega_j,\ \Omega_k$, and Ω_l; see Figure 3.12. Then, the contributions of the edge terms to $v^{(i)}$ are

$$\begin{aligned} & I^h\left(\theta_{\mathcal{E}^{ik}}\delta_j^\dagger(w^{(i)}-w^{(j)})\right)+I^h\left(\theta_{\mathcal{E}^{ik}}\delta_k^\dagger(w^{(i)}-w^{(k)})\right) \\ & +\ I^h\left(\theta_{\mathcal{E}^{ik}}\delta_l^\dagger(w^{(i)}-w^{(l)})\right). \end{aligned} \tag{3.6}$$

Let $\bar{\vartheta}_{\mathcal{E}^{ik}}$ be the finite element function, defined in Lemma 3.11, which is piecewise linear on $\tau_{h/2}$, coincides with $\theta_{\mathcal{E}^{ik}}$ on $\mathcal{E}^{ik}$, and vanishes on $\partial\widetilde{\Omega}_{i,\eta}\setminus\mathcal{E}^{ik}$ and on $\overline{\Omega_i\setminus\widetilde{\Omega}_{i,\eta}}$. Let $\widetilde{\mathcal{H}}_\eta$ be the discrete harmonic extension to the slab $\widetilde{\Omega}_{i,\eta}$, as in Definition 3.4. We consider the first term of (3.6). The edge $\mathcal{E}^{ik}$ belongs to the boundary of the face $\mathcal{F}^{ij}$, which is common to Ω_i and Ω_j. Let $\widetilde{\Omega}_{i,\eta}\subset\Omega_i$ be a slab, such that $\mathcal{F}^{ij}\subset\partial\widetilde{\Omega}_{i,\eta}$. We assume, that $\widetilde{\mathcal{H}}_\eta\left(I^h\left(\bar{\vartheta}_{\mathcal{E}^{ik}}(w^{(i)}-w^{(j)})\right)\right)$ is trivially extended by zero on $\overline{\Omega_i\setminus\widetilde{\Omega}_{i,\eta}}$. Then,

$$\begin{aligned} & \min(G_{1,i},G_{1,j})\left|\mathcal{H}_\eta\left(I^h\left(\theta_{\mathcal{E}^{ik}}(w^{(i)}-w^{(j)})\right)\right)\right|^2_{H^1(\Omega_{i,\eta})} \\ \leq\ & \min(G_{1,i},G_{1,j})\left|\widetilde{\mathcal{H}}_\eta\left(I^h\left(\bar{\vartheta}_{\mathcal{E}^{ik}}(w^{(i)}-w^{(j)})\right)\right)\right|^2_{H^1(\widetilde{\Omega}_{i,\eta})}. \end{aligned}$$

The neighboring subdomains Ω_i and Ω_j share the face $\mathcal{F}^{ij}$ and all faces are fully primal. Thus, $f_m^{\mathcal{F}^{ij}}(w^{(i)})=f_m^{\mathcal{F}^{ij}}(w^{(j)}),\ m=1,\dots,6$, and $f_m^{\mathcal{F}^{ij}}(r_n)=\delta_{mn}$ for $m,n=1,\dots,6$. Analogously to the estimates for the face terms, we obtain

$$\begin{aligned} & \min(G_{1,i},G_{1,j})\left|\widetilde{\mathcal{H}}_\eta\left(I^h\left(\bar{\vartheta}_{\mathcal{E}^{ik}}(w^{(i)}-w^{(j)})\right)\right)\right|^2_{H^1(\widetilde{\Omega}_{i,\eta})} \\ \leq\ & 2\ G_{1,i}\left|\widetilde{\mathcal{H}}_\eta\left(I^h(\bar{\vartheta}_{\mathcal{E}^{ik}}(w^{(i)}-r^{(i)}-\sum_{m=1}^{6}f_m^{\mathcal{F}^{ij}}(w^{(i)}-r^{(i)})r_m))\right)\right|^2_{H^1(\widetilde{\Omega}_{i,\eta})} \\ & +2\ G_{1,j}\left|\widetilde{\mathcal{H}}_\eta\left(I^h(\bar{\vartheta}_{\mathcal{E}^{ik}}(w^{(j)}-r^{(j)}-\sum_{m=1}^{6}f_m^{\mathcal{F}^{ij}}(w^{(j)}-r^{(j)})r_m))\right)\right|^2_{H^1(\widetilde{\Omega}_{j,\eta})} \end{aligned}$$

Here, we again have used Lemma 3.12. As before, it is sufficient to consider the first term

on the right hand side

$$
\begin{aligned}
& G_{1,i} \left| \widetilde{\mathcal{H}}_\eta \left(I^h(\bar{\vartheta}_{\mathcal{E}^{ik}}(w^{(i)} - r^{(i)} - \sum_{m=1}^{6} f_m^{\mathcal{F}^{ij}}(w^{(i)} - r^{(i)}) r_m)) \right) \right|^2_{H^1(\widetilde{\Omega}_{i,\eta})} \\
\leq \; & 7\, G_{1,i} \left\{ \underbrace{\left| \widetilde{\mathcal{H}}_\eta \left(I^h(\bar{\vartheta}_{\mathcal{E}^{ik}}(w^{(i)} - r^{(i)})) \right) \right|^2_{H^1(\widetilde{\Omega}_{i,\eta})}}_{\text{(I)}} \right. \\
& \left. + \sum_{m=1}^{6} \underbrace{\left| f_m^{\mathcal{F}^{ij}}(w^{(i)} - r^{(i)}) \right|^2}_{\text{(II)}} \underbrace{\left| \widetilde{\mathcal{H}}_\eta \left(I^h(\bar{\vartheta}_{\mathcal{E}^{ik}}(r_m)) \right) \right|^2_{H^1(\widetilde{\Omega}_{i,\eta})}}_{\text{(III)}} \right\}.
\end{aligned}
$$

Next, we will estimate the three terms (I), (II), and (III) separately.

First, we consider (I). Using Lemma 3.11, we obtain

$$
\begin{aligned}
\left| \widetilde{\mathcal{H}}_\eta \left(I^h(\bar{\vartheta}_{\mathcal{E}^{ik}}(w^{(i)} - r^{(i)})) \right) \right|^2_{H^1(\widetilde{\Omega}_{i,\eta})} &\leq C \left\| w^{(i)} - r^{(i)} \right\|^2_{L_2(\mathcal{E}^{ik})} \\
&\leq C \frac{H_i}{\eta} \left(1 + \log\left(\frac{\eta}{h_i} \right) \right) \left\| w^{(i)} - r^{(i)} \right\|^2_{H^1(\widetilde{\Omega}_{i,\eta})}.
\end{aligned}
$$

Now, we consider (II). Again, all faces are fully primal, see Definition 3.6, and we obtain

$$
\left| f_m^{\mathcal{F}^{ij}}(w^{(i)} - r^{(i)}) \right|^2 \leq C \frac{1}{\eta} \left(1 + \log\left(\frac{\eta}{h_i} \right) \right) \left\| w^{(i)} - r^{(i)} \right\|^2_{H^1(\widetilde{\Omega}_{i,\eta})}.
$$

Finally, we consider (III). Using the first inequality of Lemma 3.11, we get

$$
\left| \widetilde{\mathcal{H}}_\eta \left(I^h(\bar{\vartheta}_{\mathcal{E}^{ik}}(r_m)) \right) \right|^2_{H^1(\widetilde{\Omega}_{i,\eta})} \leq \|r_m\|^2_{L_2(\mathcal{E}^{ik})} \leq C \min(H_i, H_j).
$$

Combining the estimates for (I)-(III), we obtain

$$
\begin{aligned}
& G_{1,i} \left| \widetilde{\mathcal{H}}_\eta \left(I^h(\bar{\vartheta}_{\mathcal{E}^{ik}}(w^{(i)} - r^{(i)} - \sum_{m=1}^{6} f_m^{\mathcal{F}^{ij}}(w^{(i)} - r^{(i)}) r_m)) \right) \right|^2_{H^1(\widetilde{\Omega}_{i,\eta})} \\
\leq \; & C\, G_{1,i} \frac{H_i}{\eta} \left(1 + \log\left(\frac{\eta}{h_i} \right) \right) \left\| w^{(i)} - r^{(i)} \right\|^2_{H^1(\widetilde{\Omega}_{i,\eta})}.
\end{aligned}
$$

The third term in (3.6) can be estimated analogously. The second term in (3.6) cannot be reduced to face estimates, since the edge $\mathcal{E}^{ik}$ is shared by the subdomains Ω_i and Ω_k, which have no face in common. We have

$$\begin{aligned} & \min(G_{1,i}, G_{1,k}) \left| \mathcal{H}_\eta \left(I^h \left(\theta_{\mathcal{E}^{ik}} (w^{(i)} - w^{(k)}) \right) \right) \right|^2_{H^1(\Omega_{i,\eta})} \\ \leq \; & \min(G_{1,i}, G_{1,k}) \left| \widetilde{\mathcal{H}}_\eta \left(I^h \left(\bar{\vartheta}_{\mathcal{E}^{ik}} (w^{(i)} - w^{(k)}) \right) \right) \right|^2_{H^1(\widetilde{\Omega}_{i,\eta})} . \end{aligned}$$

The neighboring subdomains Ω_i and Ω_j share a fully primal face $\mathcal{F}^{ij}$, thus we have $f_m^{\mathcal{F}^{ij}}(w^{(i)}) = f_m^{\mathcal{F}^{ij}}(w^{(j)})$. Also Ω_j and Ω_k have a fully primal face $\mathcal{F}^{jk}$ in common, such that $f_m^{\mathcal{F}^{jk}}(w^{(j)}) = f_m^{\mathcal{F}^{jk}}(w^{(k)})$. We have

$$\begin{aligned} w^{(i)} - w^{(k)} &= \left(w^{(i)} - w^{(j)} \right) - \left(w^{(k)} - w^{(j)} \right) \\ &= \left(w^{(i)} - \sum_{m=1}^{6} f_m^{\mathcal{F}^{ij}}(w^{(i)}) r_m \right) - \left(w^{(j)} - \sum_{m=1}^{6} f_m^{\mathcal{F}^{ij}}(w^{(j)}) r_m \right) \\ &\quad - \left(\left(w^{(k)} - \sum_{m=1}^{6} f_m^{\mathcal{F}^{jk}}(w^{(k)}) r_m \right) - \left(w^{(j)} - \sum_{m=1}^{6} f_m^{\mathcal{F}^{jk}}(w^{(j)}) r_m \right) \right) . \end{aligned}$$

From this, we obtain

$$\begin{aligned} & \min(G_{1,i}, G_{1,k}) \left| \widetilde{\mathcal{H}}_\eta \left(I^h \left(\bar{\vartheta}_{\mathcal{E}^{ik}} (w^{(i)} - w^{(k)}) \right) \right) \right|^2_{H^1(\widetilde{\Omega}_{i,\eta})} \qquad (3.7) \\ & \leq 4 \; G_{1,i} \left| \widetilde{\mathcal{H}}_\eta \left(I^h (\bar{\vartheta}_{\mathcal{E}^{ik}} (w^{(i)} - r^{(i)} - \sum_{m=1}^{6} f_m^{\mathcal{F}^{ij}} (w^{(i)} - r^{(i)}) r_m)) \right) \right|^2_{H^1(\widetilde{\Omega}_{i,\eta})} \\ & + \; 4 \; G_{1,k} \left| \widetilde{\mathcal{H}}_\eta \left(I^h (\bar{\vartheta}_{\mathcal{E}^{ik}} (w^{(k)} - r^{(k)} - \sum_{m=1}^{6} f_m^{\mathcal{F}^{jk}} (w^{(k)} - r^{(k)}) r_m)) \right) \right|^2_{H^1(\widetilde{\Omega}_{i,\eta})} \\ & + \; 4 \; \min(G_{1,i}, G_{1,k}) \left| \widetilde{\mathcal{H}}_\eta \left(I^h (\bar{\vartheta}_{\mathcal{E}^{ik}} (w^{(j)} - r^{(j)} - \sum_{m=1}^{6} f_m^{\mathcal{F}^{ij}} (w^{(j)} - r^{(j)}) r_m)) \right) \right|^2_{H^1(\widetilde{\Omega}_{i,\eta})} \\ & + \; 4 \; \min(G_{1,i}, G_{1,k}) \left| \widetilde{\mathcal{H}}_\eta \left(I^h (\bar{\vartheta}_{\mathcal{E}^{ik}} (w^{(j)} - r^{(j)} - \sum_{m=1}^{6} f_m^{\mathcal{F}^{jk}} (w^{(j)} - r^{(j)}) r_m)) \right) \right|^2_{H^1(\widetilde{\Omega}_{i,\eta})} . \qquad (3.8) \end{aligned}$$

The first part of this sum can be estimated as before. We now consider the second term. Using Lemma 3.11, we obtain

$$G_{1,k} \left| \widetilde{\mathcal{H}}_\eta \left(I^h (\bar{\vartheta}_{\mathcal{E}^{ik}} (w^{(k)} - r^{(k)} - \sum_{m=1}^{6} f_m^{\mathcal{F}^{jk}} (w^{(k)} - r^{(k)}) r_m)) \right) \right|^2_{H^1(\widetilde{\Omega}_{i,\eta})}$$

$$\leq C\, G_{1,k} \left\| w^{(k)} - r^{(k)} - \sum_{m=1}^{6} f_m^{\mathcal{F}^{jk}} (w^{(k)} - r^{(k)}) r_m \right\|^2_{L_2(\mathcal{E}^{ik})}$$
$$\leq C\, G_{1,k} \frac{H_k}{\eta} \left(1 + \log\left(\frac{\eta}{h_k}\right)\right) \left\| w^{(k)} - r^{(k)} \right\|^2_{H^1(\widetilde{\Omega}_{k,\eta})}.$$

Using Assumption 3.16 for the last two terms of (3.8), i.e., $TOL \cdot G_{1,j} \geq \min(G_{1,i}, G_{1,k})$, and using again Lemma 3.11, we have

$$\min(G_{1,i}, G_{1,k}) \left| \widetilde{\mathcal{H}}_\eta \left(I^h(\bar{\vartheta}_{\mathcal{E}^{ik}}(w^{(j)} - r^{(j)} - \sum_{m=1}^{6} f_m^{\mathcal{F}^{ij}} (w^{(j)} - r^{(j)}) r_m)) \right) \right|^2_{H^1(\widetilde{\Omega}_{i,\eta})}$$
$$\leq TOL \cdot G_{1,j} \left| \widetilde{\mathcal{H}}_\eta \left(I^h(\bar{\vartheta}_{\mathcal{E}^{ik}}(w^{(j)} - r^{(j)} - \sum_{m=1}^{6} f_m^{\mathcal{F}^{ij}} (w^{(j)} - r^{(j)}) r_m)) \right) \right|^2_{H^1(\widetilde{\Omega}_{i,\eta})}$$
$$\leq C\, TOL \cdot G_{1,j} \left\| w^{(j)} - r^{(j)} - \sum_{m=1}^{6} f_m^{\mathcal{F}^{ij}} (w^{(j)} - r^{(j)}) r_m \right\|^2_{L_2(\mathcal{E}^{ik})}.$$

We obtain as before

$$\min(G_{1,i}, G_{1,k}) \left| \widetilde{\mathcal{H}}_\eta \left(I^h(\bar{\vartheta}_{\mathcal{E}^{ik}}(w^{(j)} - r^{(j)} - \sum_{m=1}^{6} f_m^{\mathcal{F}^{ij}} (w^{(j)} - r^{(j)}) r_m)) \right) \right|^2_{H^1(\widetilde{\Omega}_{i,\eta})}$$
$$\leq C\, TOL \cdot G_{1,j} \frac{H_j}{\eta} \left(1 + \log\left(\frac{\eta}{h_j}\right)\right) \left\| w^{(j)} - r^{(j)} \right\|^2_{H^1(\widetilde{\Omega}_{j,\eta})}.$$

Using identical arguments we obtain the estimates for the last term of (3.8).

To conclude the proof for the edge terms we can apply the same arguments as used at the end of the proof for the face terms.

For our analysis we have assumed that the completion of the slab can be represented as the union of finite elements. We can generalize our theory to the case where the interior boundary of the slab cuts through finite elements and where the completion of the slab cannot be represented anymore exactly as the union of finite elements. Therefore, we remesh the slab of width η using a mesh size similar to h, see Figure 2.5. Next, we use a Scott-Zhang interpolation operator to the auxiliary mesh and the associated auxiliary finite element space, respectively. Here, we only have to assume, that our irregular mesh resolves η in the sense that the incompressible inclusion is separated from the interface by at least one element; see Figure 2.5.

Let us briefly sketch the part of the proof for the face terms that is altered. The edge estimate can be carried out completely analogously. Let us denote by Π_i^h the Scott-Zhang

operator interpolating from the original finite element spaces into the space related to the auxiliary mesh. For a reference to the Scott-Zhang operator, see [56, 4]. We use the property $\Pi_i^h u \mid_{\partial\Omega_i} = u$ to insert the interpolation into (3.5)

$$\begin{aligned} & \min(G_{1,i}, G_{1,j}) \left| \widetilde{\mathcal{H}}_\eta \left(I^h(\bar{\vartheta}_{\mathcal{F}^{ij}}(w^{(i)} - w^{(j)})) \right) \right|^2_{H^1(\widetilde{\Omega}_{i,\eta})} \\ = & \min(G_{1,i}, G_{1,j}) \left| \widetilde{\mathcal{H}}_\eta \left(I^h(\bar{\vartheta}_{\mathcal{F}^{ij}}(\Pi_i^h(w^{(i)} - w^{(j)}))) \right) \right|^2_{H^1(\widetilde{\Omega}_{i,\eta})}. \end{aligned}$$

We now proceed as before for the face terms. Finally, we can remove the interpolation from the right hand side of the estimate by using the stability $\|\Pi_i^h u\|^2_{H^1(\widetilde{\Omega}_{i,\eta})} \leq C\|u\|^2_{H^1(\widetilde{\Omega}_{i,\eta})}$.

□

3.5 Numerical Results

In this section we present our numerical results for a linear elasticity problem in three dimensions, using $\mathcal{P}_2$ finite elements for the compressible hulls and statically condensated $\mathcal{Q}_2 - \mathcal{P}_0$ mixed finite elements for the inclusions. We consider almost incompressible inclusions or inclusions with a different Young modulus in the interior of the subdomains. The inclusions are always surrounded by a compressible hull with $\nu = 0.3$; see Figure 3.13. We use a FETI-DP

Figure 3.13:

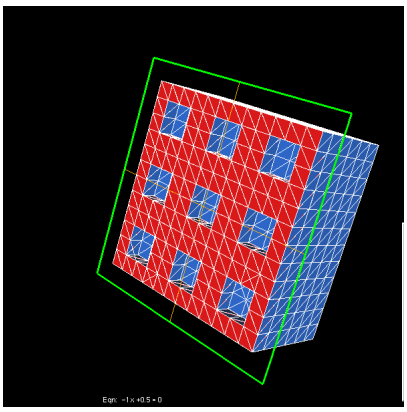

Decomposition into subdomains, hulls in red and inclusions in blue

algorithm with vertices and edge averages as primal constraints to control the rigid body modes and a relative residual reduction by $1e-10$ in the cg-method. For the algorithmic concept, see for example [37, 29, 34]. The numerical results confirm our theoretical estimates.

Table 3.1: Growing η; $H/h = 11$; $1/H = 3$; $\mathcal{P}_2/\mathcal{Q}_2 - \mathcal{P}_0$

η	♯ iterations	condition number
$1h$	32	12.366
$2h$	32	12.250
$3h$	32	12.230
$4h$	32	12.231
$5h$	32	12.233
$6h$	31	12.233
0	50	1597.8

Growing η for $3 \times 3 \times 3$ subdomains, $E = 210$ on the whole domain, $\nu = 0.499999$ in the inclusions, and $\nu = 0.3$ in the hulls. The results show only a weak dependence on η.

3.5.1 Variable η

In this subsection we present results for $3 \times 3 \times 3$ subdomains, a fixed $H/h = 11$, and a fixed Poisson ratio $\nu = 0.499999$ in the inclusions. For these computations we vary the thickness of the compressible hull from zero to six element diameters, i.e., $\eta = 0, h, \ldots, 6h$; see Table 3.1. For almost incompressibility on the whole domain, i.e., $\eta = 0$, it is not surprising that we obtain a large condition number, because we use a coarse space designed for compressible linear elasticity. But it is striking that already a hull of one element, i.e., $\eta = h$, is sufficient to obtain a good condition number which is then not improved significantly by further increasing η. As a result, the number of iteration steps needed does not change significantly for $\eta = h, \ldots, 6h$. From our theory, for this configuration of coefficients, we expect an estimate of $\kappa(M^{-1}F) \leq C \max(1, \mathsf{TOL}) \left(1 + \log\left(\frac{H}{h}\right)\right)^2 \frac{H}{\eta}$, i.e., a linear behavior in $\frac{H}{\eta}$; see Theorem 3.18, which we cannot see in the numerical results. This might be due to the fact, that our meshes are not fine enough.

3.5.2 Variable $1/H$ - Weak Scaling

In this category of tests we vary the number of subdomains from $3 \times 3 \times 3$ up to $10 \times 10 \times 10$, but we fix the number of elements in a subdomain by $H/h = 3$. We choose incompressible inclusions $\nu = 0.499999$, compressible hulls $\nu = 0.3$, and $E = 210$ in each subdomain; see Table 3.2. The results show that also in the presence of incompressible inclusions our standard coarse space is sufficient to obtain a condition number and a number of iterations which is bounded independently of the number of subdomains.

Table 3.2: Growing $1/H$; $H/h = 3$; $\eta = h$; $\mathcal{P}_2/\mathcal{Q}_2 - \mathcal{P}_0$

$1/H$	♯ iterations	condition number
3	21	5.0324
4	23	5.5950
5	24	5.6937
6	24	5.7121
7	25	5.7529
8	25	5.7820
9	25	5.8094
10	25	5.8281

Growing $1/H$; $E = 210$ on the whole domain; $\nu = 0.499999$ in the inclusions, $\nu = 0.3$ in the hulls.

3.5.3 Variable H/h

For a fixed decomposition into $3 \times 3 \times 3$ subdomains and a Poisson ratio of $\nu = 0.499999$ for the inclusion in each subdomain, we solve the linear elasticity problem for different H/h. This means, we increase the number of elements in each subdomain. We consider three cases for the thickness of the hull, namely zero, one, and two element diameters, i.e., $\eta = 0, h, 2h$; for the results see Table 3.3.

Using a hull of a thickness of only one element, i.e., $\eta = h$, already gives a good condition number; see Table 3.3 (center). Increasing the hull's width by one further element, i.e., $\eta = 2h$, has almost no additional effect on the condition number; see Table 3.3 (right). This is consistent with the findings in Section 3.5.1 and Table 3.5.1. From Figure 3.14, we see that we have numerically confirmed the polylogarithmic factor in our condition number estimate, cf. Theorem 3.18, $\kappa(M^{-1}F) \leq C \max(1, \mathrm{TOL}) \left(1 + \log\left(\frac{H}{h}\right)\right)^2 \frac{H}{\eta}$. Note that here, $\eta = h$, but we are far from the asymptotics with respect to η. In Figure 3.15 we also plot the square root of the condition number in a semilogarithmic plot of H/h. We observe the expected linear behavior in the plot. We do not include plots for $\eta = 2h$, since the results are nearly identical.

For comparison, we also provide results for the case $\eta = 0$, see Table 3.3 (left), where we have almost incompressible linear elasticity on the whole domain. Since our coarse space is designed for compressible elasticity problems it is clear that the condition number is very large, i.e., of the order of $1e3$. In this case using a different, larger coarse space is the remedy; see [42, 13, 50].

Figure 3.14:

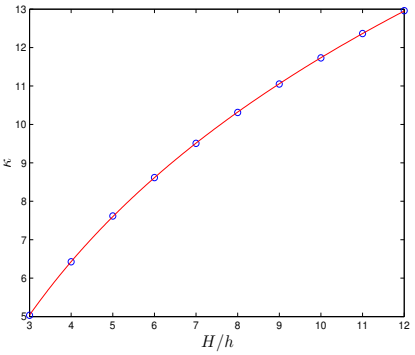

Least square fit of a polynomial in $\log\left(\frac{H}{h}\right)$ to the data from Table 3.3. Growing H/h and a hull of one element, i.e., $\eta = h$.

Figure 3.15:

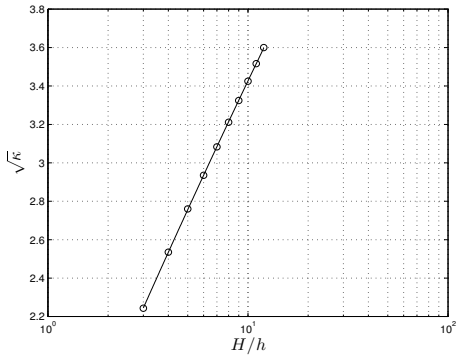

Semilog plot of $x = H/h,\ y = \sqrt{\kappa}$. We have $\eta = h$,; data from Table 3.3.

Table 3.3: Growing H/h; $1/H = 3$; $\eta = 0, h, 2h$; $\mathcal{P}_2/\mathcal{Q}_2 - \mathcal{P}_0$

	$\eta = 0$		$\eta = h$		$\eta = 2h$	
H/h	♯ iterations	condition number	♯ iterations	condition number	♯ iterations	condition number
3	38	1272.3	21	5.0324	20	5.0043
4	39	1345.6	23	6.4258	23	5.8910
5	39	1397.9	25	7.6184	25	7.6188
6	47	1440.0	27	8.6169	27	8.6056
7	44	1475.4	29	9.5066	28	9.4768
8	47	1506.2	30	10.312	29	10.261
9	47	1533.4	30	11.050	31	10.977
10	47	1557.7	31	11.731	31	11.637
11	50	1579.8	32	12.366	32	12.250
12	52	1600.0	33	12.960	32	12.824

Growing H/h for $3 \times 3 \times 3$ subdomains, $\nu = 0.499999$ in the inclusions, $\nu = 0.3$ in the hulls, $E = 210$ on the whole domain, and $\eta = 0, h, 2h$. A thickness of the compressible hull of one element is sufficient to obtain a good condition number;see also Figure 3.14 and 3.15.

3.5.4 Variable ν

We fix $H/h = 7$ and the thickness of the hull to $\eta = h$. The Poisson ratio in the inclusions is varied from $\nu = 0.4$ to $\nu = 0.499999$; see Table 3.4 (left). We see only a slight increase of the condition number and nearly no effect on the number of iterations. The condition number seems to approach a limit once a value of $\nu = 0.49999$ is reached. This clearly confirms that the condition number of the preconditioned FETI-DP method is indeed independent of the almost incompressibility in the inclusions.

The situation is identical if we choose a large Young modulus in the inclusions, i.e., $E = 1e6$, in addition to the almost incompressibility in the inclusions; see Table 3.4 (right).

It is also possible to choose more than one almost incompressible inclusion in a subdomain, see Figure 3.16. For the results, see Table 3.5. There, we have eight inclusions in each subdomain and we vary the Poisson ratio in all eight inclusions from $\nu = 0.4$ to $\nu = 0.499999$. Also for this kind of tests the condition number is quite low and seems to approach a limit.

Figure 3.16:

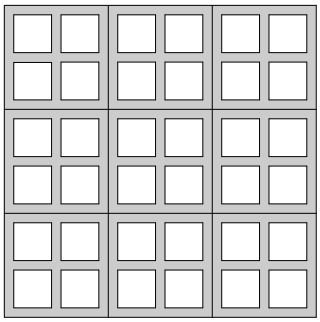

Cross section of a cube with 8 inclusions in each subdomain.

Table 3.4: Growing ν; $H/h = 7$; $1/H = 3$; $\eta = h$; $\mathcal{P}_2/\mathcal{Q}_2 - \mathcal{P}_0$

	inclusions: $E = 210$, ν variable hulls: $E = 210$, $\nu = 0.3$		inclusions: $E = 1e6$, ν variable inclusions: $E = 1$, $\nu = 0.3$	
ν	♯ iterations	condition number	♯ iterations	condition number
0.4	27	9.4841	29	11.188
0.49	28	9.5038	29	11.188
0.499	28	9.5063	30	11.188
0.4999	28	9.5049	30	11.188
0.49999	28	9.5066	31	11.188
0.499999	29	9.5066	32	11.187

Growing ν for $3 \times 3 \times 3$ subdomains, $\eta = h$.The condition number is independent of the Poisson ratio in the inclusions.

Table 3.5: Growing ν; $H/h = 7$; $1/H = 3$; $\eta = h$; $\mathcal{P}_2/\mathcal{Q}_2 - \mathcal{P}_0$; 8 inclusions in each subdomain

ν	♯ iterations	condition number
0.4	27	9.4847
0.49	27	9.5015
0.499	28	9.5025
0.4999	28	9.5041
0.49999	28	9.5041
0.499999	28	9.5041

Growing ν for $3 \times 3 \times 3$ subdomains, $H/h = 7$, and 8 inclusions in each subdomain for which the Poisson ratio is varied. The distance to the subdomain boundary and the distance to between the single inclusions is one element.

3.5.5 Variable Young's Modulus Combined with Almost Incompressibility

Now, we consider configurations of different E and ν as well as some "realistic" material properties for steel and rubber; see Table 3.6.

In a last set of experiments, we consider subdomains with inclusions of a high and low Young modulus, i.e., $E = 1e+4$ and $E = 1e-4$, either combined with a Poisson ratio of $\nu = 0.4$ or $\nu = 0.499999$. The Young modulus on the hull is always $E = 1$ and its Poisson ratio is always $\nu = 0.3$. The four different parameter settings are constructed by the number of the subdomain modulo four; see Figure 3.17. The results in Table 3.7 show that the condition number is quite small even if the thickness of the hull is only $\eta = h$. While this is a favorable result it also means that it is difficult to confirm numerically whether our theoretical bounds are sharp. Theoretically, for the most general configuration of coefficients, we could show an estimate of the condition number $\kappa(M^{-1}F) \leq C \max(1, \mathsf{TOL}) \left(1 + \log\left(\frac{H}{h}\right)\right) \left(1 + \log\left(\frac{\eta}{h}\right)\right) \left(\frac{H}{\eta}\right)^4$; see Theorem 3.18.

Table 3.6: Variable Young's modulus E; $\mathcal{P}_2/\mathcal{Q}_2 - \mathcal{P}_0$

material parameters in the inclusions		material parameters in the hulls		♯ iterations	condition
E	ν	E	ν		number
1e+6	0.3	1	0.3	23	6.4083
1e+6	0.3	10	0.3	23	6.3666
1e+6	0.3	1e-1	0.3	24	6.4087
1e+6	0.3	1e-2	0.3	24	6.4113
1e+6	0.3	1e-3	0.3	24	6.4136
1e+6	0.499999	1	0.3	25	6.4163
1e+6	0.499999	10	0.3	24	6.4098
1e+6	0.499999	1e-1	0.3	26	6.4188
1e+6	0.499999	1e-2	0.3	26	6.4652
1e+6	0.499999	1e-3	0.3	28	7.2075
steel		rubber			
21e5	0.28	0.037e5	0.485	44	18.249
rubber		steel			
0.037e5	0.485	21e5	0.28	22	5.651

Variable Young's modulus E for $3 \times 3 \times 3$ subdomains, $H/h = 4$ elements in each direction in each subdomain, and $\eta = h$. The material parameters for steel and rubber are taken from Ciarlet [8].

Figure 3.17:

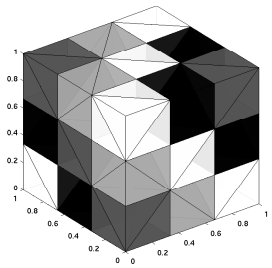

Table 3.7: Growing η; $H/h = 7$; $1/H = 3$; $\mathcal{P}_2/\mathcal{Q}_2 - \mathcal{P}_0$

distance η	♯ iterations	condition number
$1h$	36	11.956
$2h$	29	9.2575
$3h$	29	9.4767
$4h$	27	9.4812
0	> 250	13426

Growing η for $3 \times 3 \times 3$ subdomains. Four different kind of material parameter settings in the inclusions: $E = 1e+4, \nu = 0.4$, $E = 1e-4, \nu = 0.4$, $E = 1e+4, \nu = 0.499999$, $E = 1e-4, \nu = 0.499999$; and for the hulls: $E = 1, \nu = 0.3$.

3.5.6 $\mathcal{P}_2 - \mathcal{P}_0$ Mixed Finite Elements

For our theory, and also for the numerical tests presented before, we use different finite elements for the discretization of the inclusions and the hulls, namely tetrahedra for the hulls and hexahedra for the inclusions. The discretization of $\mathcal{Q}_2 - \mathcal{P}_0$ mixed finite elements is known to be inf-sup stable. We obtain similar numerical results when using $\mathcal{P}_2 - \mathcal{P}_0$ mixed finite elements as a discretization of the mixed formulation for the whole domain Ω. Although these elements are not known to be inf-sup stable in 3D. We present some numerical results in Tables 3.8 and 3.9. Let us note that these experiments are not contained in [22] due to space limitations.

Table 3.8: Growing H/h; $1/H = 3$; $\eta = 0, h, 2h$; $\mathcal{P}_2 - \mathcal{P}_0$

	$\eta = 0$		$\eta = h$		$\eta = 2h$	
H/h	♯ iterations	condition number	♯ iterations	condition number	♯ iterations	condition number
3	>250	8.528e3	22	5.0473	22	5.0129
4	119	7.610e3	22	5.9201	22	5.8386
5	>250	8.883e3	26	6.9857	26	6.9250
6	131	8.381e3	26	7.7942	26	8.1296
7	>250	9.161e3	29	9.2377	29	9.1877
8	136	8.929e3	28	9.8677	28	9.7968
9	>250	9.468e3	31	10.775	30	10.681
10	139	9.352e3	30	11.294	30	11.182

Growing H/h for $3 \times 3 \times 3$ subdomains. For $\eta = 0$, i.e., the complete domain is almost incompressible; $\nu = 0.499999$ and $E = 210$. The condition number is large since we use a coarse space designed for compressible elasticity. But it is striking that a hull of thickness of one element, i.e., $\eta = h$, is sufficient to obtain a good condition number, which is hardly improved by increasing the thickness by one further element.

Table 3.9: Growing ν; $H/h = 7$; $1/H = 3$; $\eta = h$; $\mathcal{P}_2 - \mathcal{P}_0$

	inclusions: $E = 210$, ν variable hulls: $E = 210$, $\nu = 0.3$		inclusions: $E = 1e6$, ν variable inclusions: $E = 1$, $\nu = 0.3$	
ν	♯ iterations	condition number	♯ iterations	condition number
0.4	28	8.5581	29	10.681
0.49	28	8.6064	29	10.681
0.499	28	8.6997	29	10.681
0.4999	29	8.7237	30	10.681
0.49999	29	9.1683	30	10.681
0.499999	29	9.2377	31	10.681
0.4999999	29	9.2377	31	10.669
0.49999999	29	9.2378	31	10.767
0.499999999	29	9.2379	32	10.543

Growing ν for $3 \times 3 \times 3$ subdomains, $\eta = h$.The condition number is independent of the almost incompressibility in the inclusion.

4 A New Coarse Space for Almost Incompressible Linear Elasticity

In the previous chapter we discussed linear elasticity problems with varying coefficients inside subdomains. There, we had a compressible matrix material within the hulls, which means we had a compressible neighborhood of the interface, such that we could use the standard coarse space for FETI-DP; see [22]. Now, we expand the analysis and therein the coarse space for the FETI-DP algorithm to the case, where we have an almost incompressible material on the whole domain; see also [21, Section 3]. To establish again a polylogarithmic condition number estimate for the preconditioned FETI-DP system, we need to control the rigid body modes on each face; see, e.g., [15, 50, 42]. We consider the mixed formulation, which has been introduced in Chapter 1. From [50, Lemma 3.1] or [15, Lemma 3.3] it follows that we have to impose the following zero net flux constraint

$$\int_{\partial\Omega_i} \underbrace{\left(R^{(i)} P_D w\right)}_{=:\, v^{(i)}} \cdot n \, ds = 0 \tag{4.1}$$

on each subdomain Ω_i To implement these additional constraints, we discuss two strategies. Both strategies have in common that the zero net flux condition for a subdomain is separated into constraints for each, face and edge terms. Note, that vertex terms need not to be considered since vertices are set to be primal. Additionally, in both approaches, we use projector preconditioning to establish the face constraints, i.e., instead of solving $B_B u_B = 0$ with a conjugate gradient algorithm, we iterate on $U^T B_B u_B = 0$, where the rows of U^T contain the net flux over faces; see [33] or Section 2.5 for the concept of projector preconditioning and deflation in the context of FETI-DP methods. Traditionally, in FETI-DP and BDDC methods, one normal constraint for each face is then used to enforce the zero net flux; see [42, 35, 13, 50]. In the early works [23, 24] for Neumann-Neumann methods for incompressible elasticity a coarse pressure was introduced on each subdomain.

In our new coarse space a single face constraint for each subdomain is sufficient. This

single face constraint is obtained by summing up the face contributions of each subdomain and therefore the generated new coarse space is much smaller; cf. Section 4.1.

The considered strategies here only differ in establishing the edge constraints. In the first approach, cf. Section 4.2.1, we will use primal edge averages in the normal directions to enforce the zero net flux condition for the edge terms, using a transformation of basis; see, e.g., [30, 26]. In a second approach, cf. Section 4.2.2, the zero net flux condition for edges is also enforced by projector preconditioning.

For the analysis of the zero net flux condition, we first assume that all vertices are primal. Then,

$$\begin{aligned} v^{(i)} &= \sum_{\mathcal{F}^{ij}\subset\partial\Omega_i} I^h\left(\theta_{\mathcal{F}^{ij}} v^{(i)}\right) + \sum_{\mathcal{E}^{ik}\subset\partial\Omega_i} I^h\left(\theta_{\mathcal{E}^{ik}} v^{(i)}\right) \\ &= \sum_{\mathcal{F}^{ij}\subset\partial\Omega_i} I^h\left(\theta_{\mathcal{F}^{ij}}\delta_j^\dagger(w^{(i)}-w^{(j)})\right) \\ &\quad + \sum_{\mathcal{E}^{ik}\subset\partial\Omega_i} \Big\{ I^h\left(\theta_{\mathcal{E}^{ik}}\delta_j^\dagger(w^{(i)}-w^{(j)})\right) + I^h\left(\theta_{\mathcal{E}^{ik}}\delta_k^\dagger(w^{(i)}-w^{(k)})\right) \\ &\quad + I^h\left(\theta_{\mathcal{E}^{ik}}\delta_l^\dagger(w^{(i)}-w^{(l)})\right)\Big\}. \end{aligned}$$

This means for the constraint

$$\begin{aligned} 0 &= \int_{\partial\Omega_i}\left(R^{(i)}P_D w\right)\cdot n\; ds \\ &= \sum_{\mathcal{F}^{ij}\subset\partial\Omega_i}\int_{\partial\Omega_i}[I^h\left(\theta_{\mathcal{F}^{ij}}\delta_j^\dagger(w^{(i)}-w^{(j)})\right)]\cdot n\; ds \\ &\quad + \sum_{\mathcal{E}^{ik}\subset\partial\Omega_i}\Big\{\int_{\partial\Omega_i}[I^h\left(\theta_{\mathcal{E}^{ik}}\delta_j^\dagger(w^{(i)}-w^{(j)})\right)]\cdot n\; ds \\ &\quad + \int_{\partial\Omega_i}[I^h\left(\theta_{\mathcal{E}^{ik}}\delta_k^\dagger(w^{(i)}-w^{(k)})\right)]\cdot n\; ds + \int_{\partial\Omega_i}[I^h\left(\theta_{\mathcal{E}^{ik}}\delta_l^\dagger(w^{(i)}-w^{(l)})\right)]\cdot n\; ds\Big\}. \end{aligned}$$

To fulfill this condition, we consider the face and edge terms separately.

4.1 Zero Net Flux for Face Terms

We will establish the zero net flux for face constraints by projector preconditioning; see e.g., [33, 26] for further references.

$$
\begin{aligned}
&\sum_{\mathcal{F}^{ij}\subset\partial\Omega_i}\int_{\partial\Omega_i}[I^h\left(\theta_{\mathcal{F}^{ij}}\delta_j^\dagger(w^{(i)}-w^{(j)})\right)]\cdot n\ ds\\
=&\sum_{\mathcal{F}^{ij}\subset\partial\Omega_i}\int_{\partial\Omega_i}\sum_{x\in\mathcal{F}_h^{ij}}\delta_j^\dagger\left(w^{(i)}-w^{(j)}\right)(x)\ \ \varphi_x\cdot n\ ds\\
=&\sum_{\mathcal{F}^{ij}\subset\partial\Omega_i}\sum_{x\in\mathcal{F}_h^{ij}}\int_{\partial\Omega_i}\delta_j^\dagger\begin{pmatrix}\left(w_1^{(i)}-w_1^{(j)}\right)(x)\ \ \varphi_x^{(1)}\\ \left(w_2^{(i)}-w_2^{(j)}\right)(x)\ \ \varphi_x^{(2)}\\ \left(w_3^{(i)}-w_3^{(j)}\right)(x)\ \ \varphi_x^{(3)}\end{pmatrix}\cdot\begin{pmatrix}n_1\\ n_2\\ n_3\end{pmatrix}ds\\
=&\sum_{\mathcal{F}^{ij}\subset\partial\Omega_i}\sum_{x\in\mathcal{F}_h^{ij}}\left\{\int_{\partial\Omega_i}\delta_j^\dagger\ n_1\left(w_1^{(i)}-w_1^{(j)}\right)(x)\ \ \varphi_x^{(1)}\ ds\right.\\
&\left.+\int_{\partial\Omega_i}\delta_j^\dagger\ n_2\left(w_2^{(i)}-w_2^{(j)}\right)(x)\ \ \varphi_x^{(2)}\ ds+\int_{\partial\Omega_i}\delta_j^\dagger\ n_3\left(w_3^{(i)}-w_3^{(j)}\right)(x)\ \ \varphi_x^{(3)}\ ds\right\}
\end{aligned}
$$

For all of those integrals we integrate for all $x\in\mathcal{F}_h^{ij}$ over $\partial\Omega_i\cap\mathrm{supp}(\varphi_x)\subset\mathcal{F}^{ij}$; cf. Figure 4.1. Thus, we obtain

Figure 4.1:

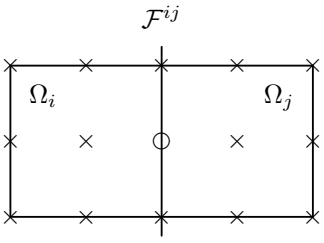

A cross section of a face shared by two subdomains Ω_i and Ω_j, containing one element each. The support of a shape function corresponding to each node on a face, here denoted by the circle, is a subset of the face.

$$
\begin{aligned}
&\sum_{\mathcal{F}^{ij}\subset\partial\Omega_i}\sum_{x\in\mathcal{F}_h^{ij}}\left\{\int_{\mathcal{F}^{ij}}\delta_j^\dagger\ n_1^{(j)}\left(w_1^{(i)}-w_1^{(j)}\right)(x)\ \ \varphi_x^{(1)}\ ds\right.\\
&\left.+\int_{\mathcal{F}^{ij}}\delta_j^\dagger\ n_2^{(j)}\left(w_2^{(i)}-w_2^{(j)}\right)(x)\ \ \varphi_x^{(2)}\ ds+\int_{\mathcal{F}^{ij}}\delta_j^\dagger\ n_3^{(j)}\left(w_3^{(i)}-w_3^{(j)}\right)(x)\ \ \varphi_x^{(3)}\ ds\right\},
\end{aligned}
$$

where $n^{(j)}$ specifies the outer normal in the direction of subdomain Ω_j. Using the short notation

$$\left(\begin{array}{ccc} a, & b, & c \end{array} \right) := \left(\begin{array}{ccc} \int_{\mathcal{F}^{ij}} \delta_j^\dagger \, n_1^{(j)} \, \varphi_x^{(1)} \, ds, & \int_{\mathcal{F}^{ij}} \delta_j^\dagger \, n_2^{(j)} \, \varphi_x^{(2)} \, ds, & \int_{\mathcal{F}^{ij}} \delta_j^\dagger \, n_3^{(j)} \, \varphi_x^{(3)} \, ds \end{array} \right),$$

we have

$$\begin{aligned} & \sum_{\mathcal{F}^{ij} \subset \partial\Omega_i} \sum_{x \in \mathcal{F}_h^{ij}} \left(\begin{array}{ccc} a, & b, & c \end{array} \right) \begin{pmatrix} \left(w_1^{(i)} - w_1^{(j)}\right)(x) \\ \left(w_2^{(i)} - w_2^{(j)}\right)(x) \\ \left(w_3^{(i)} - w_3^{(j)}\right)(x) \end{pmatrix} \\ = \; & U^T B_B u_B = 0, \end{aligned}$$

where $\sum_{\mathcal{F}^{ij} \subset \partial\Omega_i} \sum_{x \in \mathcal{F}_h^{ij}} \left(\begin{array}{ccc} \int_{\mathcal{F}^{ij}} \delta_j^\dagger \, n_1^{(j)} \, \varphi_x^{(1)} \, ds, & \int_{\mathcal{F}^{ij}} \delta_j^\dagger \, n_2^{(j)} \, \varphi_x^{(2)} \, ds, & \int_{\mathcal{F}^{ij}} \delta_j^\dagger \, n_3^{(j)} \, \varphi_x^{(3)} \, ds \end{array} \right)$ builds one row in U^T. Hence, the zero net flux condition for the face terms can be enforced by one constraint for each subdomain.

Note, that the traditional strategy, as e.g., known from [13, 35, 42, 41], is to enforce a stronger condition, i.e., a single constraint for each face. Instead of ensuring the sum over all face contributions belonging to one subdomain to be zero, we force each additive term to be zero independently. Then, we obtain one constraint for each face, such that

$$\sum_{x \in \mathcal{F}_h^{ij}} \left(\begin{array}{ccc} a, & b, & c \end{array} \right) \begin{pmatrix} \left(w_1^{(i)} - w_1^{(j)}\right)(x) \\ \left(w_2^{(i)} - w_2^{(j)}\right)(x) \\ \left(w_3^{(i)} - w_3^{(j)}\right)(x) \end{pmatrix} = 0,$$

which also satisfies the zero net flux condition.
Obviously, summing up the face contributions result in a smaller coarse space.

4.2 Zero Net Flux for Edge Terms

The zero net flux condition for the face terms is always enforced by projector preconditioning. For the edge terms we consider two possibilities to establish the zero net flux. Using the concept of a transformation of basis with partial assembly will work as well as expected from the theory. But using projector preconditioning, we obtain a good condition number only by enforcing a stronger condition; cf. Section 4.2.2.

4.2.1 Transformation of Basis

To enforce edge averages as primal constraints and hence the zero net flux condition for edges, i.e., edge averages in each component and direction of the displacement, we use a transformation of basis with partial assembly. In contrast to the well-known concept of transformation of basis with partial assembly for linear shape functions, see e.g., [37, 30], we use quadratic shape functions. The difference results in the values of the entries in the transformation matrix; see Figures 4.2 and 4.3.

We consider one edge of the reference element $[-1,1]^3$, i.e., three shape functions corresponding to the three nodes on that edge. Here, we consider the nodes $P_1 = (-1,-1,-1)\,,\ P_2 = (-1,0,-1)\,,\ P_3 = (-1,1,-1)\,$, where P_1 and P_3 are the endpoints and P_2 is the midpoint of an edge of the reference element. We integrate the corresponding shape functions over this edge, i.e.,

$$\begin{aligned}
\frac{\int_{-1}^{1} \varphi_1 \, dy}{\int_{-1}^{1} 1 \, dy} &= \frac{\frac{1}{2}\int_{-1}^{1} y^2 - y \, dy}{\int_{-1}^{1} 1 \, dy} = \frac{1}{6} \\
\frac{\int_{-1}^{1} \varphi_2 \, dy}{\int_{-1}^{1} 1 \, dy} &= \frac{\int_{-1}^{1} 1 - y^2 \, dy}{\int_{-1}^{1} 1 \, dy} = \frac{2}{3} \\
\frac{\int_{-1}^{1} \varphi_3 \, dy}{\int_{-1}^{1} 1 \, dy} &= \frac{\frac{1}{2}\int_{-1}^{1} y + y^2 \, dy}{\int_{-1}^{1} 1 \, dy} = \frac{1}{6}.
\end{aligned}$$

By assembly of the element edges, we obtain a weight of $2/3$ to $1/3$ from the midpoints to the endpoints of the element edges; see Figure 4.3.

Figure 4.2:

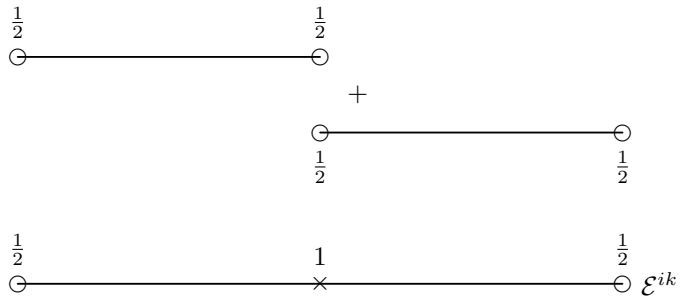

Transformation of basis for $\mathcal{P}_1$. Weights for element edges and the result after assembling.

This means, in our transformation matrix, we set $1/3$ for the endpoints of the element edges and $2/3$ as the value for the midpoints of element edges. Using this transformation of

basis, we automatically enforce the zero net flux condition for each edge in each direction of the displacement.

Figure 4.3:

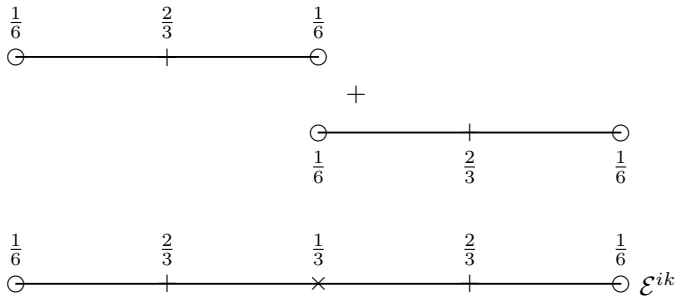

Transformation of basis for $\mathcal{P}_2$. Weights for element edges and the result after assembling.

4.2.2 Projector Preconditioning

In a second approach we establish the zero net flux condition for the edge terms by projector preconditioning. For simplicity, we first consider one edge and one jump direction, i.e., the jump between Ω_i and Ω_k; cf. Figure 4.4. Then,

$$
\begin{aligned}
&\int_{\partial\Omega_i} [I^h\left(\theta_{\mathcal{E}^{ik}}\delta_k^\dagger(w^{(i)}-w^{(k)})\right)]\cdot n\ ds \\
=\ &\int_{\partial\Omega_i}\sum_{x\in\mathcal{E}_h^{ik}}\delta_k^\dagger\left(w^{(i)}-w^{(k)}\right)(x)\varphi_x\cdot n\ ds \\
=\ &\sum_{x\in\mathcal{E}_h^{ik}}\int_{\partial\Omega_i}\delta_k^\dagger\begin{pmatrix}\left(w_1^{(i)}-w_1^{(k)}\right)(x) & \varphi_x^{(1)}\\ \left(w_2^{(i)}-w_2^{(k)}\right)(x) & \varphi_x^{(2)}\\ \left(w_3^{(i)}-w_3^{(k)}\right)(x) & \varphi_x^{(3)}\end{pmatrix}\cdot\begin{pmatrix}n_1\\ n_2\\ n_3\end{pmatrix}\ ds \\
=\ &\sum_{x\in\mathcal{E}_h^{ik}}\int_{\partial\Omega_i}\delta_k^\dagger\ n_1\left(w_1^{(i)}-w_1^{(k)}\right)(x)\ \ \varphi_x^{(1)}\ ds+\int_{\partial\Omega_i}\delta_k^\dagger\ n_2\left(w_2^{(i)}-w_2^{(k)}\right)(x)\ \ \varphi_x^{(2)}\ ds \\
&+\int_{\partial\Omega_i}\delta_k^\dagger\ n_3\left(w_3^{(i)}-w_3^{(k)}\right)(x)\ \ \varphi_x^{(3)}\ ds.
\end{aligned}
$$

Again the integrals only have a nonzero value in the intersection of $\partial\Omega_i$ with the support of φ_x. It is $\mathrm{supp}(\varphi_x)\subset\Omega_i\cup\Omega_j\cup\Omega_k\cup\Omega_l$ for all $x\in\mathcal{E}_h^{ik}$ since each subdomain contains one element; see Figure 4.4. Therefore, $\partial\Omega_i\cap\mathrm{supp}(\varphi_x)\subset\mathcal{F}^{ij}\cup\mathcal{F}^{il}$ for the jump between Ω_i and Ω_k. And we have, for one component

Figure 4.4:

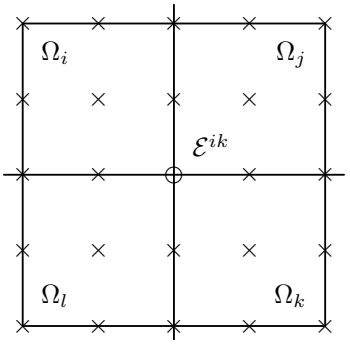

A cross section of an edge shared by four subdomains. The support of a basis function corresponding to a node on that edge, is a subset of the union of all subdomains.

$$
\begin{aligned}
&\int_{\partial\Omega_i} \delta_k^\dagger \; n_1 \left(w_1^{(i)} - w_1^{(k)} \right)(x) \;\; \varphi_x^{(1)} \; ds \\
= &\int_{\partial\Omega_i \cap \mathrm{supp}(\varphi_x^{(1)})} \delta_k^\dagger \; n_1 \left(w_1^{(i)} - w_1^{(k)} \right)(x) \;\; \varphi_x^{(1)} \; ds \\
= &\int_{\mathcal{F}^{ij}} \delta_k^\dagger \; n_1^{(j)} \left(w_1^{(i)} - w_1^{(k)} \right)(x) \;\; \varphi_x^{(1)} \; ds + \int_{\mathcal{F}^{il}} \delta_k^\dagger \; n_1^{(l)} \left(w_1^{(i)} - w_1^{(k)} \right)(x) \;\; \varphi_x^{(1)} \; ds.
\end{aligned}
$$

Thus, for all three components of a single jump, we obtain

$$
\begin{aligned}
\sum_{x \in \mathcal{E}_h^{ik}} &\int_{\mathcal{F}^{ij}} \delta_k^\dagger \; n_1^{(j)} \left(w_1^{(i)} - w_1^{(k)} \right)(x) \;\; \varphi_x^{(1)} \; ds \;\; + \;\; \int_{\mathcal{F}^{il}} \delta_k^\dagger \; n_1^{(l)} \left(w_1^{(i)} - w_1^{(k)} \right)(x) \;\; \varphi_x^{(1)} \; ds \\
&+ \int_{\mathcal{F}^{ij}} \delta_k^\dagger \; n_2^{(j)} \left(w_2^{(i)} - w_2^{(k)} \right)(x) \;\; \varphi_x^{(2)} \; ds \;\; + \;\; \int_{\mathcal{F}^{il}} \delta_k^\dagger \; n_2^{(l)} \left(w_2^{(i)} - w_2^{(k)} \right)(x) \;\; \varphi_x^{(2)} \; ds \\
&+ \int_{\mathcal{F}^{ij}} \delta_k^\dagger \; n_3^{(j)} \left(w_3^{(i)} - w_3^{(k)} \right)(x) \;\; \varphi_x^{(3)} \; ds \;\; + \;\; \int_{\mathcal{F}^{il}} \delta_k^\dagger \; n_3^{(l)} \left(w_3^{(i)} - w_3^{(k)} \right)(x) \;\; \varphi_x^{(3)} \; ds.
\end{aligned}
$$

Considering all jumps associated with a single edge, we have

$$
\begin{aligned}
&\int_{\partial\Omega_i} [I^h \left(\theta_{\mathcal{E}^{ik}} \delta_j^\dagger (w^{(i)} - w^{(j)}) \right)] \cdot n \; ds \;\; + \;\; \int_{\partial\Omega_i} [I^h \left(\theta_{\mathcal{E}^{ik}} \delta_k^\dagger (w^{(i)} - w^{(k)}) \right)] \cdot n \; ds \\
&+ \int_{\partial\Omega_i} [I^h \left(\theta_{\mathcal{E}^{ik}} \delta_l^\dagger (w^{(i)} - w^{(l)}) \right)] \cdot n \; ds \\
= \sum_{x \in \mathcal{E}_h^{ik}} &\int_{\mathcal{F}^{ij}} \delta_j^\dagger \; n_1^{(j)} \left(w_1^{(i)} - w_1^{(j)} \right)(x) \;\; \varphi_x^{(1)} \; ds \;\; + \;\; \int_{\mathcal{F}^{il}} \delta_j^\dagger \; n_1^{(l)} \left(w_1^{(i)} - w_1^{(j)} \right)(x) \;\; \varphi_x^{(1)} \; ds \\
&+ \int_{\mathcal{F}^{ij}} \delta_j^\dagger \; n_2^{(j)} \left(w_2^{(i)} - w_2^{(j)} \right)(x) \;\; \varphi_x^{(2)} \; ds \;\; + \;\; \int_{\mathcal{F}^{il}} \delta_j^\dagger \; n_2^{(l)} \left(w_2^{(i)} - w_2^{(j)} \right)(x) \;\; \varphi_x^{(2)} \; ds
\end{aligned}
$$

$$
\begin{aligned}
&+\int_{\mathcal{F}^{ij}} \delta_j^\dagger\ n_3^{(j)} \left(w_3^{(i)} - w_3^{(j)}\right)(x)\ \ \varphi_x^{(3)}\ ds \quad + \quad \int_{\mathcal{F}^{il}} \delta_j^\dagger\ n_3^{(l)} \left(w_3^{(i)} - w_3^{(j)}\right)(x)\ \ \varphi_x^{(3)}\ ds \\
&+\int_{\mathcal{F}^{ij}} \delta_k^\dagger\ n_1^{(j)} \left(w_1^{(i)} - w_1^{(k)}\right)(x)\ \ \varphi_x^{(1)}\ ds \quad + \quad \int_{\mathcal{F}^{il}} \delta_k^\dagger\ n_1^{(l)} \left(w_1^{(i)} - w_1^{(k)}\right)(x)\ \ \varphi_x^{(1)}\ ds \\
&+\int_{\mathcal{F}^{ij}} \delta_k^\dagger\ n_2^{(j)} \left(w_2^{(i)} - w_2^{(k)}\right)(x)\ \ \varphi_x^{(2)}\ ds \quad + \quad \int_{\mathcal{F}^{il}} \delta_k^\dagger\ n_2^{(l)} \left(w_2^{(i)} - w_2^{(k)}\right)(x)\ \ \varphi_x^{(2)}\ ds \\
&+\int_{\mathcal{F}^{ij}} \delta_k^\dagger\ n_3^{(j)} \left(w_3^{(i)} - w_3^{(k)}\right)(x)\ \ \varphi_x^{(3)}\ ds \quad + \quad \int_{\mathcal{F}^{il}} \delta_k^\dagger\ n_3^{(l)} \left(w_3^{(i)} - w_3^{(k)}\right)(x)\ \ \varphi_x^{(3)}\ ds \\
&+\int_{\mathcal{F}^{ij}} \delta_l^\dagger\ n_1^{(j)} \left(w_1^{(i)} - w_1^{(l)}\right)(x)\ \ \varphi_x^{(1)}\ ds \quad + \quad \int_{\mathcal{F}^{il}} \delta_l^\dagger\ n_1^{(l)} \left(w_1^{(i)} - w_1^{(l)}\right)(x)\ \ \varphi_x^{(1)}\ ds \\
&+\int_{\mathcal{F}^{ij}} \delta_l^\dagger\ n_2^{(j)} \left(w_2^{(i)} - w_2^{(l)}\right)(x)\ \ \varphi_x^{(2)}\ ds \quad + \quad \int_{\mathcal{F}^{il}} \delta_l^\dagger\ n_2^{(l)} \left(w_2^{(i)} - w_2^{(l)}\right)(x)\ \ \varphi_x^{(2)}\ ds \\
&+\int_{\mathcal{F}^{ij}} \delta_l^\dagger\ n_3^{(j)} \left(w_3^{(i)} - w_3^{(l)}\right)(x)\ \ \varphi_x^{(3)}\ ds \quad + \quad \int_{\mathcal{F}^{il}} \delta_l^\dagger\ n_3^{(l)} \left(w_3^{(i)} - w_3^{(l)}\right)(x)\ \ \varphi_x^{(3)}\ ds.
\end{aligned}
$$

To simplify our notation, we define

$$
\begin{aligned}
A &:= \int_{\mathcal{F}^{ij}} \delta_j^\dagger\ n_1^{(j)} \varphi_x^{(1)}\ ds + \int_{\mathcal{F}^{il}} \delta_j^\dagger\ n_1^{(l)} \varphi_x^{(1)}\ ds, \\
B &:= \int_{\mathcal{F}^{ij}} \delta_j^\dagger\ n_2^{(j)} \varphi_x^{(2)}\ ds + \int_{\mathcal{F}^{il}} \delta_j^\dagger\ n_2^{(l)} \varphi_x^{(2)}\ ds, \\
C &:= \int_{\mathcal{F}^{ij}} \delta_j^\dagger\ n_3^{(j)} \varphi_x^{(3)}\ ds + \int_{\mathcal{F}^{il}} \delta_j^\dagger\ n_3^{(l)} \varphi_x^{(3)}\ ds \\
D &:= \int_{\mathcal{F}^{ij}} \delta_k^\dagger\ n_1^{(j)} \varphi_x^{(1)}\ ds + \int_{\mathcal{F}^{il}} \delta_k^\dagger\ n_1^{(l)} \varphi_x^{(1)}\ ds, \\
E &:= \int_{\mathcal{F}^{ij}} \delta_k^\dagger\ n_2^{(j)} \varphi_x^{(2)}\ ds + \int_{\mathcal{F}^{il}} \delta_k^\dagger\ n_2^{(l)} \varphi_x^{(2)}\ ds, \\
F &:= \int_{\mathcal{F}^{ij}} \delta_k^\dagger\ n_3^{(j)} \varphi_x^{(3)}\ ds + \int_{\mathcal{F}^{il}} \delta_k^\dagger\ n_3^{(l)} \varphi_x^{(3)}\ ds \\
G &:= \int_{\mathcal{F}^{ij}} \delta_l^\dagger\ n_1^{(j)} \varphi_x^{(1)}\ ds + \int_{\mathcal{F}^{il}} \delta_l^\dagger\ n_1^{(l)} \varphi_x^{(1)}\ ds, \\
H &:= \int_{\mathcal{F}^{ij}} \delta_l^\dagger\ n_2^{(j)} \varphi_x^{(2)}\ ds + \int_{\mathcal{F}^{il}} \delta_l^\dagger\ n_2^{(l)} \varphi_x^{(2)}\ ds, \\
J &:= \int_{\mathcal{F}^{ij}} \delta_l^\dagger\ n_3^{(j)} \varphi_x^{(3)}\ ds + \int_{\mathcal{F}^{il}} \delta_l^\dagger\ n_3^{(l)} \varphi_x^{(3)}\ ds.
\end{aligned}
$$

Then, the zero net flux condition results in one constraint for each subdomain, i.e.,

$$
\begin{pmatrix} A, & B, & C \end{pmatrix}
\begin{pmatrix}
\left(w_1^{(i)} - w_1^{(j)}\right)(x) \\
\left(w_2^{(i)} - w_2^{(j)}\right)(x) \\
\left(w_3^{(i)} - w_3^{(j)}\right)(x)
\end{pmatrix}
$$

$$
\begin{aligned}
&+\begin{pmatrix} D, & E, & F \end{pmatrix}
\begin{pmatrix}
\left(w_1^{(i)} - w_1^{(k)}\right)(x) \\
\left(w_2^{(i)} - w_2^{(k)}\right)(x) \\
\left(w_3^{(i)} - w_3^{(k)}\right)(x)
\end{pmatrix} \\
&+\begin{pmatrix} G, & H, & J \end{pmatrix}
\begin{pmatrix}
\left(w_1^{(i)} - w_1^{(l)}\right)(x) \\
\left(w_2^{(i)} - w_2^{(l)}\right)(x) \\
\left(w_3^{(i)} - w_3^{(l)}\right)(x)
\end{pmatrix} \\
= &\begin{pmatrix} A, & B, & C, & D, & E, & F, & G, & H, & J \end{pmatrix}
\begin{pmatrix}
\left(w_1^{(i)} - w_1^{(j)}\right)(x) \\
\left(w_2^{(i)} - w_2^{(j)}\right)(x) \\
\left(w_3^{(i)} - w_3^{(j)}\right)(x) \\
\left(w_1^{(i)} - w_1^{(k)}\right)(x) \\
\left(w_2^{(i)} - w_2^{(k)}\right)(x) \\
\left(w_3^{(i)} - w_3^{(k)}\right)(x) \\
\left(w_1^{(i)} - w_1^{(l)}\right)(x) \\
\left(w_2^{(i)} - w_2^{(l)}\right)(x) \\
\left(w_3^{(i)} - w_3^{(l)}\right)(x)
\end{pmatrix}.
\end{aligned}
$$

It should be sufficient to establish the zero net flux condition (4.1) for the edge terms by one single constraint. But so far the numerical results do not correspond to this, i.e., the tests result in a large condition number.

Enforcing a stronger condition, i.e., enforcing each face integral to be zero, results in

$$
\begin{aligned}
&\begin{pmatrix}
\int_{\mathcal{F}^{ij}} \delta_j^\dagger \, n_1^{(j)} \varphi_x^{(1)} \, ds, & \int_{\mathcal{F}^{ij}} \delta_j^\dagger \, n_2^{(j)} \varphi_x^{(2)} \, ds, & \int_{\mathcal{F}^{ij}} \delta_j^\dagger \, n_3^{(j)} \varphi_x^{(3)} \, ds \\
\int_{\mathcal{F}^{il}} \delta_j^\dagger \, n_1^{(l)} \varphi_x^{(1)} \, ds, & \int_{\mathcal{F}^{il}} \delta_j^\dagger \, n_2^{(l)} \varphi_x^{(2)} \, ds, & \int_{\mathcal{F}^{il}} \delta_j^\dagger \, n_3^{(l)} \varphi_x^{(3)} \, ds
\end{pmatrix}
\begin{pmatrix}
\left(w_1^{(i)} - w_1^{(j)}\right)(x) \\
\left(w_2^{(i)} - w_2^{(j)}\right)(x) \\
\left(w_3^{(i)} - w_3^{(j)}\right)(x)
\end{pmatrix} \\
&+\begin{pmatrix}
\int_{\mathcal{F}^{ij}} \delta_k^\dagger \, n_1^{(j)} \varphi_x^{(1)} \, ds, & \int_{\mathcal{F}^{ij}} \delta_k^\dagger \, n_2^{(j)} \varphi_x^{(2)} \, ds, & \int_{\mathcal{F}^{ij}} \delta_k^\dagger \, n_3^{(j)} \varphi_x^{(3)} \, ds \\
\int_{\mathcal{F}^{il}} \delta_k^\dagger \, n_1^{(l)} \varphi_x^{(1)} \, ds, & \int_{\mathcal{F}^{il}} \delta_k^\dagger \, n_2^{(l)} \varphi_x^{(2)} \, ds, & \int_{\mathcal{F}^{il}} \delta_k^\dagger \, n_3^{(l)} \varphi_x^{(3)} \, ds
\end{pmatrix}
\begin{pmatrix}
\left(w_1^{(i)} - w_1^{(k)}\right)(x) \\
\left(w_2^{(i)} - w_2^{(k)}\right)(x) \\
\left(w_3^{(i)} - w_3^{(k)}\right)(x)
\end{pmatrix} \\
&+\begin{pmatrix}
\int_{\mathcal{F}^{ij}} \delta_l^\dagger \, n_1^{(j)} \varphi_x^{(1)} \, ds, & \int_{\mathcal{F}^{ij}} \delta_l^\dagger \, n_2^{(j)} \varphi_x^{(2)} \, ds, & \int_{\mathcal{F}^{ij}} \delta_l^\dagger \, n_3^{(j)} \varphi_x^{(3)} \, ds \\
\int_{\mathcal{F}^{il}} \delta_l^\dagger \, n_1^{(l)} \varphi_x^{(1)} \, ds, & \int_{\mathcal{F}^{il}} \delta_l^\dagger \, n_2^{(l)} \varphi_x^{(2)} \, ds, & \int_{\mathcal{F}^{il}} \delta_l^\dagger \, n_3^{(l)} \varphi_x^{(3)} \, ds
\end{pmatrix}
\begin{pmatrix}
\left(w_1^{(i)} - w_1^{(l)}\right)(x) \\
\left(w_2^{(i)} - w_2^{(l)}\right)(x) \\
\left(w_3^{(i)} - w_3^{(l)}\right)(x)
\end{pmatrix}
\end{aligned}
$$

$$
\begin{aligned}
=: \quad & \begin{pmatrix} a_1 & a_2 & a_3 \\ b_1 & b_2 & b_3 \end{pmatrix} \begin{pmatrix} \left(w_1^{(i)} - w_1^{(j)}\right)(x) \\ \left(w_2^{(i)} - w_2^{(j)}\right)(x) \\ \left(w_3^{(i)} - w_3^{(j)}\right)(x) \end{pmatrix} + \begin{pmatrix} c_1 & c_2 & c_3 \\ d_1 & d_2 & d_3 \end{pmatrix} \begin{pmatrix} \left(w_1^{(i)} - w_1^{(k)}\right)(x) \\ \left(w_2^{(i)} - w_2^{(k)}\right)(x) \\ \left(w_3^{(i)} - w_3^{(k)}\right)(x) \end{pmatrix} \\
& + \begin{pmatrix} e_1 & e_2 & e_3 \\ f_1 & f_2 & f_3 \end{pmatrix} \begin{pmatrix} \left(w_1^{(i)} - w_1^{(l)}\right)(x) \\ \left(w_2^{(i)} - w_2^{(l)}\right)(x) \\ \left(w_3^{(i)} - w_3^{(l)}\right)(x) \end{pmatrix} \\
= \quad & \begin{pmatrix} a_1 & a_2 & a_3 & & & & & & \\ b_1 & b_2 & b_3 & & & & & & \\ & & & c_1 & c_2 & c_3 & & & \\ & & & d_1 & d_2 & d_3 & & & \\ & & & & & & e_1 & e_2 & e_3 \\ & & & & & & f_1 & f_2 & f_3 \end{pmatrix} \begin{pmatrix} \left(w_1^{(i)} - w_1^{(j)}\right)(x) \\ \left(w_2^{(i)} - w_2^{(j)}\right)(x) \\ \left(w_3^{(i)} - w_3^{(j)}\right)(x) \\ \left(w_1^{(i)} - w_1^{(k)}\right)(x) \\ \left(w_2^{(i)} - w_2^{(k)}\right)(x) \\ \left(w_3^{(i)} - w_3^{(k)}\right)(x) \\ \left(w_1^{(i)} - w_1^{(l)}\right)(x) \\ \left(w_2^{(i)} - w_2^{(l)}\right)(x) \\ \left(w_3^{(i)} - w_3^{(l)}\right)(x) \end{pmatrix},
\end{aligned}
$$

this means, here we have six constraints for each edge. Note, that by enforcing this stronger constraints the zero net flux condition for edge terms is also satisfied.

For our numerical results we use the implementation of six constraints for each edge.

Figure 4.5: Outer normals of an edge

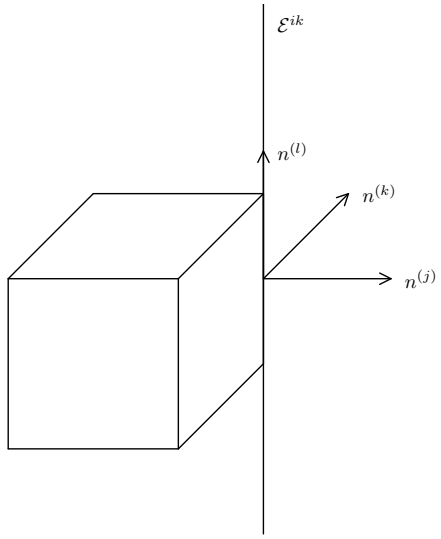

The outer normals belonging to one edge span the corresponding normal space.

4.3 Numerical Results

For all tests we use the following parameter setting. The domain Ω is discretized by statically condensated $\mathcal{Q}_2 - \mathcal{P}_0$ mixed finite elements. We consider an almost incompressible material on the whole domain Ω, i.e., $\nu = 0.499999$ and $E = 210$. Dirichlet boundary conditions are used on $\partial\Omega$ and all vertices are chosen as primal constraints. To establish the zero net flux condition for the face terms we always use projector preconditioning, as described in Section 4.1. For the edge terms, we use on the one hand the transformation of basis, see Section 4.3.1, and on the other hand we use projector preconditioning, i.e., six constraints for each edge; see Section 4.3.2.

4.3.1 Edges by Transformation of Basis

The zero net flux condition for edges is established using a transformation of basis, see Section 4.2.1, and for the face constraints we use projector preconditioning as described in Section 4.1. We run all tests on the one hand with one constraint for each subdomain, i.e., we sum up all face contributions belonging to one subdomain, and on the other hand also using all face constraints as several constraints, which enforces a stronger condition. Using this stronger condition it is not surprising, that the condition number is slightly better.

In the first set of tests, we increase the number of elements, while having a constant number of subdomains, i.e., $N = 27$; see Table 4.1. We observe only a slight difference in the condition number, but we save 50% of constraints when using our new coarse space, i.e., summing up the face contributions. Here, our stopping criterion for the cg method is the relative reduction of the preconditioned residual to $1e-14$. We have chosen a very small tolerance in order to obtain an accurate eigenvalue estimate. A least square fit of the condition number estimates with a quadratic polynomial in $\log(H/h)$ confirms our theoretical condition number estimate of $C \cdot (1 + \log(H/h))^2$; see Fig. 4.8.

Table 4.1: Growing H/h, $1/H = 3$

	New Coarse Space (=one constraint for each subdomain) # constraints: **27**		**Standard Coarse Space** (=one constraint for each face) # constraints: 54	
H/h	# iterations	condition	# iterations	condition
2	16	2.2118	15	1.9679
3	20	3.2485	19	3.0076
4	23	3.9686	22	3.6786
5	26	4.6184	24	4.2866
6	27	5.2073	26	4.8374
7	28	5.7442	27	5.3401
8	29	6.2369	29	5.8019
9	31	6.6920	30	6.2290
10	32	7.1150	31	6.6262

For a fixed decomposition in $3 \times 3 \times 3$ subdomains, we increase the number of elements in each direction in each subdomain.

In Table 4.2 we have the results for the weak scaling, i.e., we increase the number of subdomains from 8 to 1000, but the number of elements in each direction in each subdomain is fixed to $H/h = 3$. The condition number does not vary significantly and for an increasing number of subdomains the new approach is increasingly advantageous; cf. Figure 4.6. Here and for the following results, our stopping criterion for the cg method is the relative reduction of the preconditioned residual to $1e-10$.

In the next set of experiments, we consider a variable incompressibility on the whole domain, i.e., we vary the Poisson ratio from $\nu = 0.3$ up to $\nu = 0.4999999999$. We fix the number of subdomains to $N = 27$; in Table 4.3 we choose $H/h = 5$ elements in each direction in each subdomain, in contrast to Table 4.4, where we use $H/h = 8$ elements in each direction of each

Table 4.2: Growing $1/H$ - weak scaling

	New Coarse Space (=one constraint for each subdomain)			**Standard Coarse Space** (=one constraint for each face)			
$1/H$	# constr.	# its	condition	# constr.	# its	condition	constraints saved
2	**8**	10	1.7057	12	10	1.7057	33.3%
3	**27**	14	2.8989	54	14	2.5185	50.0%
4	**64**	16	3.4813	144	15	2.9639	55.6%
5	**125**	18	3.9982	300	17	3.3369	58.3%
6	**216**	19	4.0936	540	17	3.5887	60.0%
7	**343**	19	4.2320	882	18	3.7705	61.1%
8	**512**	20	4.2627	1344	18	3.8973	61.9%
9	**729**	20	4.3544	1944	18	3.9884	62.5%
10	**1000**	20	4.3630	2700	18	4.0554	63.0%

For a fixed number of elements in each direction in each subdomain, i.e., $H/h = 3$, we vary the number of subdomains from 8 to 1000. For an increasing number of subdomains the new approach generates increasingly higher savings; see also Figure 4.6.

subdomain. The condition number is bounded independently of the almost incompressibility in the domain.

In comparison to Chapter 3, we now consider a possible dependency on the thickness of a hull which has a different material parameter. We choose Young's modulus $E = 210$ on the whole domain and for the Poisson ratio $\nu = 0.3$ in the inclusions and $\nu = 0.499999$ on the hulls, conversely to the parameter settings in the previous chapter. For a fixed number of elements, i.e., once $H/h = 11$, once $H/h = 7$ and for a fixed number of 27 subdomains, we vary the thickness of the almost incompressible hull. We cannot observe a dependency of the condition number on the thickness of the hulls in the numerical results.

Table 4.3: Growing $\nu,\ H/h = 5,\ 1/H = 3$

	New Coarse Space (=one constraint for each subdomain) # constraints: **27**		**Standard Coarse Space** (=one constraint for each face) # constraints: 54	
ν	# iterations	condition	# iterations	condition
0.3	16	3.4224	16	3.2899
0.4	16	3.3552	16	3.2246
0.49	17	3.7324	16	3.1803
0.499	18	3.8820	17	3.3007
0.4999	18	3.8991	17	3.3155
0.49999	18	3.9009	17	3.3170
0.499999	18	4.1788	17	3.3171
0.4999999	18	4.6146	18	4.2847
0.49999999	18	4.6170	18	4.2768
0.499999999	19	4.6183	18	4.2838
0.4999999999	19	4.6184	18	4.2865

For a fixed number of elements in each direction in each subdomain, i.e., $H/h = 5$, a fixed number of subdomains, i.e., $1/H = 3$, we vary the incompressibility on the whole domain Ω, this means we vary the Poisson ratio from $\nu = 0.3$ up to $\nu = 0.4999999999$.

Table 4.4: Growing $\nu,\ H/h = 8,\ 1/H = 3$

	New Coarse Space (=one constraint for each subdomain) # constraints: **27**		**Standard Coarse Space** (=one constraint for each face) # constraints: 54	
ν	# iterations	condition	# iterations	condition
0.3	20	5.9482	19	4.3907
0.4	19	4.3946	19	4.2827
0.49	21	5.7142	20	4.2219
0.499	21	5.6901	20	4.2344
0.4999	21	6.2180	21	5.7185
0.49999	21	6.2364	21	5.8000
0.499999	22	6.2367	21	5.7954
0.4999999	22	6.2369	21	5.8012
0.49999999	22	6.2369	21	5.8018
0.499999999	22	6.2369	21	5.8019
0.4999999999	22	6.2369	22	5.8019

For a fixed number of elements in each direction in each subdomain, i.e., $H/h = 8$, a fixed number of subdomains, i.e., $1/H = 3$, we vary the incompressibility, this means we vary the Poisson ratio from $\nu = 0.3$ up to $\nu = 0.4999999999$.

Figure 4.6:

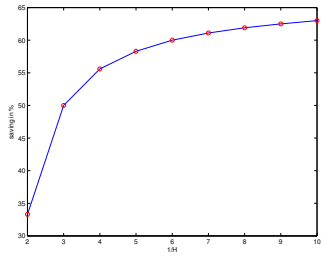

While increasing the number of subdomains from 8 to 1000 the number of saving constraints increases; data from Table 4.2. The more subdomains we choose, summing up the face contributions ensures a much smaller coarse space.

Figure 4.7: Growing H/h

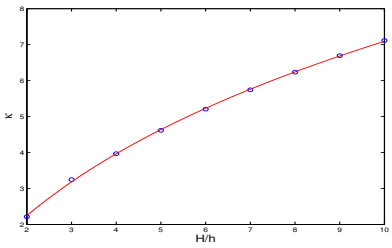

(a) Least square fit of a polynomial in $\log\left(\frac{H}{h}\right)$ to the data from Table 4.1 (left), new coarse space, i.e., one constraint for each subdomain.

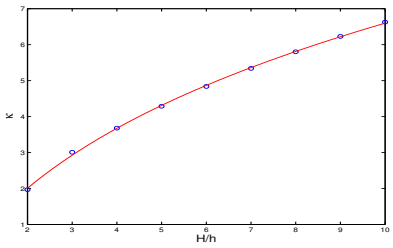

(b) Least square fit of a polynomial in $\log\left(\frac{H}{h}\right)$ to the data from Table 4.1 (right), standard coarse space, i.e., one constraint for each face.

Table 4.5: Growing η

	New Coarse Space (=one constraint for each subdomain) # constraints: **27**		**Standard Coarse Space** (=one constraint for each face) # constraints: 54	
η	# iterations	condition	# iterations	condition
0	22	7.1655	21	6.6937
h	24	7.5140	23	7.0016
$2h$	24	7.5196	23	7.0107
$3h$	24	7.5127	23	7.0011
$4h$	24	7.5107	23	6.9957
$5h$	24	7.5103	23	6.9951
$6h$	24	7.5103	23	6.9969
0	18	4.1834	18	4.0586
h	21	5.7601	20	5.3596
$2h$	20	5.7462	20	5.3356
$3h$	20	5.7433	20	5.3210

For a fixed number of elements in each direction in each subdomain, i.e., $H/h = 11$ first, in the second part $H/h = 7$, we vary the thickness of the almost incompressible hull.

4.3.2 Edges by Projector Preconditioning

In a second set of tests, we establish the zero net flux condition for faces and edges using projector preconditioning. This means, we use six constraints for each edge and run all tests with one face constraint for each subdomain, i.e., our new coarse space, and also with several face constraints for each subdomain. First we again increase the number of elements in each direction of each subdomain from $H/h = 2$ up to $H/h = 19$; see Table 4.6. We observe only a slight effect in the condition number between the new and the standard coarse space.

Table 4.6: Growing H/h

	New Coarse Space (=one face constraint for each subdomain + several edge constraints) # constraints: **243**		**Standard Coarse Space** (=one constraint for each face + several edge constraints) # constraints: 270	
H/h	# iterations	condition	# iterations	condition
2	12	2.3621	12	2.1111
3	16	4.6805	15	4.5437
4	18	5.9544	18	5.7877
5	21	7.0797	20	6.8856
6	22	8.0883	21	7.8703
7	23	9.0036	23	8.7644
8	24	9.8421	24	9.5839
9	25	10.616	25	10.341
10	27	11.336	26	11.045

For a fixed decomposition in $3 \times 3 \times 3$ subdomains, we increase the number of elements in each direction in each subdomain. In this case, we have 54 faces and 36 edges.

But, by establishing the edge constraints by projector preconditioning, the condition number is larger than by using a transformation of basis, cf. Table 4.7.

The results for the tests of the weak scaling can be found in Table 4.8. Due to the fact that we have much more edge than face constraints, using the new coarse space has only a small effect; we still need about 90% of the single constraints.

Table 4.7: Comparison

	New Coarse Space (= one face constraint for each subdomain)			
	edges using a transformation of basis		edges using projector preconditioning	
H/h	# iterations	condition	# iterations	condition
2	12	2.2118	12	2.3621
3	14	2.8989	16	4.6805
4	16	3.4495	18	5.9544
5	18	4.1788	21	7.0797
6	19	5.2044	22	8.0883
7	20	5.7437	23	9.0036
8	22	6.2367	24	9.8421
9	23	6.6920	25	10.616
10	23	7.1150	27	11.336

Comparison of the two approaches, both with the new coarse space; stopping criterion $1e-10$ in the cg method.

Figure 4.8: Comparison

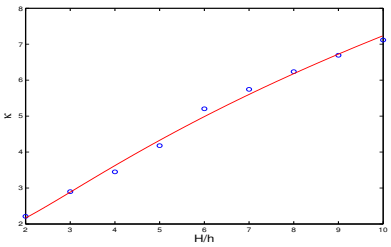

(a) Least square fit of a polynomial in $\log\left(\frac{H}{h}\right)$ to the data from Table 4.7 (left), new coarse space and edge constraints established using a transformation of basis.

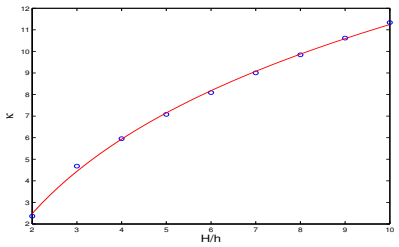

(b) Least square fit of a polynomial in $\log\left(\frac{H}{h}\right)$ to the data from Table 4.7 (right), new coarse space and edge constraints established using projector preconditioning.

Table 4.8: Growing $1/H$ - weak scaling

	New Coarse Space (=one face constraint for each subdomain + several edge constraints)			**Standard Coarse Space** (=one constraint for each face + several edge constraints)			
$1/H$	# constr.	# its	condition	# constr.	# its	condition	constraints saved
2	**43**	10	1.7751	48	10	1.7751	10.4%
3	**242**	16	4.6805	270	15	4.5437	10.4%
4	**711**	19	4.8103	792	18	4.8166	10.2%
5	**1564**	21	5.0110	1740	20	4.6073	10.1%
6	**2915**	22	5.0055	3240	22	4.9109	10.0%
7	**4879**	22	5.1967	5418	22	5.0117	9.9%
8	**7568**	22	5.2402	8400	22	5.0462	9.9%

For a fixed number of elements in each direction in each subdomain, i.e., $H/h = 3$, we vary the number of subdomains.

Bibliography

[1] Lourenco Beirão da Veiga, Carlo Lovadina, and Luca F. Pavarino. Positive definite balancing Neumann-Neumann preconditioners for nearly incompressible elasticity. *Numer. Math.*, 104(3):271–296, 2006.

[2] Dirk Böse, Sarah Brinkhues, Raimund Erbel, Axel Klawonn, Oliver Rheinbach, and Jörg Schröder. A simultaneous augmented lagrange approach for the simulation of soft biological tissue. 2011. Submitted to the proceedings of the 20th International Conference on Domain Decomposition Methods, February 07-11, 2011, San Diego, USA.

[3] Dietrich Braess. *Finite Elemente*. Springer-Verlag, 2. edition, 1997.

[4] Susanne C. Brenner and L. Ridgway Scott. *The Mathematical Theory of Finite Element Methods*. Springer-Verlag, 2008. Third edition.

[5] Franco Brezzi and Michel Fortin. *Mixed and Hybrid Finite Element Methods*. Springer Berlin, 1991.

[6] Sarah Brinkhues, Axel Klawonn, Oliver Rheinbach, and Jörg Schröder. Augmented Lagrange Methods in the Simulation of Soft Biological Tissue. *Int.J. Numer. Methods Biomed. Eng. (IJNMBE)*, 2012. In Press. Available online August 2012. http://dx.doi.org/10.1002/cnm.2504.

[7] Mario A. Casarin. *Schwarz Preconditioners for Spectral and Mortar Finite Element Methods with Applications to Incompressible Fluids*. PhD thesis, Courant Institute, New York University, 1996. Technical Report 1996-717, Department of Computer Science.

[8] Philippe G. Ciarlet. *Mathematical Elasticity, Volume I: Three-Dimensional Elasticity*. Elsevier Science Publishers B.B., 1988.

[9] Ray W. Clough. The finite element method in plane stress analysis. 1960. Proceedings,

2nd Conference on Electronic Computation, A.S.C.E. Structural Division. Pittsburgh, Pennsylvania.

[10] Jean-Michel Cros. A preconditioner for the Schur complement domain decomposition method. In O. Widlund I. Herrera, D. Keyes and R. Yates, editors, *Domain Decomposition Methods in Science and Engineering*, pages 373–380. National Autonomous University of Mexico (UNAM), Mexico City, Mexico, ISBN 970-32-0859-2, 2003. Proc. 14th Int. Conf. Domain Decomposition Methods; http://www.ddm.org/DD14.

[11] C. R. Dohrmann and R. B. Lehoucq. A primal-based penalty preconditioner for elliptic saddle point systems. *SIAM J. Numer. Anal.*, 44(1):270–282 (electronic), 2006.

[12] Clark R. Dohrmann. A preconditioner for substructuring based on constrained energy minimization. *SIAM J. Sci. Comput.*, 25(1):246–258, 2003.

[13] Clark R. Dohrmann. A substructuring preconditioner for nearly incompressible elasticity problems. Technical report, Sandia National Laboratories, Oct. 2004.

[14] Clark R. Dohrmann, Axel Klawonn, and Olof B. Widlund. Domain decomposition for less regular subdomains: overlapping Schwarz in two dimensions. *SIAM J. Numer. Anal.*, 46(4):2153–2168, 2008.

[15] Clark R. Dohrmann and Olof B. Widlund. An overlapping Schwarz algorithm for almost incompressible elasticity. *SIAM J. Numer. Anal.*, 47:2897–2923, 2009.

[16] Clark R. Dohrmann and Olof B. Widlund. Hybrid domain decomposition algorithms for compressible and almost incompressible elasticity. *Internat. J. Numer. Meth. Engng*, page 183, 2010.

[17] Maksymilian Dryja, Barry F. Smith, and Olof B. Widlund. Schwarz analysis of iterative substructuring algorithms for elliptic problems in three dimensions. *SIAM J. Numer. Anal.*, 31(6):1662–1694, December 1994.

[18] Charbel Farhat, Michel Lesoinne, Patrick LeTallec, Kendall Pierson, and Daniel Rixen. FETI-DP: a dual-primal unified FETI method. I. A faster alternative to the two-level FETI method. *Internat. J. Numer. Methods Engrg.*, 50(7):1523–1544, 2001.

[19] Charbel Farhat, Michel Lesoinne, and Kendall Pierson. A scalable dual-primal domain decomposition method. Preconditioning techniques for large sparse matrix problems in industrial applications. *Numer. Linear Algebra Appl.*, 7(7-8):687–714, 2000.

[20] Charbel Farhat and Francois-Xavier Roux. A method of Finite Element Tearing and Interconnecting and its parallel solution algorithm. *Int. J. Numer. Meth. Engrg.*, 32:1205–1227, 1991.

[21] Sabrina Gippert, Axel Klawonn, Martin Lanser, Patrick Radtke, and Oliver Rheinbach. Nonlinear Domain Decomposition, Adaptive Coarse Spaces, and a New Coarse Space for Almost Incompressible Elasticity. 2012. In preparation to the proceedings of the 21st International Conference on Domain Decomposition Methods, June 25-29, 2012, Rennes, France.

[22] Sabrina Gippert, Axel Klawonn, and Oliver Rheinbach. Analysis of FETI-DP and BDDC for linear elasticity in 3d with almost incompressible components and varying coefficients inside subdomains. *SIAM J. Numer. Anal.*, 50(5):2208 –2236, 2012.

[23] Paulo Goldfeld. *Balancing Neumann-Neumann Preconditioners for Mixed Formulation of Almost-Incompressible Linear Elasticity*. PhD thesis, Courant Institute of Mathematical Sciences, September 2003. TR-847, Department of Computer Science.

[24] Paulo Goldfeld, Luca F. Pavarino, and Olof B. Widlund. Balancing Neumann-Neumann preconditioners for mixed approximations of heterogeneous problems in linear elasticity. *Numer. Math.*, 95(2):283–324, 2003.

[25] Cornelius O. Horgan. Inequalities of Korn and Friedrichs in elasticity and potential theory. *Z. Angew. Math. Phys*, 26:155–164, 1975.

[26] Marta Jarošová, Axel Klawonn, and Oliver Rheinbach. Projector preconditioning and a transformation of basis in FETI-DP algorithms for contact problems. *Mathematics and Computers in Simulation*, 82(10):1984 –1907, June 2012.

[27] Axel Klawonn, Patrizio Neff, Oliver Rheinbach, and Stefanie Vanis. Notes on FETI-DP Domain Decomposition Methods for P-Elasticity. Technical report, Universität Duisburg-Essen, Fakultät für Mathematik, Essen, Germany, http://www.mi.uni-koeln.de/numerik/files.local/klawonn_neff_rheinbach_vanis_technical_report_p-elasticity.pdf, 2010.

[28] Axel Klawonn, Patrizio Neff, Oliver Rheinbach, and Stefanie Vanis. FETI-DP Domain Decomposition Methods for Elasticity with structural changes: P-Elasticity. *ESAIM:M2AN*, 45:563–602, 2011.

[29] Axel Klawonn, Luca F. Pavarino, and Oliver Rheinbach. Spectral element FETI-DP and BDDC preconditioners with multi-element subdomains. *Comput. Meth. Appl. Mech. Engrg.*, 198:511–523, 2008.

[30] Axel Klawonn and Oliver Rheinbach. A parallel implementation of Dual-Primal FETI methods for three dimensional linear elasticity using a transformation of basis. *SIAM J. Sci. Comput.*, 28(5):1886–1906, 2006.

[31] Axel Klawonn and Oliver Rheinbach. Robust FETI-DP methods for heterogeneous three dimensional linear elasticity problems. *Comput. Methods Appl. Mech. Engrg.*, 196:1400–1414, 2007.

[32] Axel Klawonn and Oliver Rheinbach. Highly scalable parallel domain decomposition methods with an application to biomechanics. *ZAMM Z. Angew. Math. Mech.*, 90(1):5–32, 2010.

[33] Axel Klawonn and Oliver Rheinbach. Deflation, projector preconditioning, and balancing in iterative substructuring methods: Connections and new results. *SIAM Journal of Scientific Computing*, 34(1):459 –484, 2012.

[34] Axel Klawonn, Oliver Rheinbach, and Olof B. Widlund. An Analysis of a FETI-DP Algorithm on Irregular Subdomains in the Plane. *SIAM J. Numer. Anal.*, 46(5):2484–2504, 2008.

[35] Axel Klawonn, Oliver Rheinbach, and Barbara Wohlmuth. Dual-primal iterative substructuring for almost incompressible elasticity. In D.E. Keyes and O.B. Widlund, editors, *Domain Decomposition Methods in Science and Engineering*, volume 55, pages 399–406. Springer-Verlag, Lecture Notes in Computational Science and Engineering, 2007.

[36] Axel Klawonn and Olof B. Widlund. Dual and dual–primal FETI methods for elliptic problems with discontinuous coefficients in three dimensions. In Tony Chan, Takashi Kako, Hideo Kawarada, and Olivier Pironneau, editors, *Domain Decomposition Methods*

in Sciences and Engineering: The Twelfth international Conference on Domain Decomposition Methods, held in Chiba, Japan, October 25–29, 1999, pages 28–40. ddm.org, 2001.

[37] Axel Klawonn and Olof B. Widlund. Dual-Primal FETI Methods for Linear Elasticity. *Comm. Pure Appl. Math*, 59:1523–1572, 2006.

[38] Axel Klawonn, Olof B. Widlund, and Maksymilian Dryja. Dual-primal FETI methods for three-dimensional elliptic problems with heterogeneous coefficients. *SIAM J. Numer. Anal.*, 40(1):159–179, April 2002.

[39] Axel Klawonn, Olof B. Widlund, and Maksymilian Dryja. Dual-Primal FETI methods with face constraints. In Luca Pavarino and Andrea Toselli, editors, *Recent Developments in Domain Decomposition Methods*, Lecture Notes in Computational Science and Engineering, Volume 23, pages 27–40. Springer, 2002.

[40] Jing Li. A dual-primal FETI method for solving Stokes/Navier-Stokes equations. In *Domain decomposition methods in science and engineering*, pages 225–231 (electronic). Natl. Auton. Univ. Mex., México, 2003.

[41] Jing Li. A dual-primal FETI method for incompressible Stokes equations. *Numer. Math.*, 102(2):257–275, 2005.

[42] Jing Li and Olof B. Widlund. BDDC algorithms for incompressible Stokes equations. *SIAM J. Numer. Anal.*, 44(6):2432–2455 (electronic), 2006.

[43] Jing Li and Olof B. Widlund. FETI–DP, BDDC, and Block Cholesky Methods. *Internat. J. Numer. Methods Engrg.*, 66(2):250–271, 2006.

[44] Jan Mandel and Clark R. Dohrmann. Convergence of a balancing domain decomposition by constraints and energy minimization. *Numer. Linear Algebra Appl.*, 10:639–659, 2003.

[45] Jan Mandel, Clark R. Dohrmann, and Radek Tezaur. An algebraic theory for primal and dual substructuring methods by constraints. *Appl. Numer. Math.*, 54:167–193, 2005.

[46] Jan Mandel and Radek Tezaur. On the convergence of a dual-primal substructuring method. *Numer. Math.*, 88:543–558, 2001.

[47] Gunar Matthies and Lutz Tobiska. The inf-sup condition for the mapped $Q_k - P_{k-1}^{disc}$ element in arbitrary space dimensions. *Computing*, 69:119–139, 2002.

[48] Luca F. Pavarino. Neumann-Neumann algorithms for spectral elements in three dimensions. *RAIRO Mathematical Modelling and Numerical Analysis*, 31:471–493, 1997.

[49] Luca F. Pavarino and Olof B. Widlund. Balancing Neumann-Neumann methods for incompressible Stokes equations. *Comm. Pure Appl. Math.*, 55(3):302–335, 2002.

[50] Luca F. Pavarino, Olof B. Widlund, and Stefano Zampini. BDDC preconditioners for spectral element discretizations of almost incompressible elasticity in three dimension. *SIAM J. Sci. Comput.*, 32(6):3604–3626, 2010.

[51] Clemens Pechstein and Robert Scheichl. Analysis of FETI methods for multiscale PDEs. *Numer. Math.*, 111:293–333, 2008.

[52] Clemens Pechstein and Robert Scheichl. Scaling up through domain decomposition. *Applicable Analysis*, 88(10-11):1589–1608, 2009.

[53] Clemens Pechstein and Robert Scheichl. Analysis of FETI methods for multiscale PDEs-PartII: Interface variation. *Numer. Math.*, 118(3):485–529, 2011.

[54] Oliver Rheinbach. *Parallel Scalable Iterative Substructuring: Robust Exact and Inexact FETI-DP Methods with Applications to Elasticity*. PhD thesis, Department of Mathematics, University of Duisburg-Essen, Essen, Germany, 2006.

[55] Oliver Rheinbach. Parallel iterative substructuring in structural mechanics. *Arch. Comput. Methods Eng.*, 16(4):425–463, 2009.

[56] L. Ridgway Scott and Shangyou Zhang. Finite element interpolation of nonsmooth functions satisfying boundary conditions. *Math. Comp.*, 54(190):483–493, April 1990.

[57] Andrea Toselli and Olof B. Widlund. *Domain Decomposition Methods- Algorithms and Theory*, volume 34. Springer Series in Computational Mathematics, 2005.

[58] M. Jon Turner, Ray W. Clough, Harold C. Martin, and L. J. Topp. Stiffness and Deflection Analysis of Complex Structures. *Journal of the Aeronautical Science*, 23(9):805 – 823, 1956.